Addis Ababa University

School of Earth Sciences

Integrated Analysis and Interpretation of Helicopter Borne Aeromagnetic and Gamma ray Spectrometric Data of the South Meleka

(Adola Greenstone Belt, Southern Ethiopia)

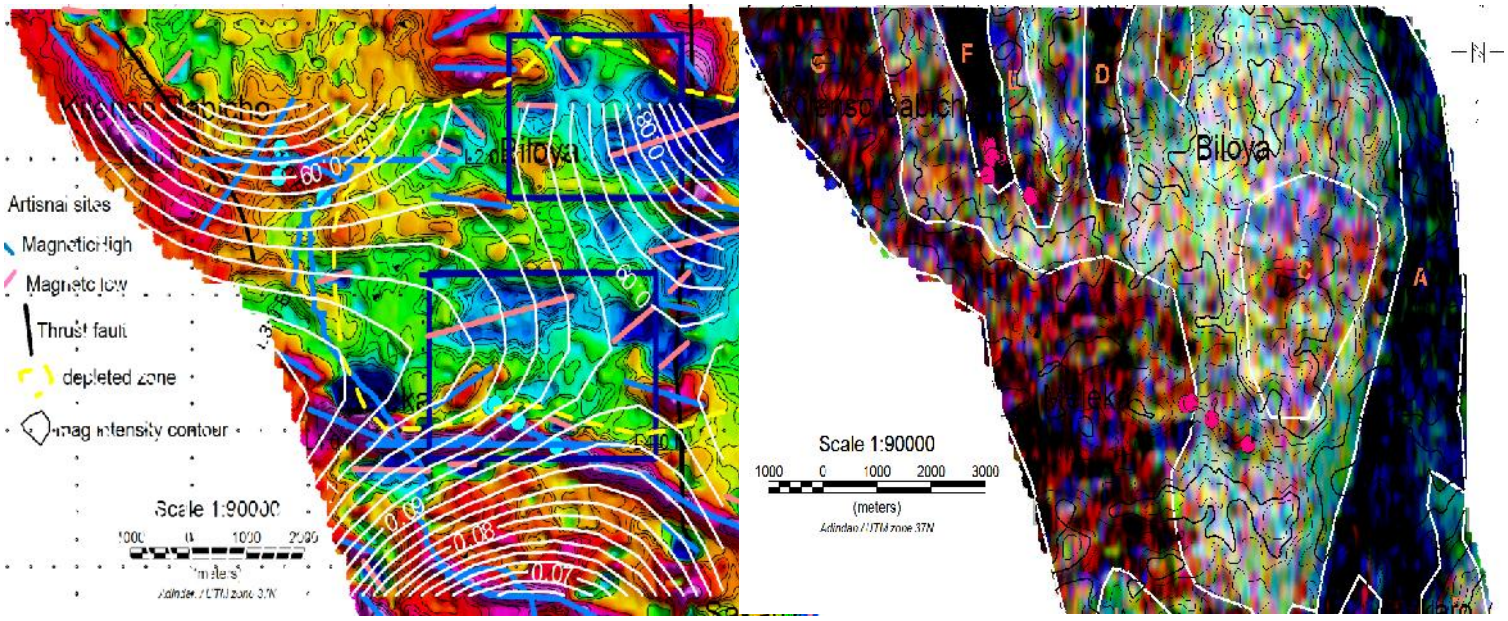

By: Behailu Mammo

July, 2015

Integrated Analysis and Interpretation of Helicopter Borne Aeromagnetic and Gamma ray Spectrometric Data of the South Meleka

(Adola Greenstone Belt, Southern Ethiopia)

A thesis presented to the school of graduate studies of
Addis Ababa University
In partial fulfilment of the requirement for the degree of
Masters of Science in exploration geophysics

By
Behailu Mammo

Addis Ababa
2015

Advisor: Dr. Abera Alemu
Co. Advisor: Dr. Mulugeta Alene
Co. Advisor: Dr. Girma Woldetinsae

Addis Ababa University

School of Earth Sciences

Integrated Analysis and Interpretation of Helicopter Borne Aeromagnetic and Gamma ray Spectrometric Data of the South Meleka (Adola Greenstone Belt, Southern Ethiopia)

By

Behailu Mammo

Department of Earth Sciences

Approved by the Examining board:

Name	Signature
Professor Tigistu Haile Examiner	
Professor Tilahun Mammo Examiner	
Dr. Abera Alemu Advisor	07-07-2015
Professor Solomon Tadesse Chairman	

Abstract

This work uses part of an airborne survey data of Adola belt generated by Geological Survey of Ethiopia in 1994. The belt has been studied by different researchers to explain the structural pattern and mineralization. Here, the different enhancing filters are applied on the aeromagnetic and gamma ray spectroscopic data and the geophysical signatures gleaned are used to explain the rock units and structural features associated to mineralization. In addition, the airborne coverage data of Ethiopia is updated with new coverage data gathered for petroleum exploration.

The Upward Continuation (UWC) filter at different height shows the effects of deeper regional source by removing the shallower effects and possible noises. Upward continued TMI (up to 500m) above the flight height of the magnetometer showed a WNW-ESE trending linear structure at the southern parts of the area. Further enhancement using tilt derivative reveals some more geological features.

The Gamma ray spectrometric data is regridded with a cell size of 15m and a bi directional line gridding is applied using Oasis Montaj, and filtered and shaded maps of the individual radio elements (U, TH, K, and TC) and a ternary image are produced. The ternary map demarcated major geological units such as basalts, gneisses and central volcano sedimentary terrain. These are peculiar signatures well marked at the eastern, western and central part of the area. The ratio map of Th/K is prepared to select the alteration zones favourable for mineralization. The Total Count map mapped the central volcano sedimentary belt with a low total count from northern end up to the southern covering a wide part of the study area. It also portrayed area around Kilenso Babicho, Meleka and north Sakaro with a high total count.

The analysis and interpretation from the ground magnetic and radiometric surveys are compared with that of the aeromagnetic and gamma ray spectrometric data on selected areas and are found to be well corroborated. From the result of all the enhanced maps the trends and dispositions of the inferred faults at the southern part are modified. Power spectrum technique is applied to estimate the depth to source of the magnetic body. The average depth for both the shallower source and deeper source anomalies using the FFT analysis method are estimated to be 11.98m and 43.54m respectively.

From all the interpreted maps composite map is produced which show the magnetic lineaments, altered zone, and selected target area for further study and follow-ups.

Acknowledgements

The ministry of Mines is acknowledged for granting permission to conduct this study and cover the cost of field work. The Geological Survey of Ethiopia kindly permitted me to use the part of the airborne data, related documents and their licensed Oasis Montaj software program..

I am very grateful to my advisor Dr. Abera Alemu for his guidance and continuous encouragement and Dr. Mulugeta Alene for his critical comments on the geology.

I would like to express my heartfelt gratitude to Dr. Girma Woldetinsae for his scientific advice guidance, constructive suggestions and all other technical and administrative supports through the Research and Development directorate of Ministry of Mines.

Mengistu Bacha and Addisu Misganaw accompanied and assisted in the ground geophysical field work. Mersha Nigussie, Asegid Ergete, Dereje Deriba and Ayele Teklu are acknowledged for their helpful support and sharing valuable experiences. Tefera Alemu, Mulumebet Fetene and Dr. Ketsela Tadesse gave me the airborne coverage data of petroleum exploration. Bekana Muleta, Dawit Mammo, Yayesh Mehrete, Etagegne Nuru, Nigat Manahel, Tesfaye Kassa, Leta Megerssa, Leule Gebre and other colleagues in Ministry of Mines provided me useful information and materials. My mother, all family members and friends thanked for their consistent support and encouragement.

Above all I like to thank almighty God who gives me everything and the Mother of Christ for being with me in every part of my life.

Table of Contents

Table of Figure

CHAPTER ONE

Introduction

1.1 Location of the study area

The study area, Meleka sheet, is located in the Oromia regional state, between Adola Rede and Ana Sora woreda (figure 1). The Ana Sora contains many kebeles from which Bwanbaw Wuha, Kilenso Babicho and Hobone kebeles are within the study area. Biloya, Meleka and Sakaro kebeles are at the middle of the study area within the Adola Rede woreda. The area is accessed from Addis Ababa by air and road. It is 420 km from Addis Ababa via Addis Ababa-Negelle road passing through the town of Mojo, Shashemene and Hawasa, which is asphalted. The sheet lies between latitude 6^0 00' and 6^0 05' N and longitude 38^0 48' and 38^0 55'E located at the northern end of Adola Greenstone Belt.

1.1.1 **Physiography**

The study area is generally found in higher altitude compared to southern and other parts of the belt which ranges between 2400 – 1500m above mean sea level (figure 2). The Digital Elevation Model (DEM) is prepared from a 30 m resolution data, gridded using minimum curvature and a cell size of 15 meters in Oasis Montaj (figure 2). Maximum elevation in the area is 2338 meters around Biloya, east of Bwanbwa Wuha and Sakaro (at the south eastern end), and the minimum extends up to 1587 meters east Biloya and south of Meleka kebele. The elevation difference between the lowest and highest point is about 751 meters and the mean elevation is 2145 meters. Central part is relatively even as compared to the south eastern rugged surface and eastern lowest place. The topographic features are controlled by the underling geology, the main tectonic episode and geomorphologic features. Most of exposed N-S trending ridges are underlain by metavolcanic and ultramafics rocks (Worku, 1996).

Two perennial and four intermittent streams cut across the study area: the Busa Idira and Haroji, and Babicho, Biloya, Getem Dida and Kilenso respectively, which flows the W-E across the N-S oriented topographic features. The Awata at the southern and Ababa at the eastern side of the study area are the two rivers in the proximity known for the artisanal works.

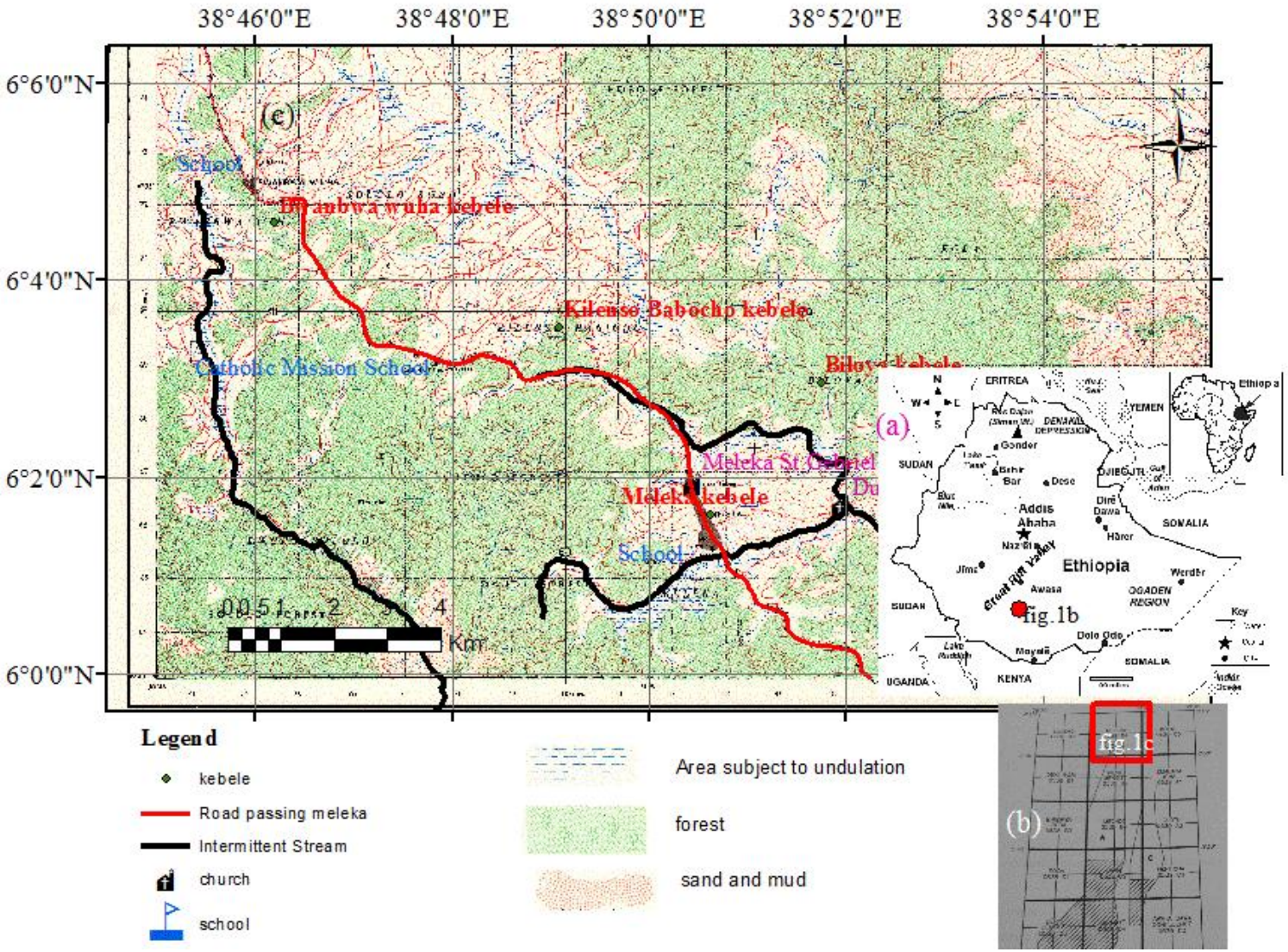

Figure 1(a) Location of Ethiopia relative to Africa. (b) Adola green stone belt survey area. (c) Location of the study area using 50, 000 topographic map

The study area predominated by warm and rainy seasons. Day time temperature during dry season ranges from 28^0c - 30^0c. September to November and March to May are the two main seasons during which most rain falls; the rest of year being relatively dry. As we have observed and the information from the local people, most of the times a rain come in the afternoon and at night. So, even if there is heavy rain falls in this season, in the morning it is possible to perform the geophysical works without much difficulty. The area is mostly covered by thick tropical rain forest hosting Wild many animals. The area surrounded by Sakaro forest at the south eastern side, Okutu forest at the south west and Kilinso forest at the western, and Anferara and Mesina forest at the southern side of the study area. The area is sparsely populated by Guji and Borena tribes of Oromia people that dominate the whole of southern Ethiopia. The inhabitants are mainly nomads and live on cattle breeding and small scale farming and some of them artisanal gold mining. They produce maize and Soya beans (Worku, 1996; Ps Mining, 2003).

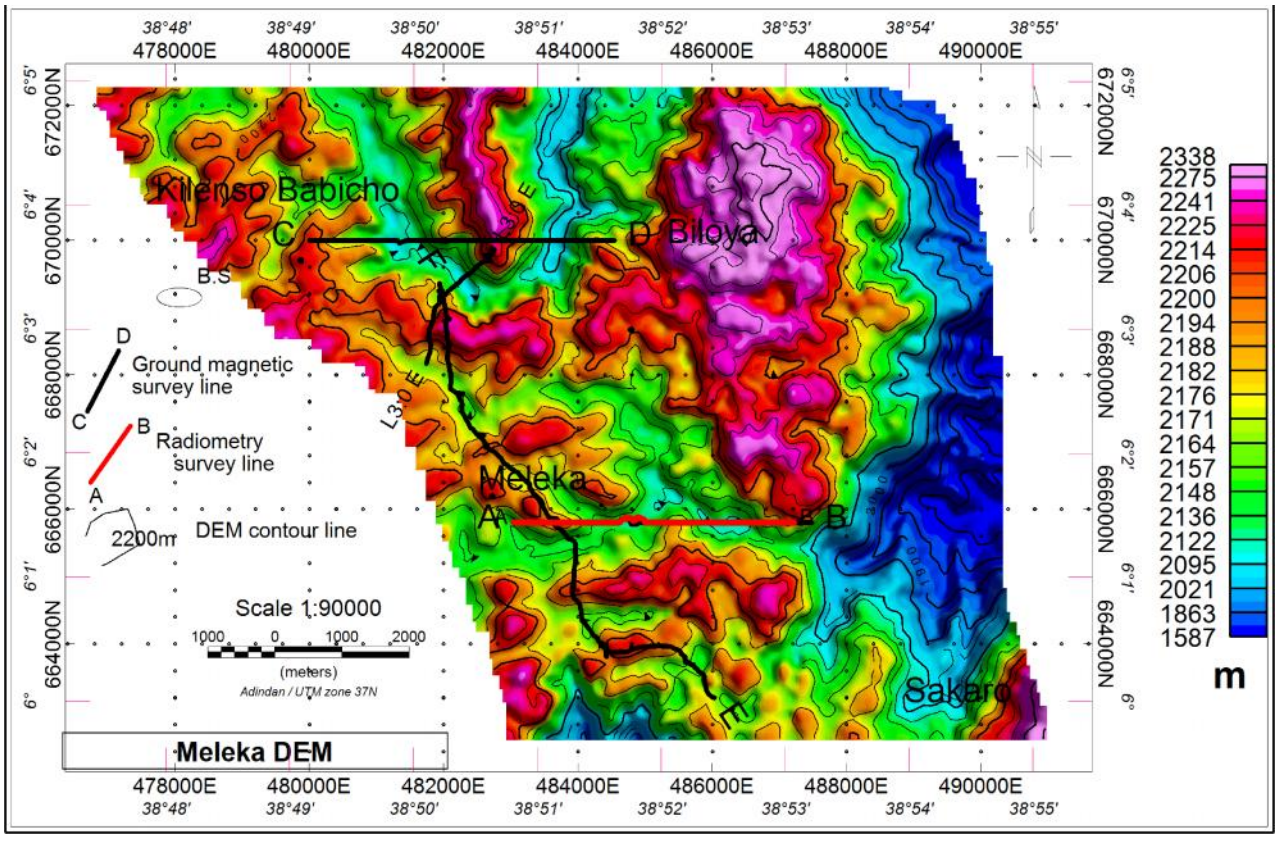

Figure 2 Digital Elevation Model (DEM) Of Meleka using a 30m resolution data gridded with a 15 m cell size using Oasis Montaj

1.2 Previous works

The Adola belt has been extensively studied since 1930 and different and different authors tried to explain the structural pattern and mineralization (Negussie, 1990; Worku, 1995, 1997, kazmin 1971, 1992; Bexell, 1948). The geological mapping and reconnaissance geochemical soil sampling were conducted at a scale of 1:50,000 in the surrounding areas of Meleka in 1989 by Geological Survey of Ethiopia (Negussie, 1990). The Canyon Resources Africa Ltd. had a 108 km^2 license area at the northern part of the study area (quarter of the study area overlap with the licence area). It contains numerous areas of placer gold mining (current artisanal mining) as well as soil geochemical anomalies and rock chip sample anomalies. The exploration result showed Structural and stratigraphic conditions for multi-million ounce gold deposit formation are present within the area (Canyon, 1998). The company completed trenching and drilling works within its license area which provided new data to better evaluate the potential for discovery of gold deposits. According to the report, visible gold has been found on outcrop within the license area in only two places to date. Sampling and panning of saprolite material from an area of high grade assay (35 g/t gold), with clear but highly weathered relict bedrock features resulted in a large number of very fine grains of gold. Visible gold was also found in a quartz vein in the southern part of the license (this part overlap with the study area). Several rock chip samples collected by Canyon have resulted in assay values greater than one gram per tonne. Artisanal placer gold mining is an ongoing practice in the entire area and every stream and locality.

In the southern part of the study area PS Mining Private Limited Company has conducted, follow-up and detail geological and geochemical exploration works at the scales of 1:25, 000 and 1:10,000 covering areas of 81.84 km^2 and 1.84 km^2, respectively. The ground magnetic survey across the strike of the rocks of the selected anomalous areas of Grid (100mX20m) was done. The main objective of the exploration activities was to follow the gold and base metals anomalies outlined during previous year of exploration within the Bulbul shear zone and to delineate target areas for trenching and IP/R geophysical survey. The exploration result revealed: the presence of competent and incompetent rocks, shearing activity and the chemistry of wall rocks are totally conducive for the flow gold-bearing hydrothermal fluids and wall rock reaction that can lead to gold deposition, hydrothermal alteration such as silicification, sulphidation, chloritization and sericitization are evidences for the flow of such hydrothermal fluids. The result also disclose the spatial overlap of gold, copper and zinc anomalies as well as magnetic anomalies supports the presence of mesothermal gold deposit containing copper and zinc mineralization area (PS Mining, 2015).

The study area doesn't have any geophysical coverage except this airborne and one ground geophysics done by GSE in 1990 covering about 85 square km area using radiometric and magnetic methods aimed assisting geologic mapping and identifying radioactive anomaly zones (Muleta, 1990). Although, the surveyed area in 1989 falls within the current study area, it doesn't have proper reference geographic coordinate (conducted using local coordinates) makes the data impossible to integrate along with this study.

Previous airborne geophysical survey in Ethiopia

Airborne geophysical surveys have been conducted in Ethiopia since 1951 with analogue recording. The surveys were for mineral exploration, petroleum exploration and geothermal exploration. Out of the total airborne geophysical surveys (figure 3) only three surveys, 1311.01 and 1313 (high resolution) and 1312.01(low resolution) were found useful for geological mapping (mineral exploration), but data of 1033, 1311 and 1312 surveys had inherent problems and could not give sound interpretation results. Other surveys employed magnetic method for Petroleum Exploration (1337.01, 1031,1035, 1238, 1335, 1337.01, 1337) to detect sediment thickness, geological structures and basement topography and for geothermal exploration (1031) (figure 3) to detect altered/demagnetized rocks as a result of high subsurface temperature and thereby to delineate geothermal field boundary (Sweth, 2009).

The total line kilometre covered from 1951 up to 1998 is 183062km both for Magnetic, radiometric and Electromagnetic

The total line kilometre covered from 1998 up to date is 245314km both for Magnetic and Gravity survey. The data doesn't include the survey currently being undertaken. Out of the total of 245314km line airborne survey 154426 km is covered by Full Tensor Gravity survey and 111624 km is covered by magnetic survey.

This study uses one of the high resolution airborne geophysical surveys (1311.01) which is found useful for geological mapping (mineral exploration) from the 1951-1998 survey coverage. The data acquisition was performed from January 26, 1993 to July 5, 1993 and January 4 1994 to March 11, 1994. The two years survey covered a total of 16,412 line kilometres of traverse and tie lines, divided in two adjacent blocks of West and East Adola area having five kilometres of distance between them (figure). The Western Adola block (A, B and D) comprises 12,927 line kilometres and the Eastern block (C) consists of 3,485 line kilometres including the tie lines (Last, 1994). These study uses block D from the West Adola area of 1994 survey (figure 4).

Table 1 compiled by GSE showing survey year, methodology, line km covered and contractor from 1951 up to 1998

Blocks from 1951- 1998

FID	Survey_No	Year	LineKm	linespace	Method	Contractor
0	1238	1951	8725	8	Mag	Rogers-Rav C.A
1	1035	1976	14345	5	Mag	Aero Service
2	1335	1976	14345	5		Aero Service
3	1311.01	1993/94	17296	0.2	Rad/Mag/EM	UNDP
4	1311.01	1993/94	17296	0.2	Rad/Mag/EM	UNDP
5	1311	1970	9726	1	Rad & Mag	UNDP
6	1337	1983	3436	3	Mag	Aero Service
7	1212	1970	15274	1	Rad & Mag	UNDP
8	1312.01	1996	12600	1	Rad/Mag/EM	Geological Survey of Finland
9	1337.01	1983	7300	7	Mag	Aero Service
10	1033	1971	35443	1	Rad & Mag	Geosurvey International GmbH
11	1031	1968	24000	10	Mag	Hunting Geology and Geophysics ltd.
12	1313	1998	3276	0.2	Rad & Mag	Geodass Ltd..RSA
Sum LineKm			183062			

Table 2 showing block names, survey year, methodology, line km covered and contractor from 1998 up to 2014 done for petroluum

FID	Block_name	years	LineKm	Method	Contractor	Current_status
0	Gambela area	2013	17772	17772 FTG	Petronas	Under South west Energy lisence
1	South Omo area	2011/12	12482	12482 FTG	Tullow Oil	
2	B17,20	2008/9	18000	18000 Mag and Grav	petronas	Under Poly GCL Petrolium licence
3	B18,19&21	2008/9	37436	5560 Mag & Grav and 31876 Mag	Gexco Exploration	Under Delovex
4	B9,13	2012	19000	FTG	South west Energy	
5	B9A	2012	19000	FTG	South west Energy	
6	B7,8	2008	33275	11547 Grav and 21728 Mag	Falcon	Under Africa Oil licence
7	Afar block	2014	0	Grav	GPB	not finished
8	Afar block	2014	0	Grav	GPB	not finished
9	Rift Vally block	2013	36522	FTG	Africa Oil	
10	Rift Vally block	2013	0	FTG	Africa Oil	
11	Adigala block	2009	16252	5820 Gravity & 10432 Mag	Lundin east africa	Under New Age licence
12	Afar	2007	2300	Grav & Mag	Afar Exploration	
13	B2,6	2008	33275	11547 Grav and 21728 Mag	Lundin east africa	Under New Age licence
Sum LineKm			245314			

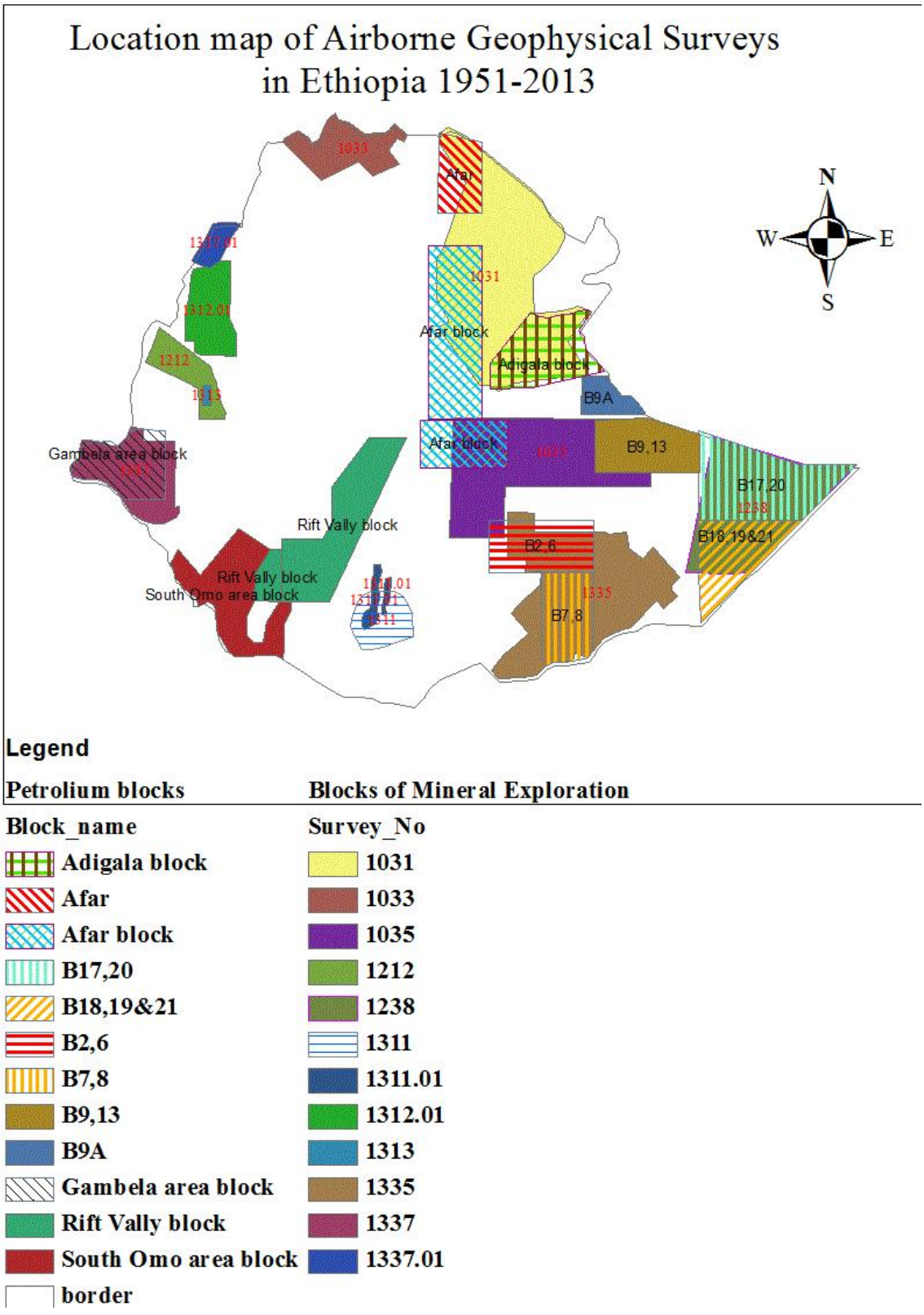

Figure 3 Airborne coverage of the country

The purpose of the survey was to provide information that could be used to map the geology and structure of the survey area, and to indicate potential mineralized areas which might have similar geological settings to known mineralized sites.

This data is part of the airborne survey conducted by Dighem, a division of CGG Canada Ltd under contract to the United Nations Department of Economic and Social Development (UNDESD) for the Geological Survey of Ethiopia, Ministry of Mines (Last, 1994).

The acquisition was accomplished by using a DIGHEM multi coil, multi frequency electromagnetic system, supplemented by a high sensitive, Picodas 3340 Optically Pumped, Cesium Vapour Magnetometer and a 256 channel GR-820 Airborne Spectrometer. A GPS electronic navigation system ensured accurate positioning of the geophysical data with respect to the UTM grid

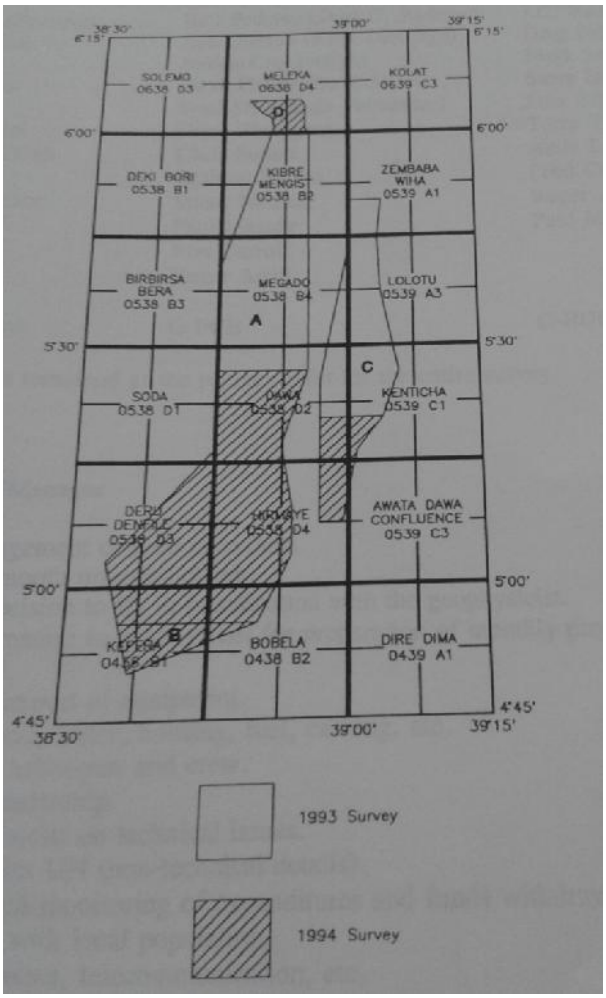

Figure 4 The 1993 and 1994 Adola area survey for mineral exploration (this study uses D block from 1994 survey labelled D)

1.3 Problem statement

An airborne geophysical work, including magnetic, radiometric and electromagnetic techniques, was done by Geological Survey of Ethiopia (GSE) covering the Adola belt in 1994. This geophysical work covers the southern part of Meleka sheet, which is found at the northern end of Adola belt. The area's airborne data hasn't been interpreted yet integrated with other geophysical and geological data.

The present geophysical work is planned to locate and delineate the mineral potential of the area by identifying geological boundaries and anomalous zones of mineralization for a further ground follow up using different filter types to enhance the raw data and improve previous models of interpretation.

1.4 Objectives of the study

1.4.1 General Objective

The general objective of this project is to use both aeromagnetic and gamma ray spectrometric data together with available ground geophysical and geological information of the southern Meleka sheet for identification of target anomalous zones of mineralization for a further ground follow up and integrated interpretation.

1.4.2 Specific Objectives

- Process the available existing aeromagnetic and spectrometric data using different types of filters and prepare composite geophysical map.
- Integrate the processed aeromagnetic and spectrometric data with other existing data (remote sensing, geology and ground geophysics) available for the area.
- Identify anomalous zones of mineralization for a further ground follow up and detailed studies.
- Delineate simple geological boundaries revealed by the study
- Assess the mineral potential on the selected area

1.5 Methodology

In order to meet the objectives outlined above, the methodology used can be divided as follows (figure 5);

1. Carrying out a literature review to find out any previous works done in the area. Any previous geophysical and other geo data exist in the area, relevant information is

collected. Previous geological study shows the area is covered by a low grade belt of metavolcanic and metasedimentary rocks bounded by a higher grade schists and gneisses.

2. Selection of Meleka's airborne data from the 1994 Helicopter Born geophysical survey in the Adola area was the next step in the process. This data is part of the airborne survey conducted by Dighem, a division of CGG Canada Ltd under contract to the United Nations Department of Economic and Social Development (UNDESD) for the Geological Survey of Ethiopia, Ministry of Mines (Last, 1994). The data was collected using Picodas 3340 Optically Pumped Cesium Vapour Magnetometer and GR-820 Airborne Spectrometer for aeromagnetic and radiometric survey respectively.

3. Processing the aeromagnetic and spectrometric data is done on the corrected data. For a better interpretable results image enhancement such as reduction to Pole/Equator, vertical derivatives, Tilt derivative and downward/upward continuation is done. There are different softwares used to do the processing. These include: Oasis Montaj gridding, processing and mapping system (using geological survey licence), Arc GIS, Global Mapper and MS Office 2000.

4. Merge the processed airborne and geophysical data to compile a composite geophysical map of the study area for a further interpretation. Integrate other geo data (remote sensing, geology and ground geophysics) for an improvement of data quality and to avoid ambiguity problems during the interpretation. Based on the results of integrated data, profiles that crosses observed anomalous sites were selected for field test.

5. Conducting ground magnetic survey along the selected profiles is followed. These survey profiles is selected from the result of interpreted airborne data

6. Finally reinterpret the data collected during the follow up survey to extract additional information using different software's like Geosoft, surfer and Arc GIS, and exercise 2D modelling.

.

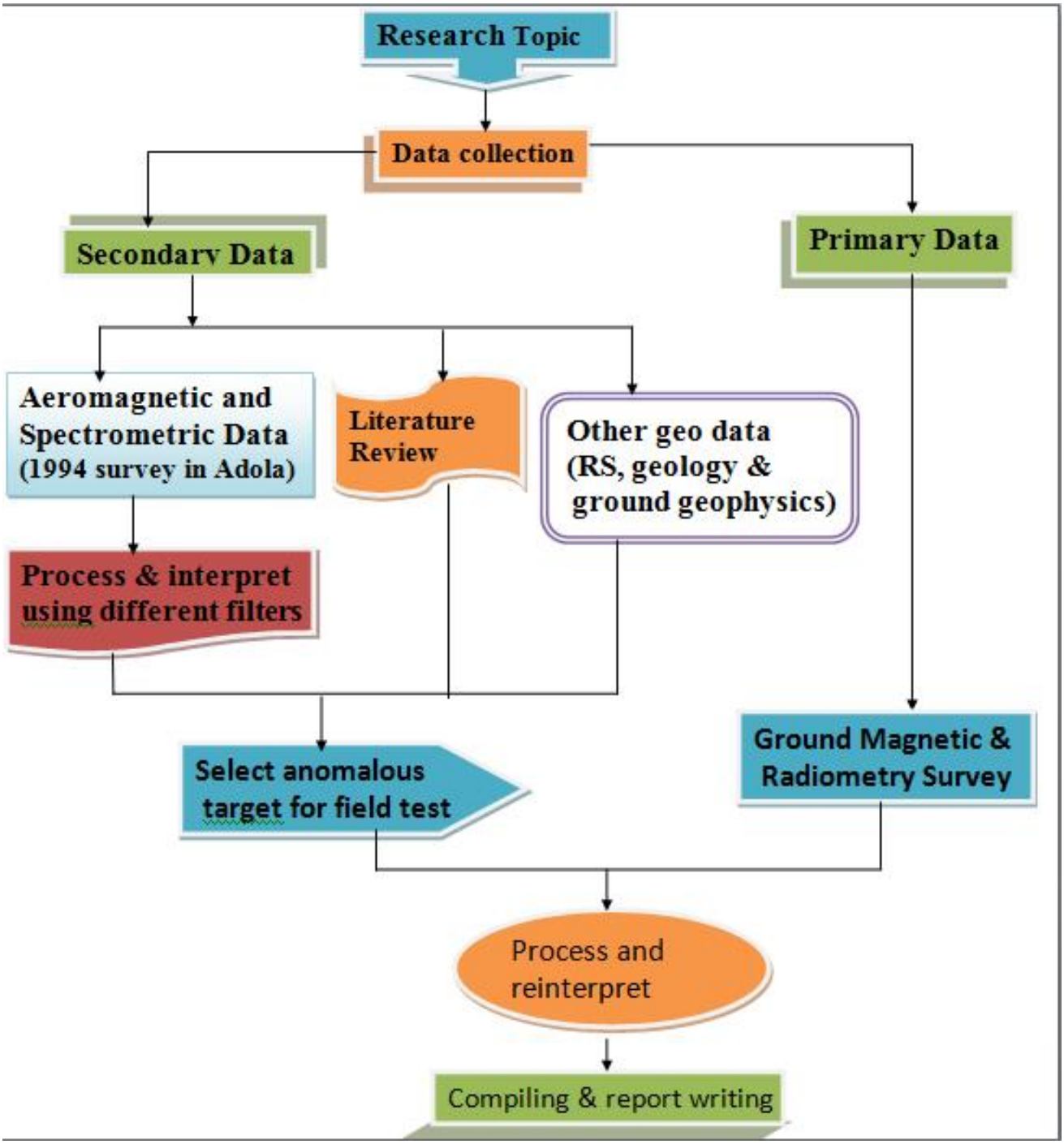

Figure 5 Flow model of the project

CHAPTER TWO

Geological Background

2.1 Regional Geological Setting

2.1.1 Geology of southern Ethiopia

Recent suggestion for the Ethiopian basement is grouped in to two major blocks of volcano sedimentary terrane and Gneissic migmatitic terrane separated by numerous Ophiolitic Sutures (Asrat et al., 2001)

Based on the distribution of magmatic and sedimentary rocks and on deformational and metamorphic criteria, rocks of southern Ethiopia can be subdivided into two major lithologic domains that form distinctive intercalated packages separated by major tectonic boundaries: i) the gneiss and schist domain, a complex and heterogeneous association of high grade, polydeformed and metamorphosed granitoid gneisses, pelitic and psammitic gneisses/schists migmatites and associated mafic-ultramafic schliem and enclaves, all of which are intruded by syn- to post-collision granitoids, ii) low-grade Metavolcano-sedimentary successions and associated mafic-ultramafic complexes forming distinctive N-S- trending belts

The gneissic rocks of southern Ethiopia were locally subjected to medium to high grade metamorphism with local areas of granitization and migmatization. Occurrences of granulites of Pan-African age are reported from the western part of southern Ethiopia. The occurrence of Pan-African granulites in southern Ethiopia is interpreted as representing the roots of the Pan-African collision zone, which were consequently trusted/ uplifted to a higher level during late-stage tectonism. Although the nature of Pre- Pan-African protoliths in the gneisses is difficult to reconstruct, it is evident that the gneisses have suffered deformation and metamorphic episodes which were not shared by the metavolcano-sedimentary sequences. However, both rock groups seem to have suffered similar deformation sequences during the Pan-African. The high-grade rocks comprise the Awata and Mormora Groups in which Mormora Groups overlays the Awata.

The gneissic layering in the high-grade rocks, which are folded into recumbent folds (or intrafolial folds), form the earliest recognizable structural feature. This deformation event is not well represented in the metavolcano-sedimentary rocks apparently because the deformation and metamorphism in the latter rocks occurred at relatively higher structural level. In southern Ethiopia, the eastern part of the ANS/MB is a moderately west-dipping

thrust that displaced the metavolcano sedimentary as well as the basement rocks to the southeast, contrary to the general West-verging thrusts in western Ethiopia. These thrust zones form part of the complicated thrust system involving basement and cover, representing typical transpressional features on a regional scale that formed during the final cratonization (Kazmin, 1978; Kazmin et al., 1978, Worku, 1996; Solomon, 2009; Tadesse, 2010, Alemu, 2001).

The low-grade metavolcano-sedimentary sequences and associated mafic-ultramafic rocks occupy a 5-16 km wide and about 100 km long distinctive zone confined to the Megado Terrain. The succession consists of metavolcanics and pyroclastics, graphitic schists, graphitic quartzites, metasandstone, metaconglomerate, ultramafic rocks and is intruded by gabbro and tonalite. Excluding the intrusive and ultramafic rocks, this rock association was considered to form the Adola Group. Most of the known metallic mineralizations hosted in these low grade metamorphic rocks are known over a little area in the east exhibiting lead and copper anomalies (Solomon, 2009).

In the Precambrian of Southern Ethiopia distinct lithotectonic terrains, which are mainly represented by Moyale Belt, Adola Belt, and Bul Bul Belt are recognized. The Adola Belt is a late-Precambrian, north-south trending fold and thrust belt of volcanic-sedimentary and ophiolite-like units overlying 'basement rocks' (gneisses and granitic gneisses). Structural analysis reveals that the Adola Belt has undergone three major deformational events (Solomon, 2009). The earliest deformational event produced low-angle thrusts, recumbent folds and associated flat-lying foliation. The second deformational event gave rise to upright folds, north-south trending and generally west dipping regional schistosity and oblique to reverse sense shear zones. The third deformation reactivated the earlier structures and produced sub vertical, discrete strike-slip shear zones along previous discontinuities

The basement in the south of the country where granitic rocks and gneisses predominate has been more strongly metamorphosed.

The Adola Fold belt is comprised of metasedimentary, metavolcanic, mafic and ultramafic rocks metamorphosed to greenschist and amphibolite metamorphic facies. The metasedimentary rocks appear to be predominantly pelitic with some chemical sediment (mainly siliceous) while the metavolcanic rocks are predominantly basic, basalts and Komatiitic basalts. The package of rocks is contained within a higher grade unit of rocks, commonly granite gneiss, which forms a fairly distinct eastern and western boundary to the belt. There are occasional granitic bodies which represent post deformational intrusions

within the belt. Sparse outcrops, thick soil and vegetation cover and a truncated soil profile inhibit area (Canyon, 1997, 1998, 1999).

2.2. Geology of Meleka

A complete and detailed description of the study area, where the research specifically lies is compiled by Negussie Tilahun during Mineral Exploration Training Project ETH/86/034 under GSE in 1990. Based on the result of the project report, the observed and identified geological make up of the area is classified as gneissic rocks and metasedimentary-metavolcanic assemblages.

The metamorphic rocks of Meleka are parts of the MB/ANS and the northern extension of the Adola belt. The rock types and structural trends are very similar to the rocks present in the southern part of the Adola zone. The metavolcanic and metasedimentary rocks are bordered by older gneisses rocks which dip towards each other forming a mega synform. The rocks generally trend north south with minor deviations to NE and NW. The various lithologic units identified are gneisses (biotite - gneiss); schists (Psammo pelitic schist), metavolcanics, amphibolite/amphibole schist, gabbro amphibolites, ultramafics (serpentenite, talc - tremolite schist), meta granodiorite, granite, basalt and various quartz and pegmatite veins. Other than these basaltic flows of Tertiary age and recent lateritic surface covered the area. (Negussie, 1990; Solomon, 2009)

According to the report (Negussie, 1990) the following is a lithologic description base on field observation, thin section analysis and relevant interpretation of the rocks of the area is made (figure 6).

Description of major rock units

Biotite – gneiss (Bg)

A large part of this rock is exposed near the western part of the study area. Except in few places exposed fresh rock is not found in the area. Hence the presence of the rock is deduced from sandy gray soil with abundant floats of quartz vein. The unit dips steeply near the contact with the ultramafics, otherwise dips to the east gently. The rock shows a regular compositional banding. These bands are formed distinctly by feldspar, biotite/ amphibole the rock contains garnet and magnetite as accessory minerals.

Plenty of quartzite and some pegmatite veins are characteristics of this gneiss. Some of the veins are discordant to the general foliation.

Psammo pelitic schist (Ps)

This unit is commonly exposed along sterms cuts as well as on top hills. It also occupies the central portion of the area and also found intercaleted in the amphibole schist. The rock is composed of quartz, magnetite and graphite. The unit shows compositional layering.

Amphibolite / Amphibole schist (A)

This rock crops out along hill tops, hill sides as well as stream cuts. This rock is the one exposed in the area with the wider coverage. Textural variation is one of its peculiar characteristics. Qaurzo-feldspathic gneiss is found in a minor extent. The strike of the rock is north south as usual with its dip direction to the east and to the west.

In most of the places where the rock is exposed sulphide mineralization is observed. Magnetite is also found but not as often as sulphides. From description of different thin section the metamorphic grade of the rock is low to medium.

Metagabbro, Gabbro amphibolite (Ga)

The rock is found randomly in the fine grained amphibolite almost always. It is coarse grained massive and generally composed of amphibole, palgioclase and minor quartz.

Sulphide mineralization is common and relicit igneous textures are clear from hornblend and palgioclase grains.

Metaultramafics (Um)

These rocks copmrise massive serpentenite, talc-chlorite schist, tremolite actinolite schist and talc- tremolite.

Talc Tremolite schist (Tts)

The rock It is exposed in deeply cut valley but the most extensive part of the unit is exposed in the western and eastern parts of the studied area. This schist exposed in the western part is dipping gently to the east and that exposed in the east is dipping to the west.

Characteristically it is being cut by pegmatite veins that cross the foliation.

Zircon has a typical sedimentary shape.mica are anastomising around garnet (which is older thanthe micas). This unit has an intercalated gneissose variety often.

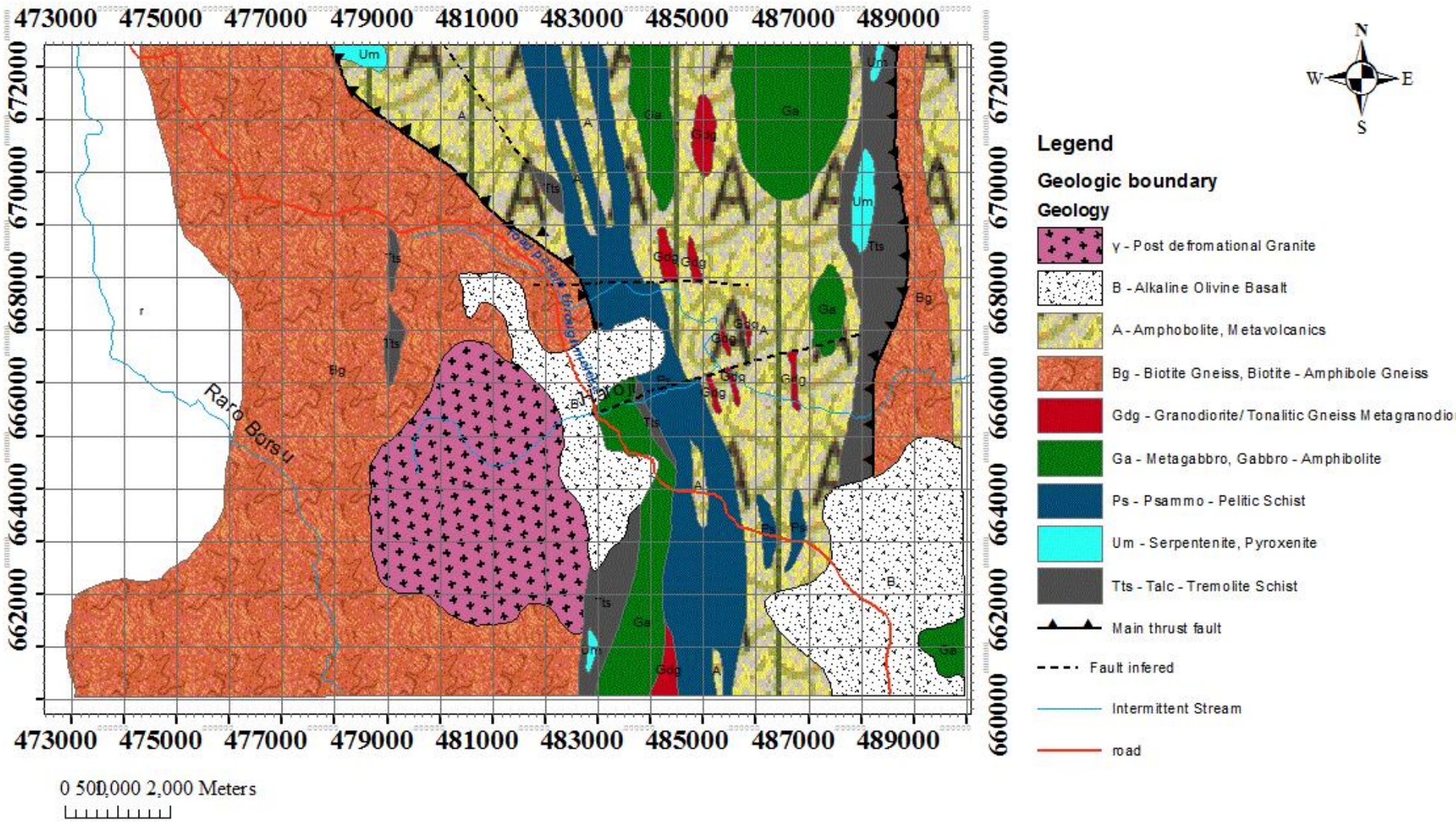

Figure 6. Geological Map of Meleka (modified from Geological Map of Adola Area by GSE and Nigussie)

Granodiorite / Tonalitic gneiss (Gdg)

Exposed in stream cuts and is found in the amphibolite/ amphibole schist in the northern and central portion of the area. Generally the rock contains quartz, feldspar, amphibole, biotite and minor garnet.

The rock is being changing from medium to low grade of metamorphism. This is clear from the reaction between biotite and chlorite. In addition to this biotite and hornblende are both green indicating that the rock is at its medium grade of metamorphism.

Post deformational granite (γ)

This is granite exposed in the central portion of the study area. It is light gray in color and weathers to pinkish. Shows ex-foliation and is coarse grained and massive.characteristically the garnet is jointed. And there are three main directions east-west, north south, north west and south east; these joints are sub – vertical and few of them are horizontal. Quarz veins and veinlets are commonly found in the rock.

Veins and veinlets

Various quartz -and pegmatite veins are observed in all the metamorphic rocks of the area. These vains cut accross and intrude along the foliation of the rocks.

Quartz veins and veinlets

These are generally colorless to whitish in color and sugary to glassy in texture. Most of these veins are fractured and medium to coarser grain sizes. At least three directions of veining are observed. Two of which are crossing general foliation third is parallel to it.

These directions of veining are N-S, E-W and MW-SE. the veins vary in width from a mm to 30 meters (for example near Babicha river). Very thin veinlets are most common than large size veins and are better mineralized than bigger ones. It is noted that the veins which are parallel to the foliation, and are more fractured than the rest.

Basalt (B)

The basalt covers a considerable area at three places (figure 7). It is aphanitic to very fine grained. Pentagonal columnar jointing and an irregular fracturing characterize the unit. The columnar joining dips in a wide range (30^0-90^0). Weathering colours of the basalt are variable. It weathers along the joint planes but spheroidally weathered surfaces are observed.

At places it is vesicular and these vesicles are filled by secondary minerals namely, silica and calcite. This basalt is Porphyritic due to bigger crystals of olivine and plagioclase.

Lateritic surface

It is a recant minor unit exposed usually near swampy areas and grass covered places. Mainly composed of weathered material except some quartz grains and boulders. With some exception the typical ranges from brown to reddish. Not only later silica precipitation is visible but also other big cobbles of quartz and magnetite are sticked to the latereite. These materials look foreign in appearance to

the unit. The lateritic unit develops with many lithologies. It is exposed in moderate to flat topographies and in grass covered areas, it has a light tone aerial photographs characteristic. Although not always, clayey horizon underlies this surface.

2. 3 Metamorphism

The area mapped is underlain by different litho1ogic units which are subjected to metamorphism of different pressure- temperature conditions. So, different grades of metamorphism have been recognized on the basis of both field observation (megascopic analysis of minerals in the rock and different penetrative structures) and thin section (microscopic) analysis.

Generally the area comprises the volcano sedimentary rocks which form a low /very low grade linear belt with some variation in grades of metamorphism and it is bounded by the older, medium grade schists and gneiss.

Therefore the metamorphism of the area ranges from low to medium grade.

Very low and low grade (Greenschist faces)

The ultra mafic rocks of the area are found to be very low grades of metamorphism. Serpentenite, for instance can result from very low grade metamorphism of ultramafic rocks i.e simple addition of excess H_2O and CO_2 or SiO_2 to ultramafic rocks (olivine and orthopyroxenes). Also the mineral assemblage of the rock, as can be seen in the thin section, (serpentenite+talc+magnetite+/-Mg-chlorite +/- magnetite) is typical of very low grade metamorphism. In addition the mineral assemblage of the talc-tremolite schist (tremolite + talk+ Mg-chlorite + opaque) indicates a rock which belongs to very low grade of metamorphism (Miyashiro, 1979).

The strong association in occurrence of this rock with serpentenite suggests that they belongs to low grade of metamorphism too.

The other rock unit which belongs to the green schist facies (low grade) is the metavolcanic rock having a mineral assemblage of the following type: actinolite+ tremolite + plagioclase (albite) + quartz + epidote +/- zoisite =/- opaque

Upper low grade to medium grade (epidote -amphibolite to amphibolite facies)

The rock units included in this range of metamorphism are the amphibole schist and the gabbro amphibolite. Their mineral assemblages which are (actinolitic hornblend + albite – oligoclase + quartz +/= zoisite +/- sphene +/- limonite) for gabbro amphibolite confirm that they belong to a metamorphism ranging from upper green schist faces to the lower (threshold of) amphibolite faces (Myashiro, 1979).

Figure 7 Columnar basalt cross cut at Meleka kebele by the road

.

Medium grade (Amphibolite facies)

The rest of rock units including the various schist and gneisses are subjected to medium grade of metamorphism. This is evidenced in various ways among which are

1. Staurolite, kyanite and garnet have been identified within the various schsits and gneisses
2. Panning of heavy concentrate sample collected from streams draining these rocks indicated that the rocks contain staurolite and garnet.
3. The mineral assemblages of the rocks, as can be deduced from thin section analysis, are typical of the amphibolite facies. Moreover the occurrence of hornblend e the gabbro amphibolite indicates the same facies.

2.4 Structural Setting of the Study Area

The region consists of linear zone bounded by older schists and gneisses, separated by the big tectonic contact. From the nature of the rocks it is clear that there was earlier basin for the deposition of graphitic quartzite and associated basic volcanics that form the linear low grade belt.

These volcanic and sedimentary rocks are folded and metamorphosed with later deformational episodes together with the older schist and gneisses. In association with later tectonic events of the area, post tectonic granitic bodies and basaltic flow affected the region.Different microscopic, mesoscopic and megascopic structures are observed and described. Most of the structures are found on the bounding schists and gneisses rather than in the lower grade linear metavolcano-metasedimentary belt. These structures are: foliations (schistosity or granitic layering), minor and major folds, large scale faults, joints or mesoscopic faults, shear zones, boundungs and lineations.

Lineation

Linear structures include mineral lineations, crenulations or intersection lineation and striations. As described in thin sections of oriented samples, some minerals show two preferred alignment directions. But most of the minerals (amphibole) are aligned with their plane perpendicular to the foliation. As the foliation is sub vertical, the lineations are sub horizontal. The dominant direction is parallel to the major faults on which the courses of the big rivers of the area are controlled.

Mesoscopic folds

F1- folds:- these are recumbent to gently plunging and are exposed locally in the quartz- micas schist at Dalore. The foliation S1- surface which is developed parallel to the axial surface of F1-folss dips $50^0/240^0$. Clear mica rich and quartz rich layers are observed which could be original sedimentary layers (S_0) . Most of these minor folds are observed on veins of secondary minerals of igneous intrusions that have been plastically deformed withor around the foliation. In thinsection, from oriented sample the tremolites are seen to form microscopic folds as in kink band formation.

F2-folds:- These minor folds are more abundant than the F1-folds, although both are found in the same unit. The axial trace of F1- folds is usually parallel to the dominant foliation.

F2 folds are close folds with the interlimb angle of 40^0 - 46^0 as measured in reference plane that srtikes N94W ^{0} – and dips 85^0. Its trend and plunge being $180^0 / 45^0$.

F3- folds:- these are megascopic folds which are interpreted from the map pattern of the lithologic units. This is the result of the third phase of deformation that affected the existing regional foliation but so slight that it haven't produce its own foliation. The trace of axial surfaces of these folds are nearly east – west and they are open folds. This third phase of deformation is the cause of bulges of the lithologic units and the formation of the youngest folds of the area.

Shear Zones

Brittle and ductile minor shear zones are observed. In the serpentenite a brittle shear zone is observed in a highly deformed ultramafic rock unlike its massive character. Many quartz veins are fractured with variable joint spacing i.e other than these minor shear zones. The quartz mica schist seems

to be sheared near the contact with the ultramafics defining a major shear zone that must be related to the strike slip movement of D_2.

A minor brittle ductile type of shear zone is noted within the biotite gneiss cropping out at Dalore area. In this outcrops a vein cuts across the foliation obliquely. The foliation is dragged, where it is cut by the vein. From the displacement a dextral sense of movement is deduced. Both the foliation and veinlets are used as indicators of the displacement

The Lega Dembi – Aflata shear zone identified by Hailu Worku continues further north and is conspicuous in this region along the contact of the quartz mica schist and the ultramafic rock units. This mega shear zone is expected to extend even further north.

Foliation

These are the most prominent tectonic structures that are developed as compositioinal layering , schistosity and gneissic layering . These planar structures are defined by preffered orientation of platy and acicular minerals like mica(biotite and moscovite), amplhiboles(hornblend, actinolite, tremolite) and talc. These tectonically formed fabrics in the present erosional level dip steeply in the linear metavolcanic and metasedimentary belt and gently to steeply dipping in the bounding higher grade schists and gneisses.

Two of foliation planes (S1and S2) are recognized in the study area. These planes are preserved in folds (f1) , but are now become to be parallel and form the dominant foliation that srtikes meridionally with some 20^0 variation to the west or east.

In the western part of the area, where the feldspare, quartz biotite gneiss and the quartz mica schist crop out, the foliation generally dips to the west. In the central part however dips to either directions have been measured .

Faults

As the result of the last tectonic activity (brittle deformation) in the low grade belt, medium grade schists and gneisses several faults have been formed showing E-W, N-S and NW-SE trends. Among these three sets the N-S trending ones are dominant. But if the length is taken in to consideration the NW-SE ones could be dominant. All units except the basalt are affected, but clear lithologic displacements are not commonly seen the field. However, the Psammo pelitic schist and the minor units granodiorite which is hosted in the amphibolite are examples of displaced units showing dextral sense of movement.

Joint

Joints affected all rocks of the study area. Although all rocks are affected by joints, the most prominent joints are the post deformational granite.

Detail investigation of joints on granite has shown that there is one major dominant striking direction which is established i.e. $290^0 – 310^0$.

Micro scale faults that displace quartz veins in sinistral sense with little variation in degree from the regional jointing direction are observed in the gneiss.

2.5 Mineralization

The occurrence of mineralization is observed in some lithologic units and pegmatites /quartz veins of the area. These are

Sulphides (chalcopyrite, pyrite and pyrrhotite)

The sulphide minerals occur as disseminated and layered. They are usually associated with gabbro amphibolite and less commonly found in the amphibole schist. Sugary and fractured which intrudes the amphibole schist near Babicho River contains pyrite and chalcopyrite.

Oxides

Magnetite is the common oxide mineral which occurs in ultramafic rocks, graphitic quartzite, gabbro amphibolite and in quartz mica schist. Magnetite is found in Psammo pelitic schist as thin layered and disseminated forms. Lateritic surface developed on the ultramafic rocks contains blocks of magnetite ranging in diameter from 10-12 cm. Disseminated and finely layered forms of magnetite are also very common in the ultramafic unit. Magnetite appears to have well developed crystals in the gabbro amphibolite. In addition chromite grains are observed in the ultramafic unit. Columbo – Tantalite grains are also found in the region.

Kaolin

This mineral is developed from weatherd biotite gneiss. Kaolin occurs in the northern part of the study area. The exact location of the mineralization is 6^0 1’ N - 6^0 5’ N and 38^0 47’ N -38^0 50’ (North West of Meleka)

Gold Occurrences in the region

The rocks of the Adola gold belt commonly host gold occurrences. The Lega Dembi mine contains gold associated with a series of en echelon, northerly plunging, quartz veins within a shear zone sandwiched between the eastern granite gneiss and a meta gabbro body to the west and is apparently controlled by a very dominant flexure in the eastern bounding shear zone around the meta gabbro body. Quartz veins containing gold has been found in nearly all stratigraphic horizons of the Megado belt. Placer gold has been mined by a state enterprise throughout the region since the mid 1930's and artisanal

mining has become common in the past five years with the essential elimination of the enforcement of restrictions on artisanal mining.

There are a number of primary gold occurrences, most discovered during the Soviet supported Adola Gold Project of the 1970'sand 80's. These occurrences have been studied over the past several years by the state mining corporation and the EIGS. Two of the surface primary gold occurrences, Lega Dembi and Sakaro, discovered by the Adola Gold Project have become deposits which have been mined. Of particular interest is the fact that it appears that the litho-structural units which contain both the Lega Dembi and Sakaro deposits trend into Meleka (Canyon, 1993).

Occurrence of placer gold is indicated by panning of heavy mineral concentrate samples collected from various localites in the area. Samples taken from one of the eastern tributaries if Borsu river, for example contains two flaky gold grains. In the south, local people are panning for gold in the Awata river and in its tributary Teda stream. The tributaries of Babicha and Borsu river are also places of panning (by local people) for gold in the area (Tilahun, 1990). During the field survey, we saw many artisanal miners panning for gold following the rivers Babicho, Biloya, Busa Hariji and at the northern end Hobone (figure 8).

Figure 8 Artisanal miners digging a pit in search for quartz following the river Babicho

CHAPTER THREE

Aeromagnetic and Gamma ray Spectrometric methods of investigation

Airborne geophysical surveying is a process of measuring the variation of physical or geochemical parameters of the Earth. The parameters to be measured include the magnetic susceptibility, conductivity, density, and radioactive element concentration. Any variation on the Earth's surface that could cause a measurable change in these parameters is a potential application for airborne geophysics.

There are variety of method to use in the survey such as Airborne magnetic surveys, Gamma-ray spectrometric surveys, Electromagnetic surveys and Airborne gravity surveys to map the variation of the magnetic susceptibility due to changes in the magnetite content of the rock, to measure the radiation of one or more of the natural radio elements (potassium, uranium, or thorium, or a specific man-made radioelement), to map the three-dimensional variation in conductivity caused by changes in mineralogy, intensity of alteration, water content or salinity, and to map density variations within the Earth respectively. Here, the study focuses on aeromagnetic and gamma-ray spectrometric survey methods to map the geological boundaries and identify anomalous zones of mineralization.

3.1 Magnetic method

Magnetic prospective is the oldest and the cheapest of the geophysical method used to explore both oil and mineral (Parasnis, 1975). The measurements for exploration are acquired from the ground, in the air, on the ocean, in space, and down boreholes, covering a large range of scales and for a wide variety of purposes (Nabighian et.al, 2005). It is now possible to map the entire crustal section at a variety of scales, from strongly magnetic basement at regional scale to weakly magnetic sedimentary contacts at local scale.

Fundamental Principle of Magnetic Method
Magnetic Force

An expression for the magnetic force, F, between two magnetic poles of strength m_1 and m_2 separated by a distance r is given by

$$F = \frac{m_1 m_2}{\mu r^2} \qquad (1)$$

Where the constant μ known as the magnetic permeability, is a property of the material in which the two monopoles, m_1 and m_2 are located. If they are in a vacuum, μ is called the magnetic permeability of free space. It depends up on the magnetic properties of the medium in which the poles are situated.

Magnetic field

A magnetic field is the space in which a magnetic pole experiences a force or it is the space around a magnet in which the influence of the magnet is felt. The magnetic field strength vector B (magnetic induction), is defined as the magnetic force experienced by a unit pole placed at that point (Telford et al., 1990). If a magnetic pole of strength m placed at a point in a magnetic field experiences a force F, the magnetic induction at that point is:

$$B=\frac{F}{m} \qquad (2)$$

Where, m is unit pole

Magnetic properties of materials

Magnetizing field

The magnetic field used to magnetise a material is called the magnetising field. It is denoted by H.

Magnetic permeability (u)

Magnetic permeability is the ability of the material to allow the passage of magnetic lines of force through it. Magnetic permeability u of a medium is also defined as the ratio of magnetic induction B inside the medium to the magnetising field H inside the same medium.

$$u = \frac{B}{H} \qquad (3)$$

Induced and remanent magnetism

Magnetic anomalies in the Earth's magnetic field are caused by two types of magnetism: induced and remanent magnetism. The induced magnetism of the body is in the same direction as the Earth field whereas the remanent magnetism need not be in the same direction and could even oppose the earth's field. If the Earth's field could be removed the induced magnetism would disappear but remanent magnetism would remain.

Induced magnetism (J_i)

When a magnetisable material is placed in a magnetic field it will become magnetised in the direction of the applied field. This phenomenon is called induced magnetisation. The intensity of the induced magnetisation of a magnetic material is defined as the magnetic moment per unit volume of the

material, i.e.,

$$J_i = \frac{M}{V} \quad (4)$$

The magnetic moment of a magnet (M) is defined as the product of the pole strength and the distance between the two poles.

The intensity of the induced magnetisation, J_i, is proportional to the strength of the magnetic field (and is in the direction of the field) and to the ability of the material to enhance the local field, a property called magnetic susceptibility.

$$J_i = kH \quad (5)$$

Where,

J_i = Intensity of Magnetisation

k = magnetic susceptibility (unit less) H = Field intensity in Tesla (T)

If J_i is constant and is in the same direction throughout the body, the body is said to be uniformly magnetised by induction. For most rock materials k is much less than 1 and usually of the order of 10^{-3} in SI units.

Remanent magnetism (J_r)

This is due to the previous history of the rock. Remanent magnetisation is the permanent magnetisation of a material in the absence of an external magnetic field, and thus occurs only in the materials which exhibit hysteresis, i.e. irreversibility of magnetic behaviour with applied field (Hunt et al., 1994). The direction of this magnetisation, J_r, may not necessarily be in the direction of the inducing vector (Earth's magnetic field) and could even oppose the field.

The ratio between J_r and J_i is called the Konigsberg ratio, Q. Konigsberg ratios confirms the comparative importance of remanent and induced magnetisation, with remanence dominant for Q>1 and induced for Q<1 (Mahanyele, 2010).

The direction and strength of the present Earth's field is known. However, we may know nothing about the remnant magnetisation of a rock. For this reason, and because in strongly magnetised rocks the induced field dominates, it is often assumed that all the magnetisation is induced. The true magnetisation is the vector sum of the induced and remnant components, i.e.:

$$J = J_i + J_r \quad (6)$$

Magnetic susceptibility (k)

Magnetic susceptibility is a property which determines how easily and how strongly a material

can be magnetised. Susceptibility of a magnetic material is defined as the ratio of intensity of magnetisation J_i induced in the material to the magnetising field H in which the material is placed (or the amount of magnetic minerals, mainly magnetite and pyrrhotite, contained within a rock). Rock forming minerals (quartz, feldspar, etc) are virtually non-magnetic so the magnetic susceptibility is related to the amount of minor accessory minerals in a rock which contains iron such as magnetite and pyrrhotite.

From equation 6, magnetic susceptibility k becomes:

$$K = \frac{J_i}{H} \qquad (7)$$

Elements of the Earth's magnetic field

The magnetic field at any point on the Earth's surface is a vector field and can be described by the following 5 components of Earth's magnetic field.

In the southern hemisphere the Total field vector, T, is directed upwards and away from the south magnetic pole. It makes an angle Iº (the inclination) to the horizontal component H and is negative. The horizontal component H has an angle Dº (declination) from the geographic north. At the magnetic equator the magnetic field is horizontal (I = 0) and at the magnetic poles the field is vertical (I = 90)

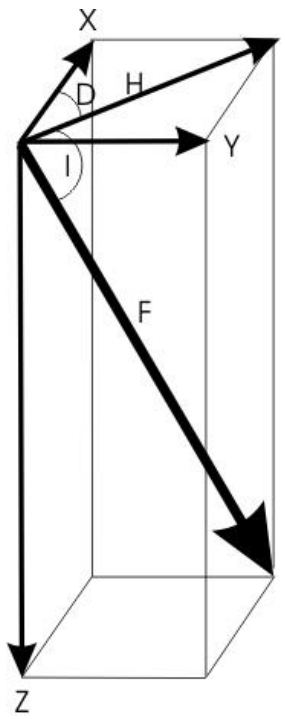

Figure 9.Components of the Earth's magnetic field.

$$
\left.
\begin{aligned}
H &= F \cos(I) \\
Z &= F \sin(I) = H \tan(I) \\
X &= H \cos(D) \\
Y &= H \sin(D) \\
X^2 + Y^2 &= H^2 \\
X^2 + Y^2 + Z^2 &= F^2 = H^2 + Z^2
\end{aligned}
\right\} \qquad (8)
$$

where H- Horizontal field, Z - Vertical field, F - Total field, D - Declination, I - Inclination

Aeromagnetic surveying is the most common airborne survey type conducted for both mineral exploration and hydrocarbon exploration. The survey can be regional or detail depending on the objective. For regional surveys (geological mapping, mapping basement lithology and structure, and depth to basement mapping for petroleum, coal and other non metallic exploration) traverse line spacing is more than 500m and cover a minimum of 5,000 km^2. The detail survey line spacing is less than 500 meters and made for prospecting magnetic ores like iron ores, chrome, asbestos-bearing ultra mafic rocks, or kimberlites and also for mapping weak magnetic lineation related to faulting within the sedimentary section.

The three most commonly used magnetometers in the airborne survey are the Fluxgate, Proton Precession and Optically Pumped (Alkali or He vapour) magnetometer, which are used to collect various data by mounting on the chosen aircraft system. The flight height, traverse line separation and traverse line orientation should be considered as important factors in the survey (e.g. Reeves, 2005; Nabighian et.al, 2005). For example, a magnetic surveys with 30m line spacing and 20m altitude is more detail and give much information than a survey with a parametre of 200m line spacing and 80m altitude. But it is more expensive and the flying is less safe (Jessel, 2002).

Changes in magnetic susceptibility often allow rock units to be differentiated based on the total field magnetic response. Geophysical classifications may differ from geological classifications if various magnetite levels exist within one general geological classification. Geometric considerations of the source such as shape, dip and depth, inclination of the earth's field and remanent magnetization will complicate such an analysis.

In general, mafic lithologies contain more magnetite and are therefore more magnetic than many sediments which tend to be weakly magnetic. Metamorphism and alteration can also increase or decrease the magnetization of a rock unit. Hydrothermal alteration may destroy magnetite, producing a broad, smooth magnetic low (Ford, et.al, 2007)

Textural differences on a total field magnetic contour colour or shadow map due to the frequency of activity of the magnetic parameter resulting from in homogeneities in the distribution of magnetite within the rock, may define certain lithologies. For example, near surface volcanics may display highly complex contour patterns with little line-to-line correlation.

Rock units may be differentiated based on the plan shapes of their total field magnetic responses. Mafic intrusive plugs can appear as isolated "bulls-eye" anomalies. Granitic intrusive appear as sub-circular zones, and may have contrasting rings due to contact metamorphism. Generally, granitic terrain will lack a pronounced strike direction, although granite gneiss may display strike.

Linear north-south units are theoretically not well-defined on total field magnetic maps in equatorial region due to the low inclination of the earth's magnetic field. However, most stratigraphic units will have variations in composition along strike that will cause the units to appear as a series of alternating magnetic highs and lows.

Faults and shear zones may be characterized by alteration that causes destruction of magnetite (e.g., weathering) that produces a contrast with surrounding rock. Structural breaks may be filled by magnetite-rich, fracture filling material as is the case with diabase dikes, or by non-magnetic felsic material.

Faulting can also be identified by patterns in the magnetic total field contours or colours. Faults and dikes tend to appear as lineaments and often have strike lengths of several kilometres. Offsets in narrow, magnetic, stratigraphic trends also delineate structure. Sharp contrasts in magnetic lithologies may arise due to large displacements along strike-slip or dipslip faults (Bruce. et al., 2007).

3.2 Radiometric method

Radiometric surveys detect and map spontaneous gamma ray radiation, on account of the element’s interaction with other substances, from rocks and soils. The basic purpose of radiometric surveys is to determine either the absolute or relative amounts of U, Th., and K in the surface rocks and soils and their by to map lithological units.

No other geophysical method, and probably no other remote sensing method, requires us to consider so many variables in order to reduce the observational data to a form that is useful for geological interpretation. Meteorological conditions, the topography of the survey area, the influence of the planets cosmic environment, the speed of the aircraft and the height of the sensor above ground are just a few of the variables which affect radiometric measurements, and which can bias our analysis unless we deal with them very thoroughly. For example, gamma-ray flux decreases exponentially with distance from the source (e.g. Urquhart, 2013).

A single AGRS measurement provides an average surface concentration over a wide area, composed of variable proportions of bedrock, overburden, soil moisture, water and vegetation. So usefulness of AGRS to geological mapping and mineral exploration depends on two factors. The first is the extent to which radioelement distribution relates to bedrock differences and the extent to which these are recognizably modified by mineralizing processes. The other factor is extent to which bedrock radioelement content is reflected in surficial materials that can be spatially related to bedrock sources (e.g. Jessel, 2002)

In Gamma Ray Spectrometry Surveys different corrections and calibration applied on the observed counting rates that are measured in the three spectral windows. Since the count rate is related to the sensitivity of instrument; controlling the temperature of the crystal, photomultiplier tubes and the detector and a daily calibration checks should be the first step during operation.

Then correcting measurements for cosmic ray background effect, atmospheric noise, and Compton scattering should be done.

Dead time correction considers the missing counts during the time that it takes the instrument to measure and analyze the scintillation from a single gamma photon. Since the instrument is “dead” during this period which last for only a few microseconds. In most cases the dead time correction is insignificant for airborne survey data, but can be important for data collected during borehole logging.

The background correction refers to the general background count rate that prevails in each channel, or spectral window, that is due to non-geologic sources, primarily atmospheric radon and cosmic rays.

In order to increase the accuracy of airborne radiometric data sometimes additional processing such as smoothening, micro-levelling and calculation of ratio is done. Airborne radiometric surveys can be applied to geological/geochemical mapping, exploration for uranium deposits, porphyry copper deposits and radioactive haloes, and exploration for gold. Unlike the other airborne geophysical methods, there are no mathematical models that will allow us to calculate the theoretical radiometric response of a specific source. Interpretation of radiometric data is, therefore, more similar to interpreting the results of a conventional geological survey (e.g. Urquhart, 2013; Kearey,2002).

CHAPTER FOUR

Data acquisition and processes

The following is a summarized technical specification of the helicopter borne geophysical survey of Adola;

The flying was carried out during February - July 1993 and January – March by a high performance Aerospatiale SA315B Lama with high lift and good altitude characteristics, capable of carrying a simultaneous package of frequency-domain electromagnetics, multi-channel spectrometry and magnetometer, and also of maintaining tightly-specified flight path and terrain clearance

The survey cover a total of 3000 km^2 area corresponding to 16,412 km line (including tie lines) in 1993 and 1994. Figure 4 above shows the area covered which represents the zones considered to be of prime importance for gold and rare metals exploration in the Adola area..

The traverse line interval was 200 m. The direction of the traverse lines was E-W (090/270) in all areas except Block B, where it was 135/315.

The nominal control line interval was 5 km or 25 times the line spacing, not to exceed 7.5 km at any point. The direction of the control lines was perpendicular to the traverse lines in all areas.

The nominal survey height was 60 m above the terrain for the helicopter (and the spectrometer), corresponding to 30 m above the ground for the EM sensor and 40 m above the ground for the magnetic sensor. The tolerance on the flying height was ±5 m subject to safety considerations. The speed of the aircraft was not to exceed 100 km/hr.

Navigation and flight path recovery employed the NAVSTAR Global Positioning System (GPS). Real-time differential (RTD) GPS navigation and positioning, using a base station with a repeater station, was employed.

4.1 Aeromagnetic Survey

A Scintrex CS2 cesium vapour split beam magnetometer was used, together with several similar base stations at various times, subsequent diurnal corrections. The magnetic field was sampled by airborne and ground magnetometers at 0.1 second intervals, with a sensitivity of 0.01 nT

The magnetic data were: (i) corrected for diurnal variations by subtraction of the digitally recorded base station magnetic data and (ii) interpolated onto a regular 25 m grid using a modified akima (1970) technique. Final image quality grids were verified using the VISION imaging system. Regional variation (IGRF) for the epoch of the survey was removed from the levelled magnetic data using the IGRF model year 1990. The residual data were adjusted back to the nominal total magnetic field at Shakiso (Last, 1994).

The final products of an aeromagnetic survey is one or more maps such as the contoured total magnetic field, coloured and/or shaded maps of the total field or a parameter derived from the total field, and a digital data file recorded on a convenient medium that contains the time, location and value of each measurement and any other information relevant to that measurement. Because we actually measure the field only at discrete points in time and along flight lines, all maps, other than profile maps, are an interpolation of the measured data. The selection of survey parameters by the exploration manager, such as line spacing, altitude, and the orientation of the traverse lines as well as compilation and presentation procedures and an evaluation of the anticipated noise - both temporal and geological - should all be made with the desired accuracy of the final products as guide (Urquhart; Reeves, 2005).

Additional processing such as reducing the data to the magnetic north pole/Equator is done. This reduction to the pole (RTP) shifts magnetic highs directly over the causative body instead of being located slightly to the south (e.g. Reeves, 2005). The RTP magnetic data processing could be done using appropriate software like oasis Montaj (Oasis Montaj). Other than this RTP aeromagnetic data run through a series of filter to highlight deep and shallow magnetic features. These include Tilt derivative, analytic signal, first vertical derivative, directional cosine filtering, and upward/downward continuation (e.g. Nabighian, 1972). Interpretation of all the processed geophysical data can be carried out by integration of aeromagnetic data with, radiometric data, remote sensing and GIS geological information.

4.2 Gamma Ray Spectrometry Surveys

A state-of-the-art Exploranium GR-820 256-channel spectrometer was used. This spectrometer employs automatic gain stabilization using a selectable radioelement peak. This may be an artificial source, e.g. ^{137}Cs, or a commonly occurring radioisotope from the ground, e.g. ^{4o}K or ^{208}Tl (from the decay series of ^{232}Th). In this case the potassium peak was used in the 1994 flying season.

The spectrometer was used in conjunction with a detector package consisting of 16.8 1 of downward-looking crystals (1024 cubic inches or 4 crystals) and 4.2 1 of upward-looking crystal (256 cubic inches or 1 crystal). The detector package was installed in the Lama basket, to the side and below the fuel tank.

The sampling interval for the radiometric data was 1 second. Test line data were used for calibration of the upward detector. Spectrometer data processing consisted of: Live time correction, Aircraft and cosmic background corrections, Radon background removal, Compton stripping, Height attenuation corrections, Conversion of corrected count rates to apparent radioelement concentrations.

In addition to recording 256 channels for both the downward- and upward looking detectors, the following IAEA-recommended windows (IAEA 1991) were recorded (table 3):

Table 3 IAEA-recommended windows (IAEA 1991)

Window	Energy range (KeV)
Total Count:	410 - 2810
Potassium	1370 – 1570
Uranium (up and down):	1660 – 1860
Thorium:	2410 - 2810
Cosmic:	3000 – infinity

4.3 Ground Surveys

A fieldwork for ground investigation was carried out from April 24th to 6th May, 2015. During the fieldwork, ground magnetic and radiometric data were collected. Magnetic data were collected along three profiles while the radiometric data were collected on only one line.

4.3.1 The Magnetic Survey

Instrumentation

ENVI PRO is used for magnetic survey (figure 10). It is portable, proton-precession magnetometers which measure the scalar amplitude of the total magnetic field vector.

It has Interactive menus for easy operator use with selectable sampling rates as fast as 2 times per second. It has WALKMAG mode for rapid data acquisition and single-frequency GPS antenna allowing the user to acquire non-differential positional data along with the magnetometer data. Large internal memory, expandable to 188,000 readings, easy to read and large LCD screen that display data both graphically and numerically (Breiner, 1999).

The complete ENVI PRO consists of several basic modules

- Lightweight console with a large screen alphanumeric display and high capacity memory
- GPS receiver antenna
- Staff or back-pack mounted sensor and sensor cable
- Rechargeable lead-acid battery and battery charger
- RS-232 cable for downloading data

Data Acquisition

The magnetic data were collected perpendicular to the strike along two selected lines oriented East- West, one line approximately along NW-SE direction following the direction of the road passing through the study area and one line along NE-SW direction at the north western end. The two East – West profiles at 665800N and 670000N covered a lateral distance of 4.5km and 4.48km respectively, the NW-SE directed profile covered a total of 8.58km and NE-SW profile covers only 2.12km. Each of the

profiles sampled at a station interval of 20 m orienting the sensor coils aligned perpendicular with the Earth's magnetic field (the N mark points to the north).

Figure 10 Data acquisition using ENVI PRO portable, proton-precession magnetometer in Biloya kebele where artisanal miners work following the river Biloya

A fixed base station for all profiles was established at the point (478113 E, 669064 N) before any measurement taken. In the survey only one magnetometer was used for both the field and for base station reading. This technique the most cost-effective as it only requires one magnetometer but is not accurate as using two magnetometers. The reading was taken on foot and reoccupied for the purpose of diurnal correction. If the field is not changing rapidly, it is quite adequate to locate an anomaly. Totally nine hundred seventy five (975) data were collected from the five lines.

The positions of the magnetic data points were determined using the hand-held GPS. The GPS used was Garmin e Trex Legend. It can locate the coordinate of the area with an accuracy of less than 2m of accuracy.

Data Reduction and Processing

The raw data collected on the field sheet were transferred on the excel sheet for diurnal and IGRF corrections. The corrected data prepared to be suitable to the software and processed for effective interpretation of the subsurface mineralized zones (faults and fractures) geometry.

Diurnal Variation Correction

After the data collection, the diurnal effect was calculated from a fixed base station and the magnetic data were filtered in order to correct for drift or diurnal effect in the magnetic readings. Noise due to secular change or epoch was considered negligible since the measurements taken at the base station were consistent. The correction to the readings taken at each station was made using the diurnal correction formula:

$$\gamma (ci) = \gamma_i \pm (\Delta\gamma/\Delta T) (\Delta Ti) \quad (9)$$

where, $\gamma_{(ci)}$ = diurnally corrected data measured at time t_i.

γ_i = Magnetic field measured at time t_i

γ_1 = Base station magnetic reading at the beginning of the survey.

γ_2 = Base station magnetic reading at the end of the survey.

T_1 = Base station time reading at the beginning of the survey

T_2 = Base station time reading at the end of the survey

$\Delta\gamma = \gamma_2 - \gamma_1$, $\Delta T = T_2 - T_1$, $\Delta Ti = t_i - T_1$

The unit of measurement of the magnetic field is nano-Tesla (nT)

Calculation and Removal of the Geomagnetic Field

After correcting the observed total field magnetic data for the diurnal effect, the theoretical geomagnetic field (IGRF), for that specific location was determined from the Geosoft eXecutable (GX) program attached to the main menus in the system. It can give inclination, declination and geomagnetic field based on the dates, elevation and geographical locations (latitude and longitude) corresponding to each point. The average geomagnetic field of 34970 nT, inclination of -5.25 and declination of 1.60 is found in the study area. The IGRF was then subtracted from the observed magnetic values for each station to determine the residual magnetic field due to anomalous contribution from local magnetic sources in the area. This residual magnetic field is adjusted back to the nominal total magnetic field at Meleka by adding the average value 34970 nT to compare with the aeromagnetic data.

Magnetic Data Presentation

After the correction is made the corrected data were processed and plotted on Oasis Montaj mapping and processing software. The results are presented in a profile forms for visualization and further enhancements. The data is up ward continued to 40m using one dimensional Fast Fourier Transform (1DFFT) to compare with the aeromagnetic data on the selected profile (Oasis Montaj).

4.3.2 Radiometric survey

A battery-operated Scintrex GAD-6 4-channel spectrometer (fig. 11) measuring total count (TC), potassium (K), uranium (U) and thorium (Th) was used in conjunction with a GSP-4 stabilized sensor.

Readings were taken at 20m intervals. The instrument was held at knee-height to smooth out purely local effects. No further corrections were made to the data,

GAD-6 K, U and Th data were converted to equivalent potassium eK (%), thorium eTH (ppm) and uranium eU (ppm) radioelement concentrations, using as an approximation the GSP-4 sensitivities for semi-infinite 2pi geometry and GAD-6 windows as follows:

K: 3.4 cps/% for 1.38- 1.56 MeV window

U: 0.36 cps/ppm for 1.66-1.90MeVwindow

Th: 0.13 cps/ppm for 2.44-2.77MeV window

The most common use of GSP-4 is in making radiometric anomalies of rock out crops to determine their K, U or Th content (Scintrex).

Energy calibration was the first step made before the survey began to ensure that the GAD -6 accurately records the gamma radiation energies detected by the sensor. This was achieved by using a disc-shaped thorium calibration sample following the steps given on the GAD-6 manual (Scintrex, 1979).

Before starting measurement each morning, a daily energy calibration cheek is made to ensure the validity of data.

GAD-6 operate properly anywhere between -20^0c and 55^0c. But, serviceability of the battery will greatly decrease at lower temperatures.

Th radiometric data is collected along one E-W profile line at 665800N line only, due to the failure of our GSP-4 sensor. 4.221 km line is collected with a station interval of 20m. Totally 209 reading was taken for each of TC, K, U and TH.

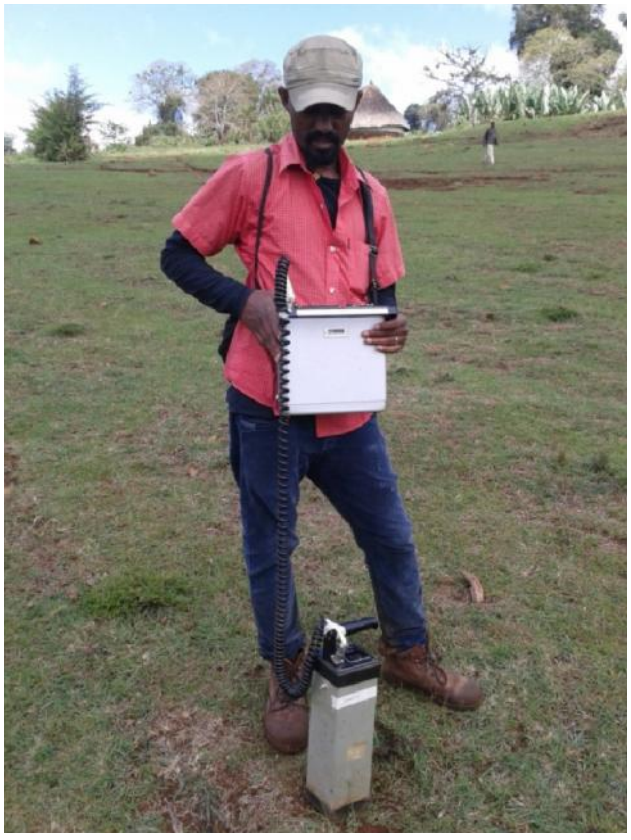

Figure 11 Data acquisition by the researcher using GAD-6 Four-channel spectrometer together with GSP-4 stabilized sensor in Meleka

CHAPTER FIVE

Geophysical data Enhancement, Analysis and Interpretations of results

5.1 Geophysical data Enhancement

The Main task involved in this study is image enhancement of existing aeromagnetic and gamma ray spectrometric data sets acquired by Dighem, for the Geological Survey of Ethiopia in 1994.

Both the gamma ray spectrometric and aeromagnetic data were given on a grid format. The first step is to build the data base for the TMI, U, TH, K and TC using the Geosoft, oasis Montaj. Additionally, ground magnetic and radiometric data is used together with the existing aeromagnetic and gamma ray spectrometric data.

Image enhancement deals with the procedure of making a raw image better interpretable for a particular application using various enhancement techniques to improve the visual impact of the original data for the human eye.

MAGMAP applies filters in the wave number or Fourier domain. To do this requires a number of steps in the MAGMAP system. Pre-processing steps involve the preparation of the original space domain grid for filtering, after which filters are applied. Post-processing involves returning the filtered data to the same size and shape as the original grid and replacement of a regional trend (Oasis Montaj)

The Fourier transformation was done using MAGMAP 2D FFT system exists in Geosoft, eXcutable. Mathematically, the Fourier transformation of a space domain function F(x, y) is defined to be:

$$\bar{f}(\mu,\nu) = \int_{-\infty}^{\infty}\int_{-\infty}^{\infty} f(x,y)e^{-i(\mu x+\nu y)}dxdy \qquad (10)$$

The reciprocal relation is

$$F(x,y) = \int_{-\infty}^{\infty}\int_{-\infty}^{\infty} \bar{f}(\mu,\nu)e^{-i(\mu x+\nu y)}d\mu d\nu \qquad (11)$$

Where μ and n are wave numbers in the x and y directions respectively, measured in radians per meter if x and y are in units of meters. These are related to spatial frequencies f_x and f_y in cycles per meter (Oasis Montaj).

MAGMAP is commonly used to enhance information of interest in a given 2D data set, either by removing features considered as “noise”, or by enhancing the features of interest. Some of the enhancement filters used are;

5.1.1 Upward continuation

Upward continuation is a mathematical technique that project data taken at some plane of observation to a higher elevation. This is considered a clean filter because it produces almost no side effects that may require the application of other filters or processes to correct. Because of this, it is often used to remove or minimize the effects of shallow sources and noise in grids, the opposite is true for downward continuation where special techniques, including filter response tapering and regularization, have to be applied in order to control noise (Nabighian, et al., 2005; Oasis Montaj).

The effect of upward continuation is that short wavelength features are smoothed out because one is moving away from the anomaly. It is a way of enhancing large scale (usually deep) features in the survey area. It attenuates anomalies with respect to wavelength; the shorter the wavelength, the greater the attenuation. It is a way of enhancing large scale (usually deep) features in the survey area. Also upward continuation tends to accentuate anomalies caused by deep sources at the expense of anomalies caused by shallow sources (Mekonnen, 2004).

There is a partial correlation between the wavelength of an anomaly and the depth of its source. The high-frequency signals are identifiable if the sensor is close to the source. Lower frequencies (long wavelength) are observable at greater distances between the sensor and the source (e.g. Jessell, 2002). As a result, a magnetic data measured on a given plane can be transformed to data measured at a higher or lower elevation, thus either attenuating or emphasizing shorter wavelength anomalies

$$L(r) = e^{-hr} \qquad (12)$$

Where h = the distance in meters continue up relative to the plane of observation.

Also, upward continued data may be interpreted numerically and with modelling programs. This is not the case for many other filter processes. Even if it may not show the corresponding details of the subsurface as the continuation distance increase it shows the regional and deeper structures clearly.

5.1.2 First Vertical Derivative

This helps to sharpen the anomaly the shallower features. The first vertical derivative computation in an aeromagnetic survey is equivalent to observing the vertical gradient with a magnetic gradiometer and has the same advantages, namely enhancing shallow sources, suppressing deeper ones and giving better resolution of closely spaced sources (Mekonnen, 2004). Generally, the enhancement of the shallow features either by a first or second vertical derivative filters is at the expense of anomalies

caused by deeper sources. Low-pass filter is also used with this filter to remove the high wavelength noise.

5.1.3 Tilt derivative

It is based on a combination of gradients in three spatial directions (x, y and z). The tilt derivative is used for mapping shallow basement structures and mineral exploration targets (e.g. A.Almasi et.al, 2014, Oasis Montaj). It is defined by a mathematical formula

$$TDR = \arctan \frac{VDR}{THDR} = \arctan = \frac{\frac{\partial M}{\partial z}}{\sqrt{\left(\frac{\partial M}{\partial x}\right)^2 + \left(\frac{\partial M}{\partial y}\right)^2}} \qquad (13)$$

where VDR and THDR are the first vertical derivative and total horizontal derivative

5.2 Analysis and Interpretations

5.2.1 Gamma-ray Spectrometer data

The radiometric surveys, as in the other parts of the Adola area, helped a lot in identifying and delineating the main lithological units (EIGS, 1993). The alteration zones related to mineralization targets are also clearly defined.

5.2.1.1 Total Count

The total counts map (figure 12) is the sum of a major radioactive elements K, Th and U, regridded with a cell size 7.5 and passed three times through a 3x3 hanning filter. It is overlaid with points showing kebeles of the two woredas which falls within the study area and the geology of Meleka represented with line.

The area around Kilenso Babicho, Meleka and north Sakaro portrayed with a high total count. The high count at Kilenso Babicho and northern Sakaro area is related to gneissic terrain while Meleka's is related the basaltic rock. Radiometric signature at Kilenso is a NW-SE trend while that of Northern Sakaro is N-S trend becoming wider on the side of the Sakaro and thinner going south.

Around 481000E east of Kilenso there is one NW-SE trending triangular shaped high total count recorded which falls within the amphibolite in the areas. This specific trend uniquely depicted high count from the wide amphibolite region with a low count in the surrounding. This high total count found near the inferred fault with a NW-SE trend at the North Western end. Probably this high count variation is related to flow of hydrothermal solution which makes the area favourable for mineralization and target area for further study.

The central part of the area also show low total count from northern end up to the southern covering a wide part of the study area. This is related a typical of the mafic –ultramafic rock units such as amphibolite, gabbro-amphibolite, talc tremolite schist and serpentenite. Regionally this is within the Megado volcano sedimentary belt.

The magnitudes of T.C. and K are found relatively greater than those of U and Th at the eastern side of the area which is related with felsic lithology of Biotite Gneiss (figure 12). This high potassium anomaly could be due to potassium enrichment associated with hydrothermal alteration.

In Lega Dembi and Sakaro zone, which fall in the same belt along with study area, have a known gold mineralization associated with sediments relatively enriched in thorium and less enriched in potassium compared to other felsic lithologies. As in Lega Dembi and Sakaro zone metasediments in the study area are in close special association with (mineralized) altered zones, particularly close to the contact with mafic rocks (EIGS, 1993).

5.2.1.2 Ternary radiometric map

The ternary map of the survey area (figure 13) is produced using the three radio elements (K, Th and U) and color model CMY (cyan, magenta and yellow) respectively and the colouring method of histogram equalization shading with the DEM. This type of display allows distinguishing between lithology, similar to a geological map, as the variations are shown as colour variations due to the different mineral abundances of potassium, thorium and uranium.

From the ternary map different lithologies can be seen with distinct colours. The light color in the central region (labelled as J) indicates the Volcano-sedimentary rocks with a north south trend which is due to low radioelement concentration. At the eastern side a closed region (labelled as A) having dark blue color, and a triangular shaped region widening towards the south and narrowing to the northern side is related to an biotite gneiss. This is the eastern boundary of the volcano sedimentary belts. It contains a potassium rich rock which shows distinct radiometric signatures clearly seen on the percent potassium map (figure 12).

Similar to other known primary gold occurrences in the area apparently associated with the contact between metavolcano-sedimentary rocks of the Greenstone Belt and the gneisses of the Gneissic Terrain of the area (last, 1994) this region could be selected as a primary target area for further investigation.

The ternary map also perfectly shows the thrust fault at the eastern side with a North - South trend at the lithologic contact between the gneissic terrain and volcano sedimentary belt. The thrust fault at the North Western part with a NW-SE trend is also seen with some modification at the North Western side.

Western part generally having mixed color of brownish and light blue (labelled G) is the western boundary of the volcano sedimentary belt.

At the center of the central part of volcano sedimentary belt one circular region (labelled as C) is distinctly seen related with metagabro, gabbro- amphibolite.

5.2.1.3 Th/k Ratio map

The abundance ratios are often more diagnostic of changes in rock types, alteration, or depositional environment than the values of the radio-isotope abundances themselves, which are subject to wide variations due to soil cover, etc. Ratio values, U/Th, U/K and Th/K, tend to closely approximate values at ground level. Ratio patterns can enhance subtle variations in elemental concentrations due to lithological changes or alteration processes associated with mineralization (e.g. Jessell, 2002). The U/ Th ratio, for example, decreases in weathered rock since uranium is easily oxidized to a water-soluble form and Thorium has no soluble ion and therefore tends to remain with the parent rock or is transported over relatively short distances in the form of solid mineral grains (e.g. Urquhart, 2013).

A low Th/k ratio is good indicator of potassic alterations that have exploration significance since hydrothermal alteration is associated with potassium enrichment. Thus profiles that include this ratio are often very useful for picking specific target anomalies for ground follow-up.

Figure 14 shows two distinct areas of low Th/k values which indicate zones of potassic alteration. One below Meleka at the south western end, where the talc tremolite schist and gabbro amphibolite are indicated and the other is at the eastern part, where the biotite gneiss is mapped. This eastern region is has a triangular shaped widening in the southern part.

It is also possible to see the low Th/k values with in the central volcano sedimentary zone bounded by the gneisses.

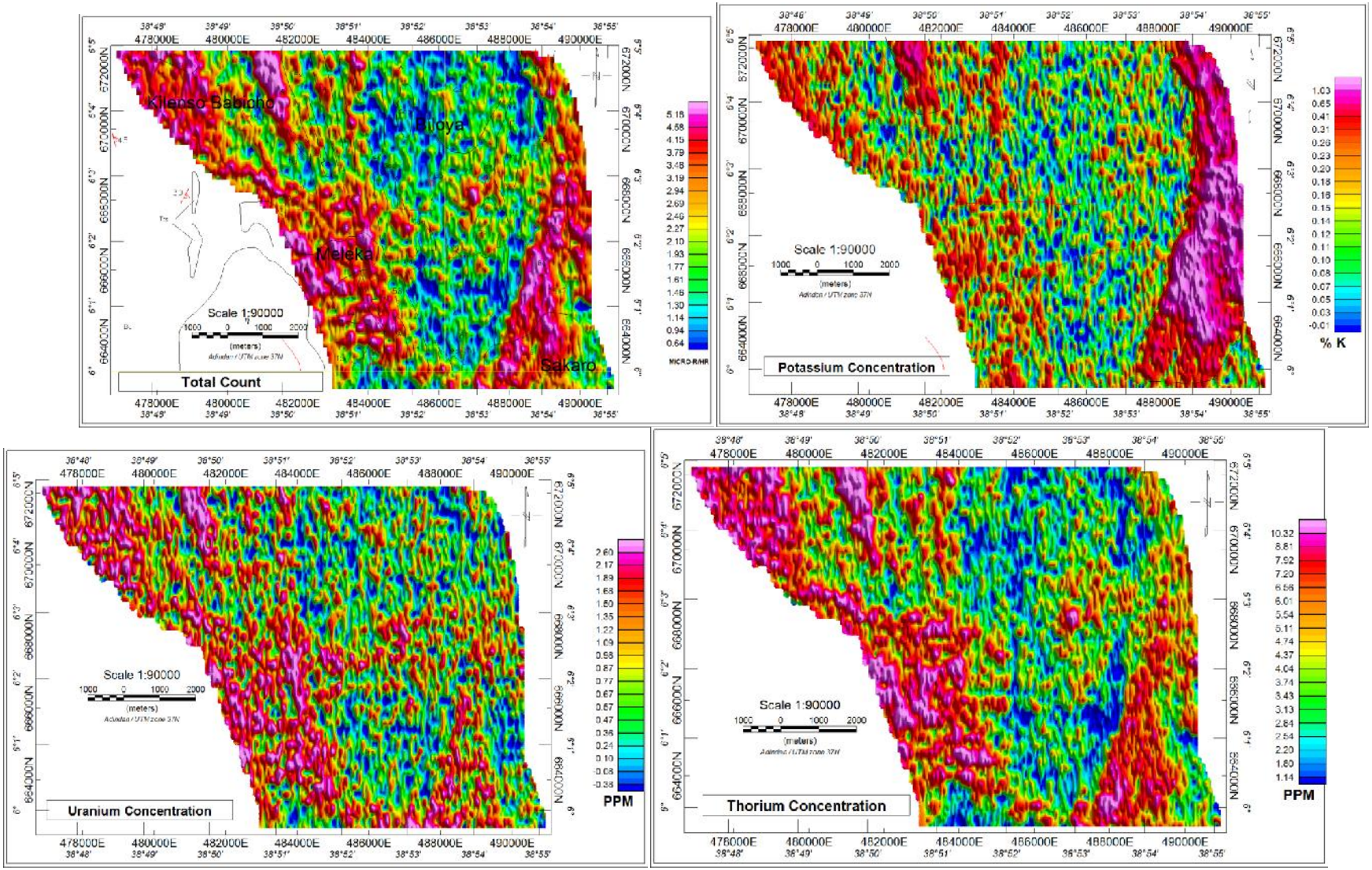

Figure 12 Total Count prepared with a cell size of 7.5m, 3x3 hanning filter with an overlaid geology and kebeles, Potassium, Uranium and Thorium Concentration maps

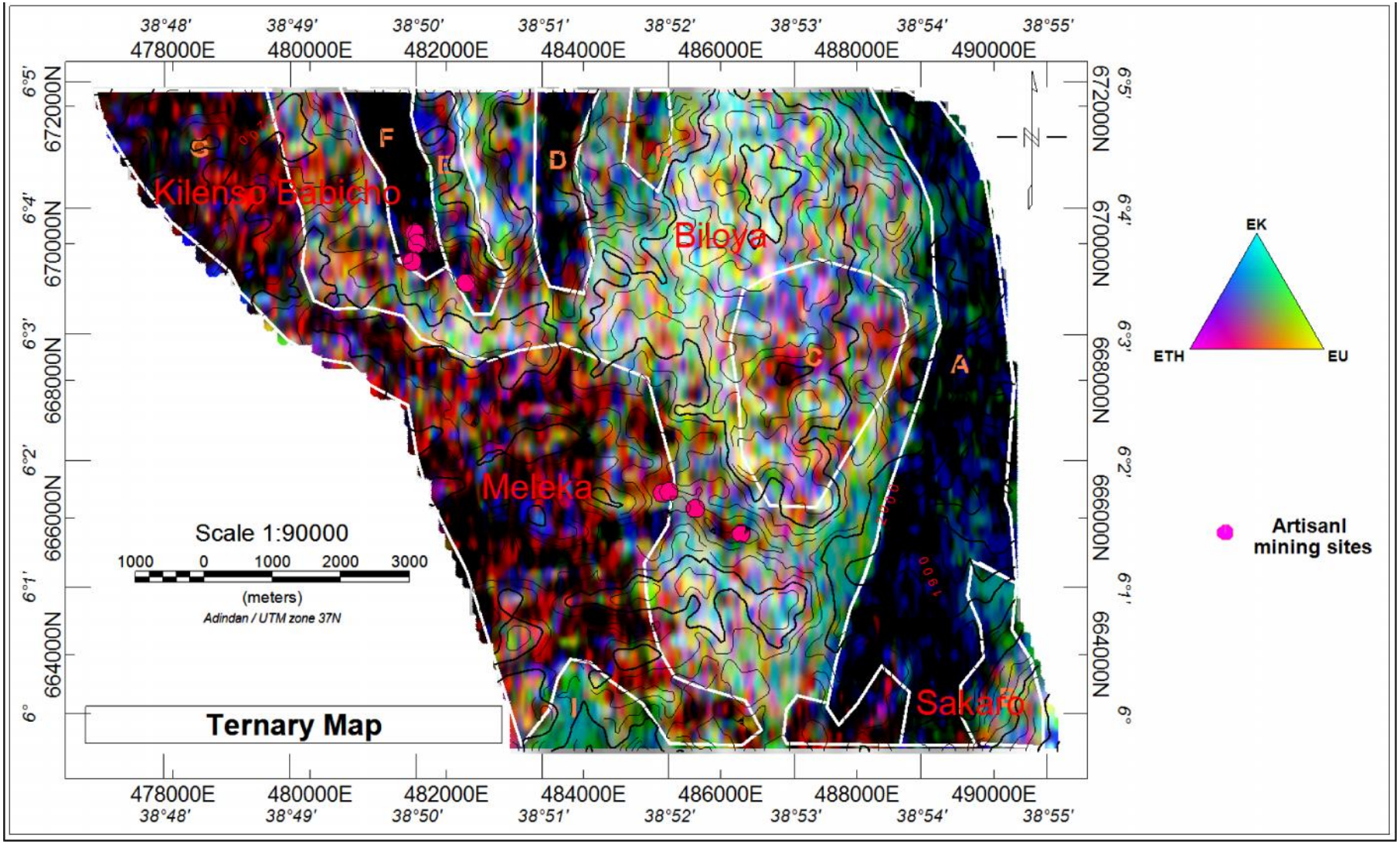

Figure 13 Meleka Ternary map (produced using the three radio elements and shaded with the DEM)

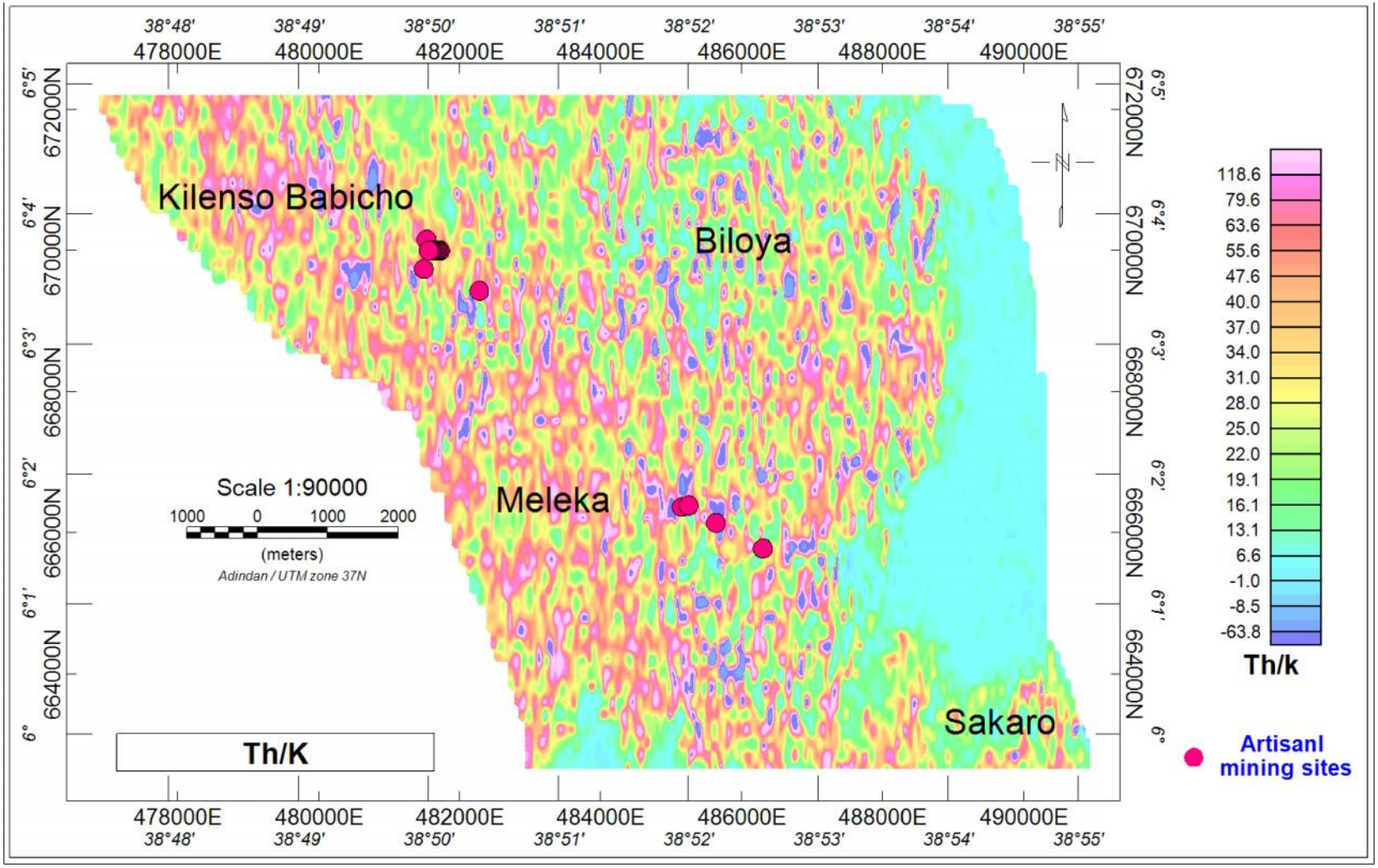

Figure 14 Th/k map re gridded with a cell size of 5m and filtered with 3x3 convolution filter

5.2.2 Aeromagnetic data

5.2.2.1 The TMI anomaly map

The measured total magnetic field provides information on the magnetic properties of the earth materials in the survey area. The information can be used to locate magnetic bodies of direct interest for exploration, and for structural and lithological mapping.

The total magnetic field response reflects the abundance of magnetic material in the source. Magnetite is the most common magnetic mineral. Other minerals such as ilmenite, pyrrhotite, franklinite, chromate, hematite, arsenopyrite, limonite and pyrite are also magnetic, but to a lesser extent than magnetite on average (Bruce, et al., 2007).

The TMI map (figure 15) regridded with a bidirectional line gridding with a cell size of 12 m (≈ 1/16 of the line separation) and displayed with a histogram equalization color method, normal brightness, 60^0 inclination and 45^0 declination for a better presentation of geophysical data and interpretation.

The TMI map exhibits different types of high and low magnetic anomalies. Broadly, the southern part of the TMI map shows magnetically high and complex region. The eastern part is magnetically depleted semi circular region with some minor close-ups inside which could probably be shear zones giving high values. It outlines the thrust fault with a N-S trend at the eastern side with a dipolar magnetic field. The thrust bounds old rock of biotite gneiss on the eastern side and soft talc tremolite schist on the western side. The gneiss gets narrow and the schist wider as it goes further north. The fault is truncated in the southern part near Sakaro by large alkaline olivine basalt around 664000N and continues further south up to Shakiso, Lega Dembi Au open pit mining area with the same bounding rocks on either side of the thrust fault similar to the study area. The thrust fault on the North Western side with a NW-SE trend also indicated on the TMI following the northern edge of high magnetic trend. This thrust bounds old rock of biotite gneiss on the western side and amphibolite on the western side. Similar to the Eastern side thrust fault this fault is truncated in the southern part near Meleka by large alkaline olivine basalt around 667000N and continues further down beyond the study area. The thrust is on the younger rocks on both the Eastern and North Western thrust fault. The semi circular depleted region is bounded by the two thrust faults in the eastern and western side and by the linear high magnetic zone in the southern side. This zone is 8005 m wide E-W and 5815 m wide along the North south direction. The artisanal sites in the area also follow this zone and the fault which make it interesting for further follow ups. Magnetically complex region of deeply seated

ultramafic units is delineated at the North Western end, along the eastern thrust fault and at the southern end. This unit is also delineated on the upward continued maps. The ultramafic units in the area contains up to 20% magnetite (Weldehaimanot, 1995) which make the high magnetic signatures to be seen. The ultramafic rocks in the Adola Belt are exposed along major tectonic discontinuities in two parallel zones. They are interpreted as belonging to different suites related to different stages of crustal break-up (Worku, 1996) intruding the host.

However, the map discloses prominent high magnetic features in elongated shapes distributed at the north western, central and southern parts of the mapped area.

The aeromagnetic anomalies ranges from 33137 to 35959 nT are characterized by both low and high frequencies of anomalies. The southern part of the map area reveals some major magnetic belts. The first major belt is nearly a NW– SE positive magnetic anomaly around 666000N extending from the middle part of the map, around 485000E, continued to south-eastern part beyond the study area and almost east west trending linear structure starting from western part of the area up to 485000E. Parallel to this NW– SE positive magnetic anomaly another trend at 664000N is seen. These two linear structures at the Southern part of the sheet could be associated to an inferred fault. Even though the direction of the inferred fault from the geological interpretation is different. For example, the direction of an east west trending structure is similar with the geophysical response, but the other one is in the NE- SW direction. This probably is inferred from displacement of the Amphibolite unit as can be seen from the geology, but from the geophysical response it should be modified to NW– SE direction. The fault on the upper side of the parallel structure is discontinued around 485000E.

The main thrust fault at the eastern side of the area at the boundary between the gneissic terrain and the schist is seen with a dipolar anomaly which crosses the NW-SE trending inferred fault around 489000E and discontinued by the basalt found at the South Eastern part of the study area.

The map unveil that the high magnetic anomalies have a NW-SE trending elongated structure at the North Western end related to the main thrust contact. The Eastern part of the area is occupied by low magnetic region with circular and irregular shaped high values inside related with ultramafics. Also, there are moderate anomalies at the north western with an irregular shapes due to amphibole, metavolcanics.

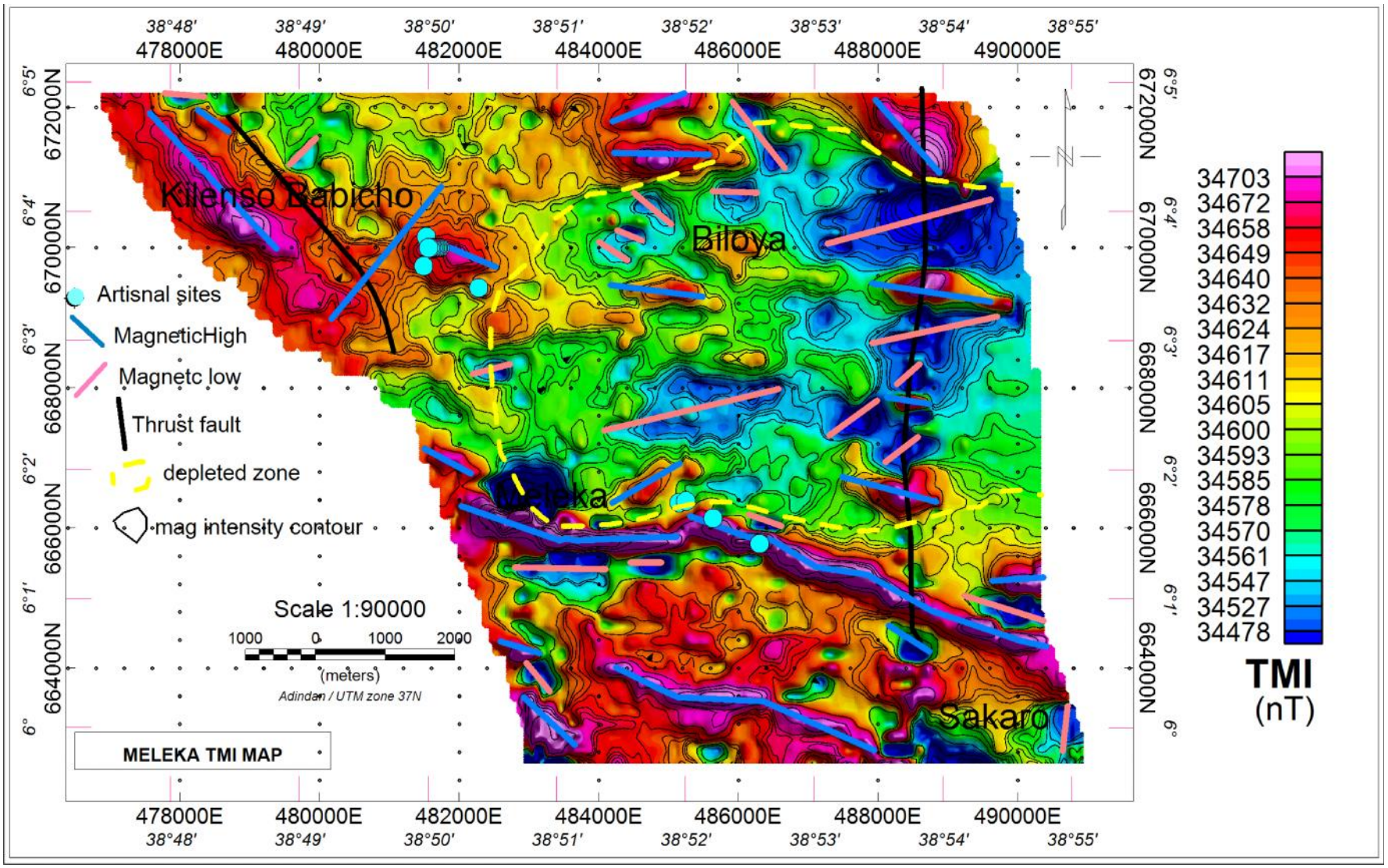

Figure 15 Total Magnetic Intensity Map (displayed with colour shaded grid, multiple contour intervals, overlaid with interpreted lineaments and zone, and artisnal sites)

5.2.2.2 Upward-downward continuation

Here the TMI map is processed using upward continuation (UWC) filter at different heights (figure 16) to enhance the regional effect and remove effects from shallow sources. For example, those dipolar features at the eastern part of TMI between 488000N and 489000N, and at the northern end around 485000N is seen on the UWC100 map but on the upward continued maps beyond 350m these features eliminated which clearly shows the effect from shallower source is attenuated as the continuation distance increase. On all the UWC maps linear features at the southern portion and north western end is seen. This show the structures are deeply rooted. But at lower distances than this continuation height, it is possible to see some anomalous features of shallower source at the central, northern and north eastern end. Also some localized anomalies at eastern part of the maps are seen. On the UWC 350 and UWC 500 map the discontinuity on the WNW-ESE trending structure is large.

Derivative Maps

5.2.2.3 First Vertical Derivative

On the first vertical derivative map (figure 17) the north south trending thrust fault at the eastern side is clearly demarcated. The two inferred fault with a modified direction is also depicted on this map. Shallower source anomalies also seen scattered within the volcano sedimentary belt bounded with the two fault structures.

5.2.2.4 Tilt derivative

The tilt derivative map (figure 18) is prepared from the TMI using the MAGMAP Filter on the Geosoft and upward continued to 40 m above the flight height to enhance the mapped structure. The map is displayed as color shaded grid image with normal shading effect, histogram equalization color method, the Canadian "gsc.tbl" color table and 45^0 illumination directions to a better presentation of the map.

As tilt derivative is adequate for mapping shallow basement features, the map shows a major direction of the structures along E-W and EW-SE with some minor N-S and NE-SW trends. The dominant features identified are an E-W trending elongated shallow features around 670000N at the eastern side related to the ultramafic rocks and around 484000E northern part due to the gabbro amphibolite rock. These features were not clearly seen on the TMI map

The inferred faults at the southern part also clearly demarcated on this derivative filter. But, there are discontinuities along the trend which were not visible in TMI map on this trend. Also the N-S thrust fault at the eastern side is hidden.

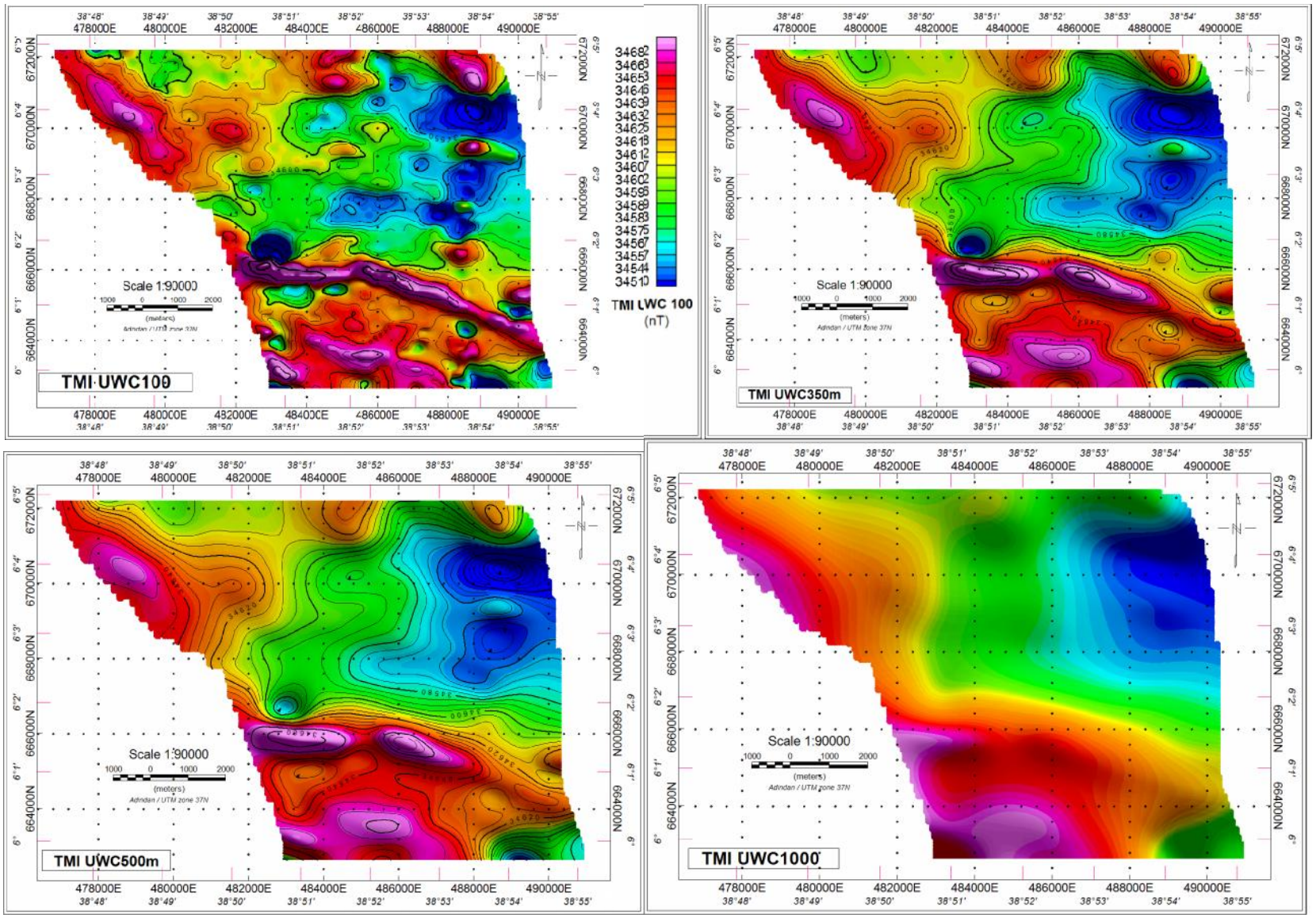

Figure 16 Total Magnetic Intensity map upward continued at 100, 350, 500 and 1000m above the survey height

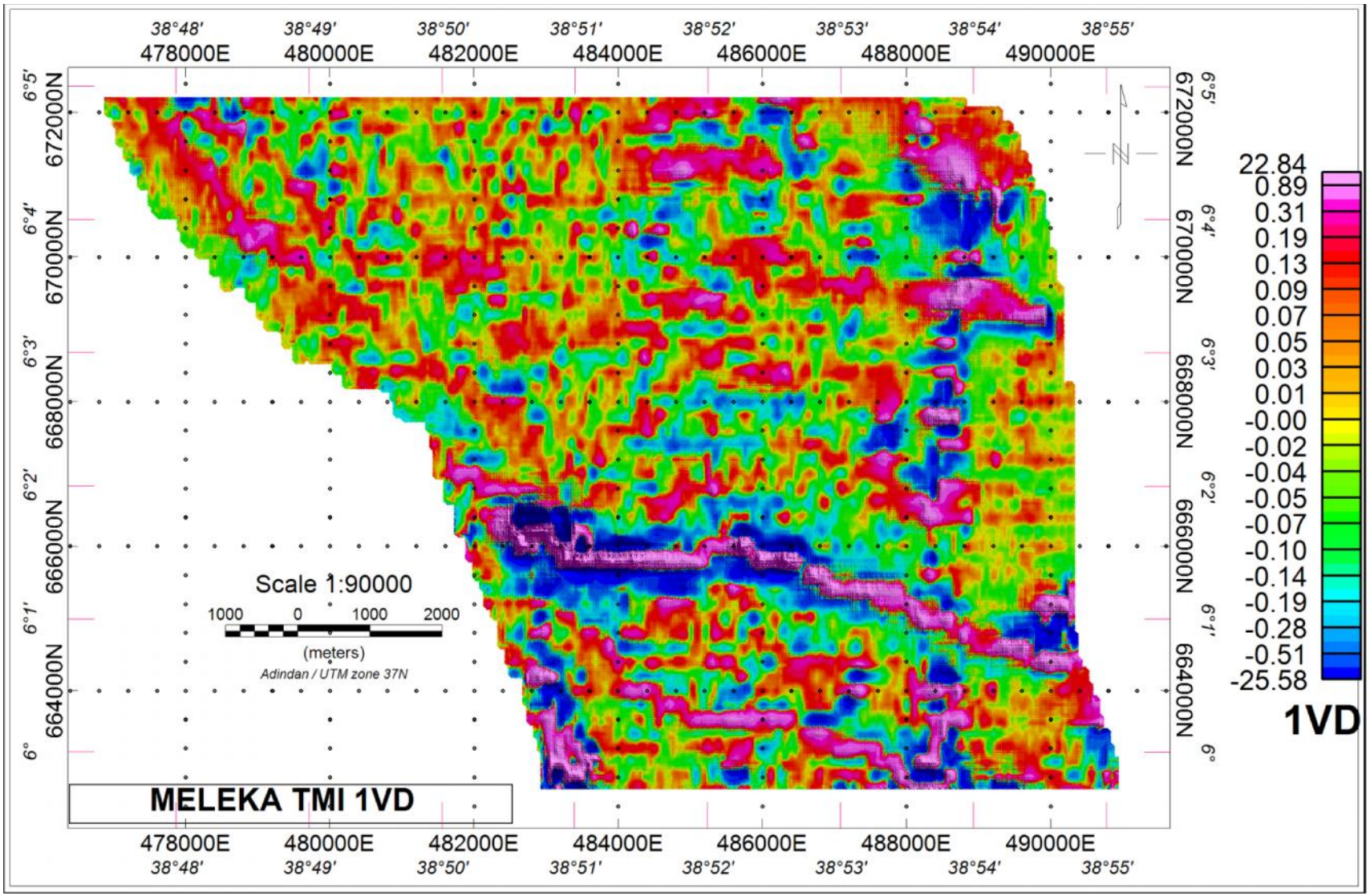

Figure 17 First Vertical derivative

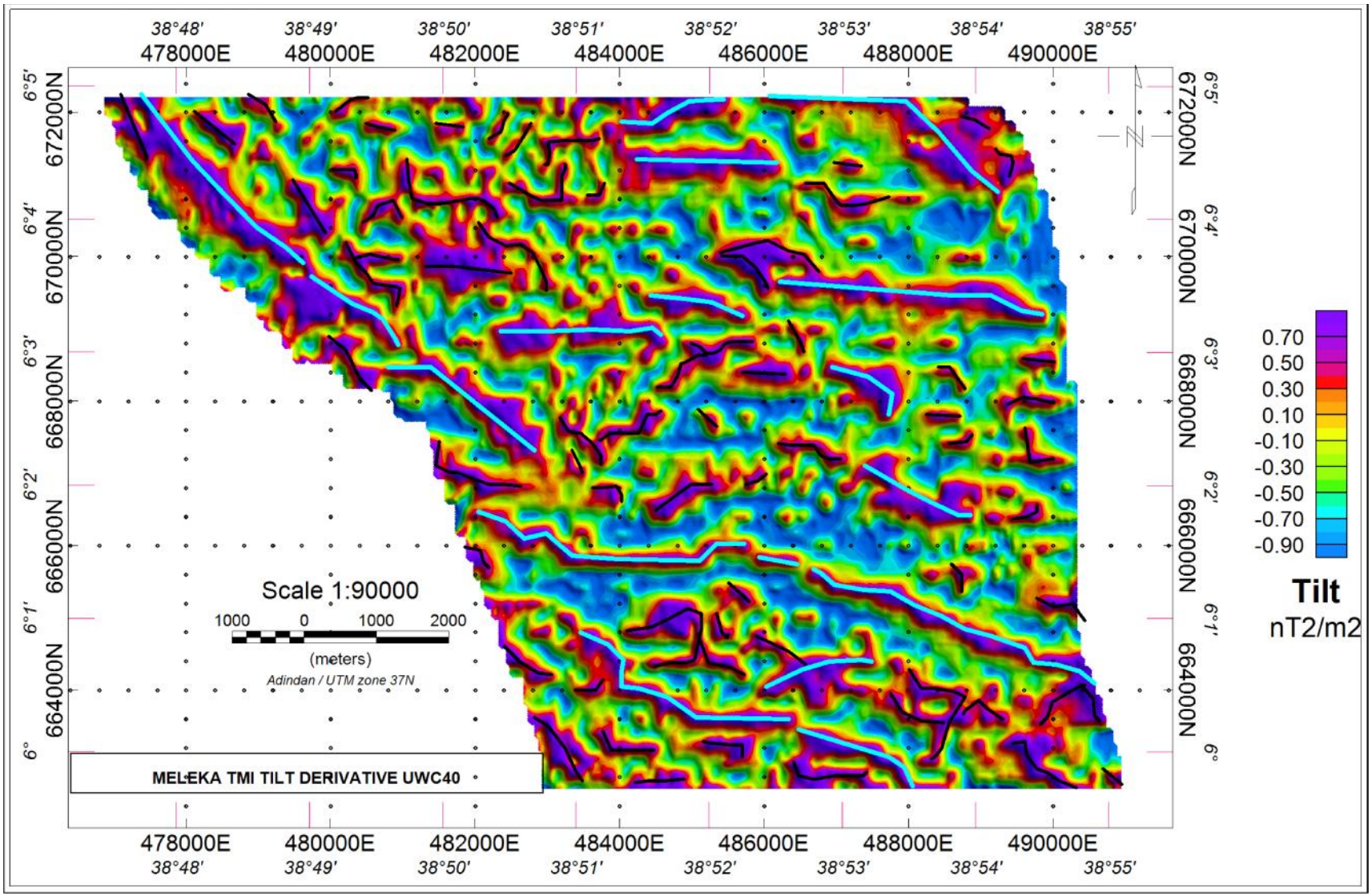

Figure 18 Tilt derivative ("gsc.tbl" color table is used to display as a shaded map)

5.2.2.5 Regional and residual separation

The aim of the separation is that, shallow and deep structures in most cases appears together, which makes difficult to differentiate the source of the anomaly. Thus, under such circumstances, separation of anomalies will be a desirable step.

The process is done by determining the cut off frequence from the radially average spectrum curve. The regional field is produced by applying low pass filter to the TMI with the cutoff frequency 2.6465719. The residual field is determined by subtracting the regional field grid from the TMI grid. Further, a 3x3 hanning filter is applied to smooth the resigual map.

Long wavelength anomalies with broad and slow changes in the potential fields may be attributed to sub crustal sources/deep seated structures, whereas the shallow or near surface (short wave length) residual anomalies are attributed to lithological features (e.g. Woldetinsae et.al, 1995).

Regional (long wave length) anomaly map

The depth estimate is a plot of the 5-point depth data from the spectrum file. The average depth estimated to the source of this anomaly is around half kilometres (figure 21a). The estimation can be used as a rough guide to the depth of magnetic source populations.

On this anomaly map (figure 19) there is a clear zone between the southern high magnetic field and low magnetic field zone in the north western part. An east west trending high magnetic linear zone centered on 666000N is also well delineated. This is related to the inferred fault. From the depth estimate value it tells us that the fault goes at relatively deeper depth,

Residual (short wave length) anomaly map

The residual magnetic field anomalies (figure. 20) are caused by sources at relatively average depth of 300meters (figure 21b). These are rough estimates of the depth from the radially averaged spectrum.

To have a better estimate for depth the method of spectral analysis as given by Spector and Grant (Woldetinsae, 1997) is used.

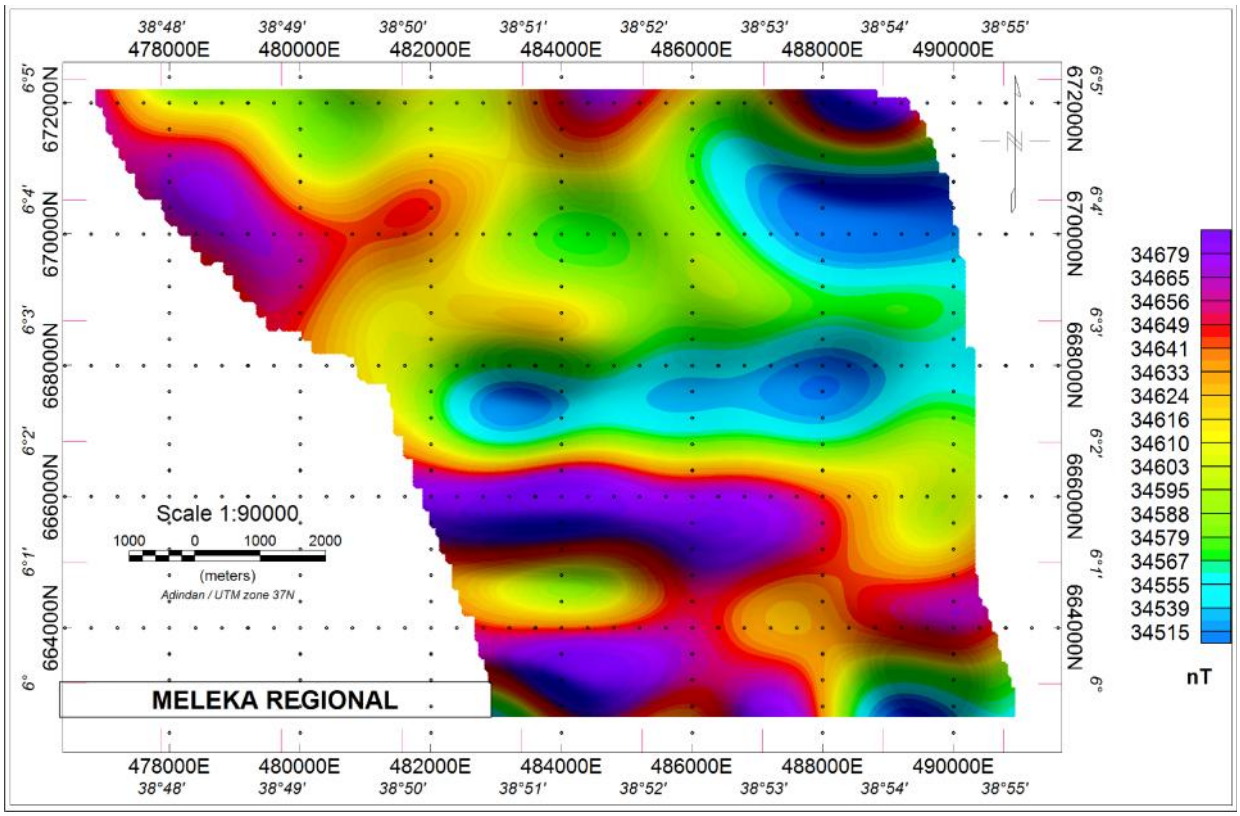

Figure 19 Regional map

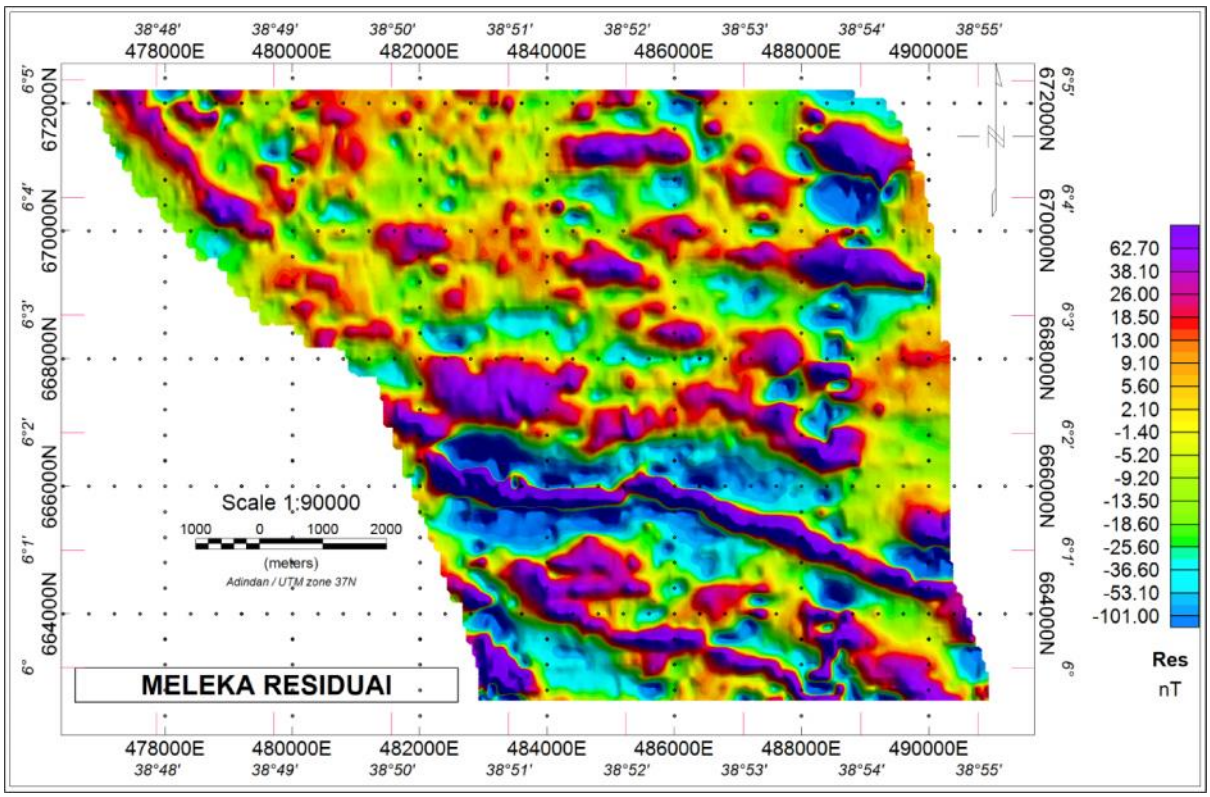

Figure 20 Residual map (the map is displayed as a color shaded grid image with "gsc" color table and 0.1 contour intervals)

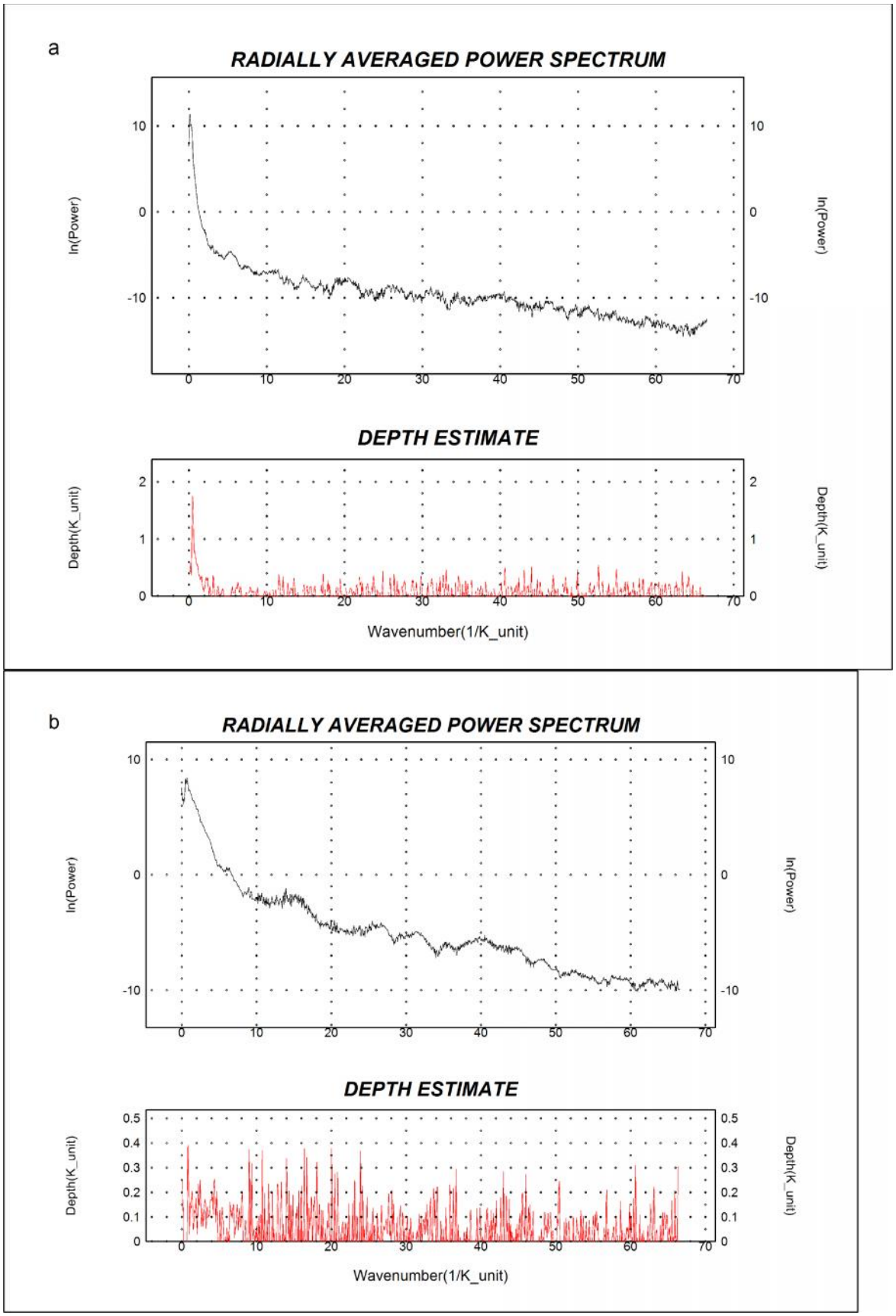

Figure 21 Power spectrum and Depth estimate curve for regional (a) and residual (b) field

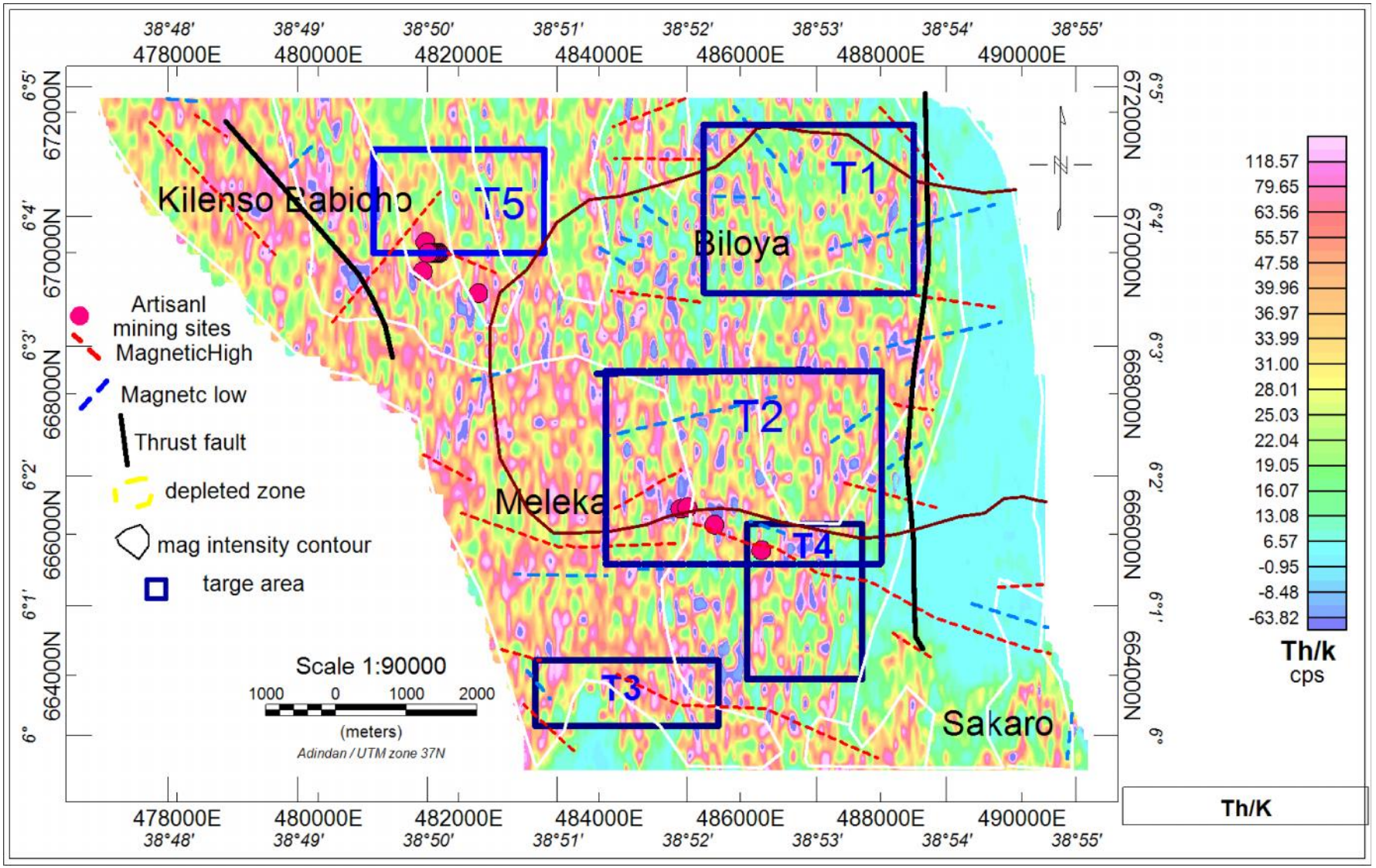

Figure 22 Composite interpreted map with follow up targets overlaid on Th/k map

5.2.2.6 Composite interpreted map with follow up targets

From the figure 22

T1= this target is at the boundary between the megado volcano sedimantsry belt and the gniessic terrain. The zone has low total count mark. The Th/K ratio map show pottasium alteration. The target is situated on the elevated part of the area, Sakaro. Follow up method recommended is geochemical survey to see the level of alteration in the area.

T2 = Magnetically depleted zone which is bounded by the thrust. This also falls within the volcano sedimentary belt. Just above the junction point of a north - south and north west- south east trending fault. the target area is known for its artisnal works. It is at intermediat topography.

T3= This block show low Total count and and pottasic alteration zone. Magnetically high due to the ultramafic rock.

T4= This target is at the boundary between biotite gneiss and the volcano sedimentary. It has high radimmetric value, low Th/k value which show high pottasic alterations. The area crosses the infered fault and artisnal gold mining is done extensively. The area is relatively at moderate topography. Recommended follow up methods are IP/resistivity, detail magnetic and radiometric survey.

T5= Around 481000E east of Kilenso there is one NW-SE trending triangular shaped high total count recorded which falls within the amphibolite in the areas. This specific trend uniquely depicted high count from the wide amphibolite region with a low count in the surrounding. This high total count found near the inferred fault with a NW-SE trend at the North Western end. Probably this high count variation is related to flow of hydrothermal solution which makes the area favourable for mineralization and target area for further study.

5.2.2.7 FFT analysis on the blocks to prepare a2D model

This analysis is done by dividing the the grid in to many sub grids (figure 23) to perform power spectral analysis on each of them and determine depth of source. This analysis can be done MAGMAP in Oasis montaj. Several researchers used the overrlapping of grid cells to calculate the depth to magnetic markers in the penisular sheld of India (e.g. Woldetinsae, 1997). The method assumes an aeromagnetic anomaly is due to ensemble od vertical prism.

From the spectrum curve (figure 24 and 25) of each block two depth h_1 for deeper source and h_2 for shallower source is determined. From the two depth average depth is calculated to aid an interpritation. Results are gridded and contoured to produce the basement map for deeper and intermediate magnetic reflectors. The average map of the two also producced.

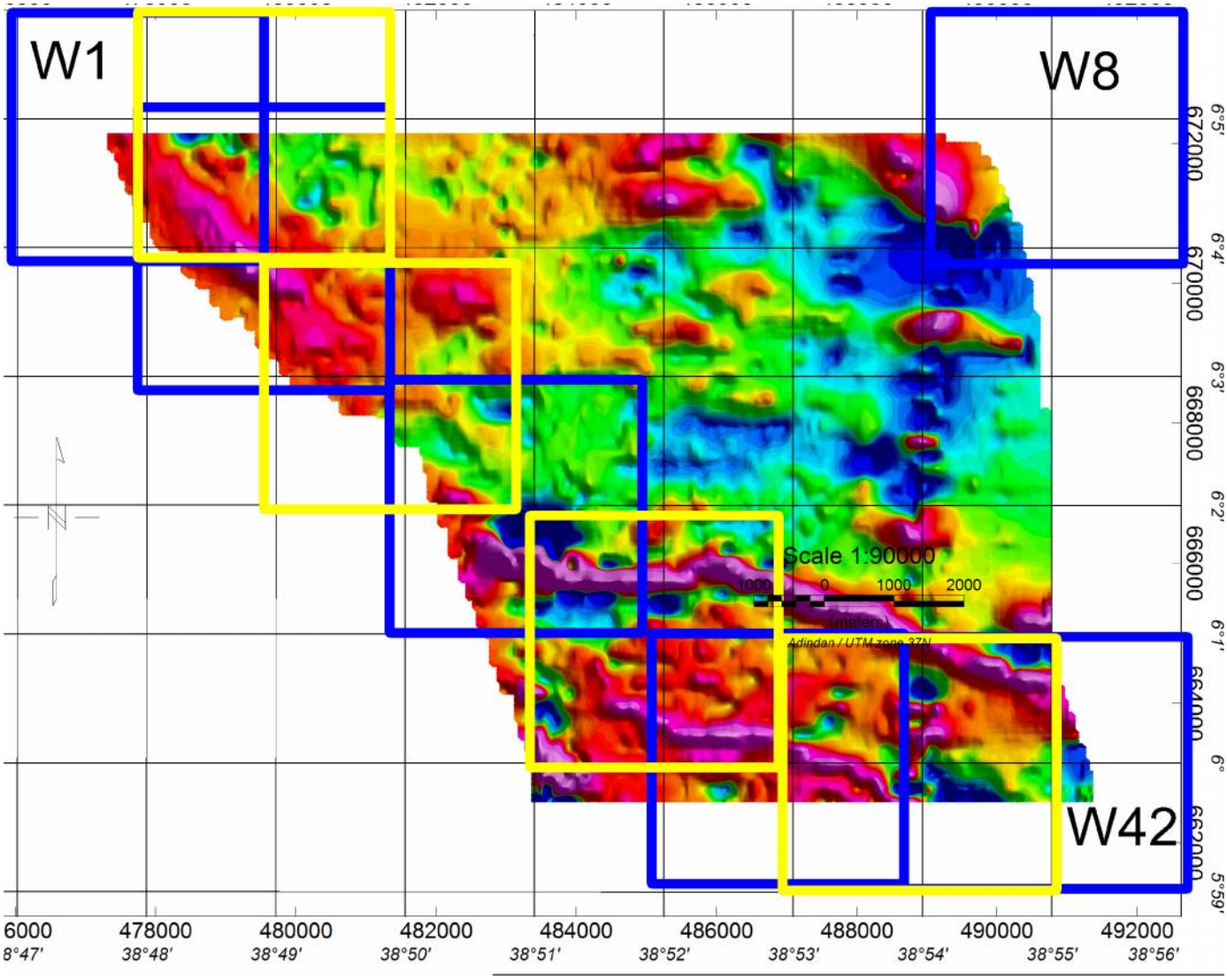

Figure 23 Original grid subdivision in to 42 equal sub grids to do FFT analysis on each of them

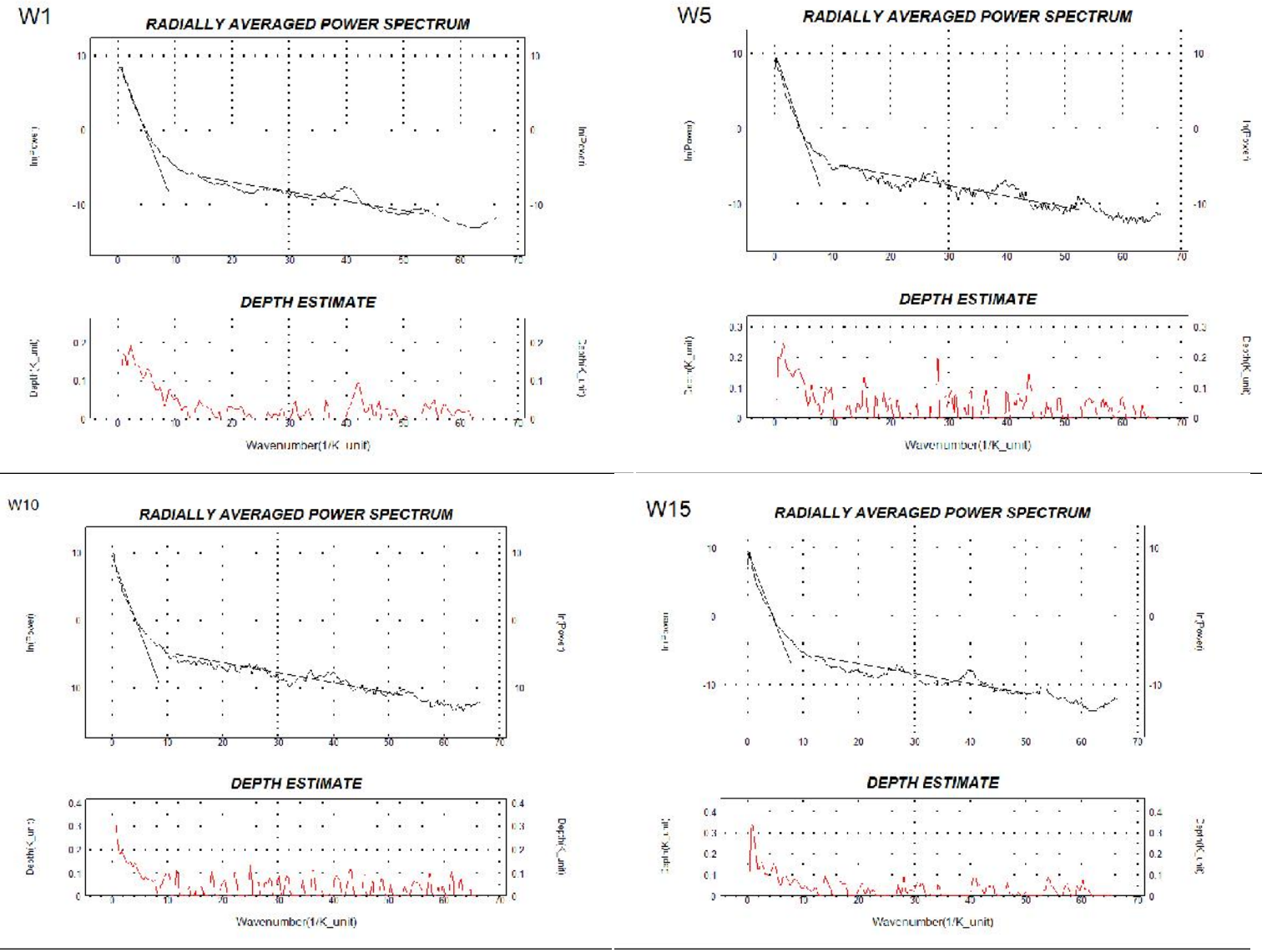

Figure 24 Selected power spectrum and depth estimate curve for shallower and deeper depth (W1, W5, and W10&W15)

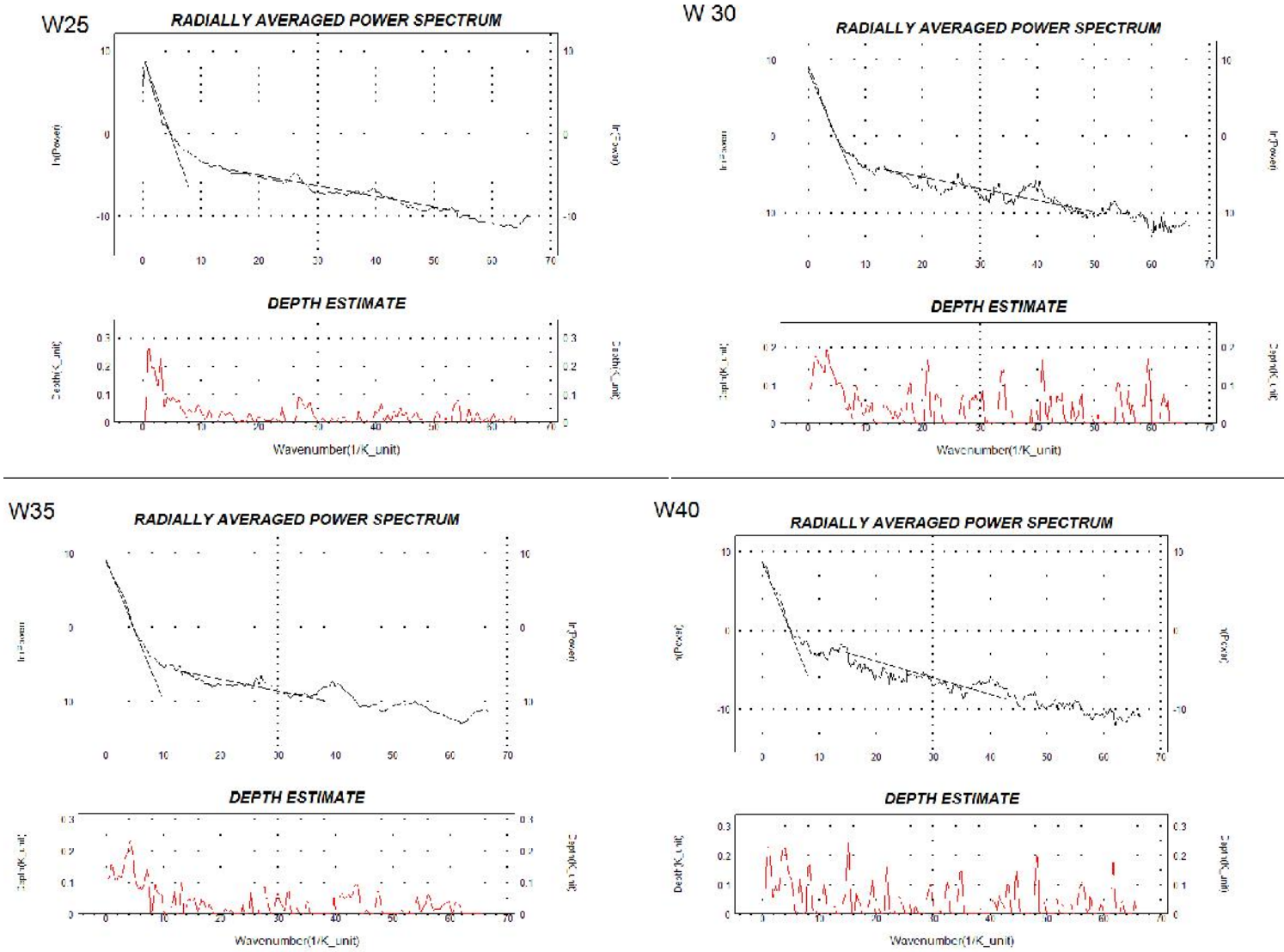

Figure 25 Selected power spectrum and depth estimate curve for shallower and deeper depth (W25, W30. W35 & W40)

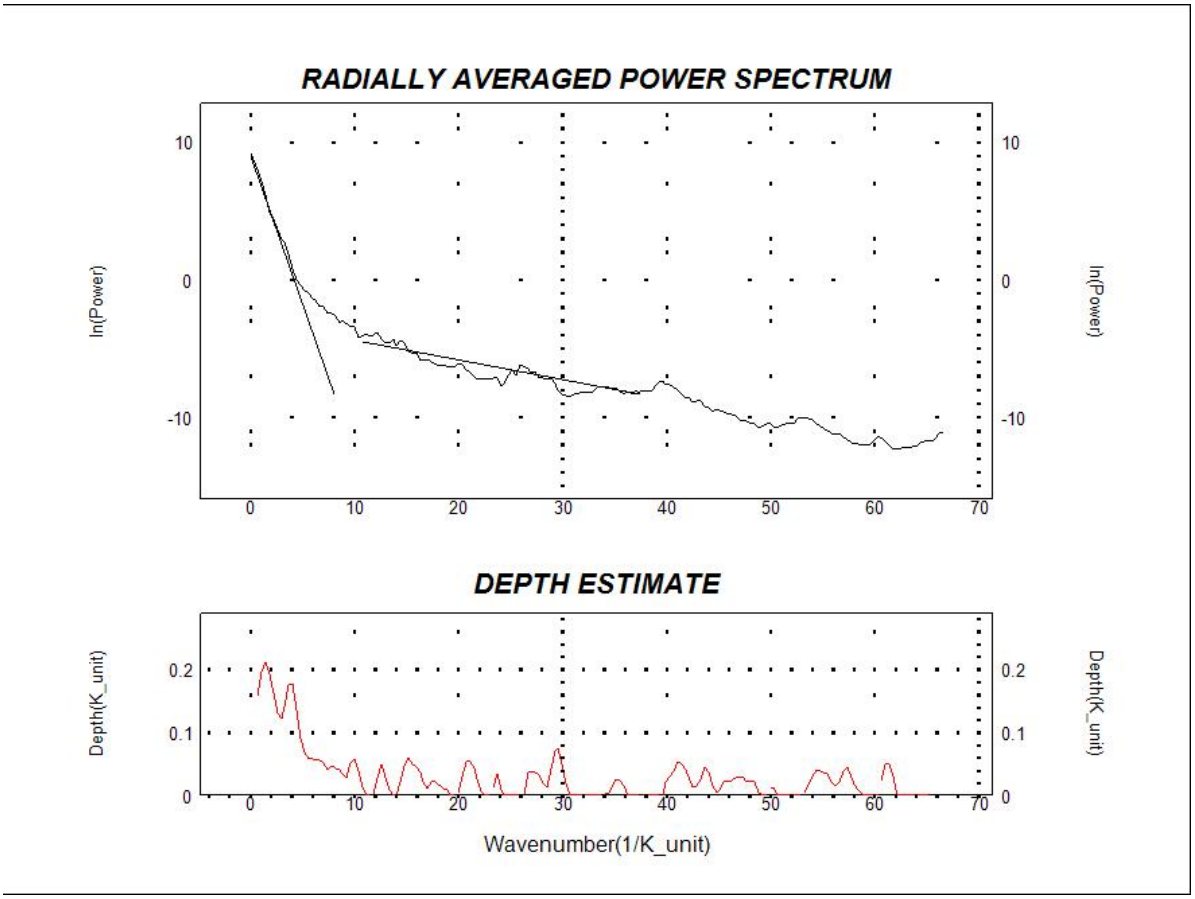

Figure 26 Power spectrum and depth estimate curve for shallower and deeper depth (W42)

From the above curves (figure 24 – figure 26) the following depths (Table 5) are calculated using the depth to a statistical ensemble of sources expression:

$$h = -s/ 4\pi \qquad (74)$$

where:

h is depth

S is the slope of the log (energy) spectrum (Oasis Montaj)

The map for each of the three depths (deeper, shallower and average depth) is gridded using the Geosoft, Oasis Montaj (figure 27). Each of the depth calculated represent the central point of respective block.

The depth contour from shallower source is overlaid on the residual map (figure 29) , the depth contour from deeper source is overlaid on the regional map (figure 28) and the average depth contour is overlaid on the TMI map (figure 30) to correlate the anomalies with depths to the source of the body.

Table 5 depths calculated for deeper source (h1), shallower source (h2) and the average of the two (h_{ave})

Block	X	Y	h1*1000	h2*1000	h ave*1000
W1	477833	672405	42.9106	10.0387	26.474646
W2	479681	672405	39.8089	11.3767	25.592824
W3	481524	672405	46.4922	13.9897	30.240932
W4	483411	672405	40.2161	12.6873	26.451689
W5	485224	672405	38.0942	11.698	24.896122
W6	487072	672405	34.9112	12.7236	23.817372
W7	488885	672405	56.0015	10.2733	33.137366
W8	490733	672405	49.4596	12.5015	30.980538
W9	477833	670557	36.8674	12.7847	24.826037
W10	479681	670557	37.155	12.9353	25.045155
W11	481524	670557	41.509	11.5522	26.530586
W12	483411	670557	34.3659	13.1684	23.767158
W13	485224	670557	31.9681	10.9718	21.469945
W14	487072	670557	35.004	12.6223	23.813179
W15	488885	670557	38.9728	11.4061	25.189444
W16	490733	670557	41.4131	11.1336	26.273349
W17	477833	668710	37.1379	11.894	24.515913
W18	479681	668710	36.3698	11.9729	24.171339
W19	481524	668710	41.8254	11.0217	26.423546
W20	483411	668710	39.9489	11.0516	25.500287
W21	485224	668710	43.6126	10.6376	27.125131
W22	487072	668710	38.1595	10.4478	24.303628
W23	488885	668710	47.3883	10.2888	28.838572
W24	490733	668710	44.864	10.0373	27.450654
W25	479681	666861	39.5273	10.6131	25.070215
W26	481524	666861	50.0955	11.1127	30.604098
W27	483411	666861	53.3358	8.12427	30.730024
W28	485224	666861	50.1519	10.2434	30.197637
W29	487072	666861	45.0186	9.99207	27.505327
W30	488885	666861	48.7316	11.8776	30.304613
W31	490733	666861	48.3773	15.6695	32.02339
W32	481524	665014	49.1404	15.2688	32.204556
W33	483411	665014	47.1907	8.2846	27.73765
W34	485224	665014	50.2556	13.7967	32.026146
W35	487072	665014	43.0685	11.5769	27.322722
W36	488885	665014	44.7412	14.894	29.817602
W37	490733	665014	42.1196	12.7461	27.432804
W38	483411	663167	68.6504	9.94582	39.298097
W39	485224	663167	42.3819	14.8192	28.600569
W40	487072	663167	46.9955	16.545	31.770272
W41	488885	663167	42.9286	14.6396	28.784068
W42	490733	663167	37.5911	11.4876	24.539339

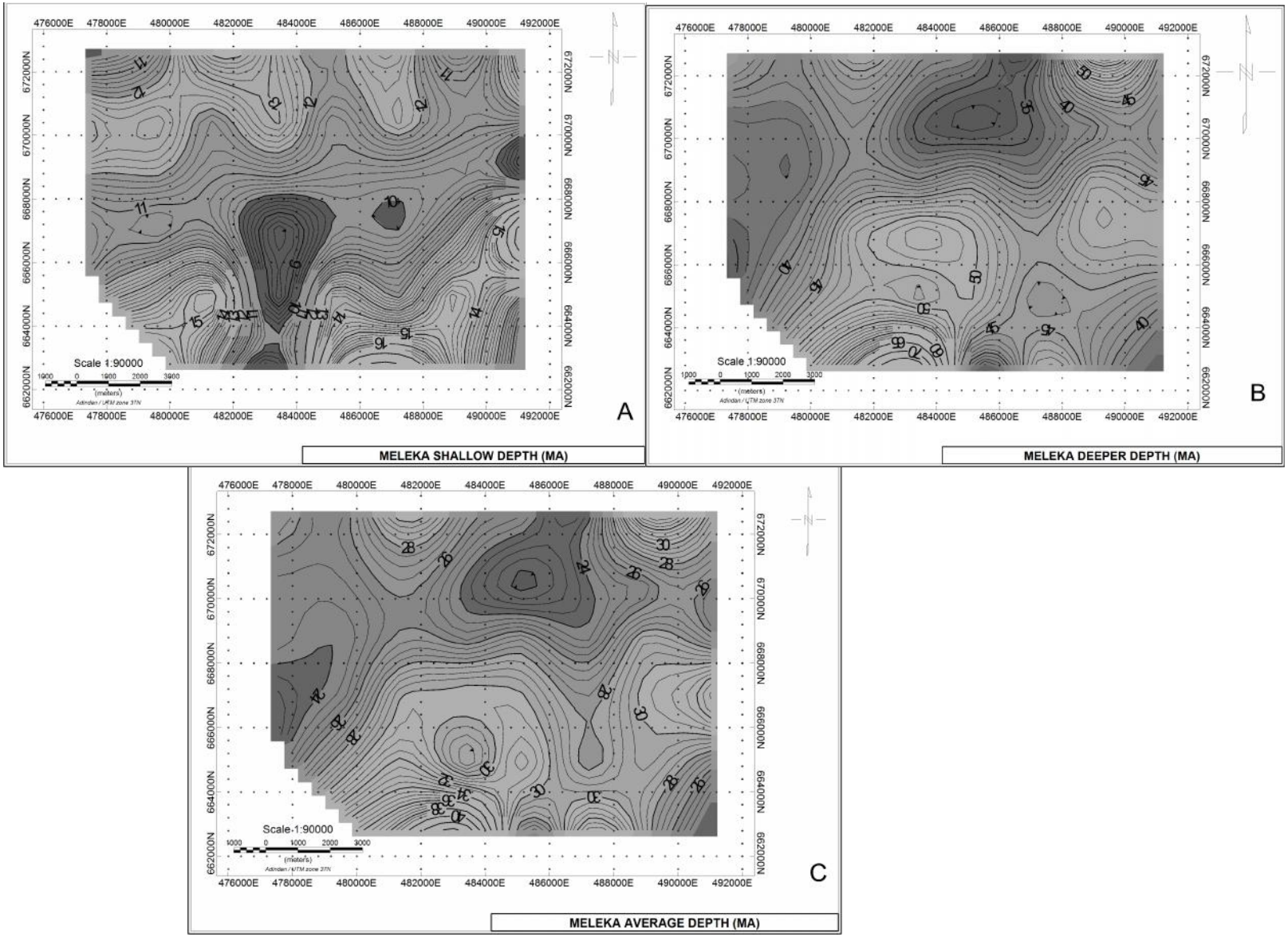

Figure 27 Gray scale maps for shallower (A), deeper (B) and average(C) depth with contour

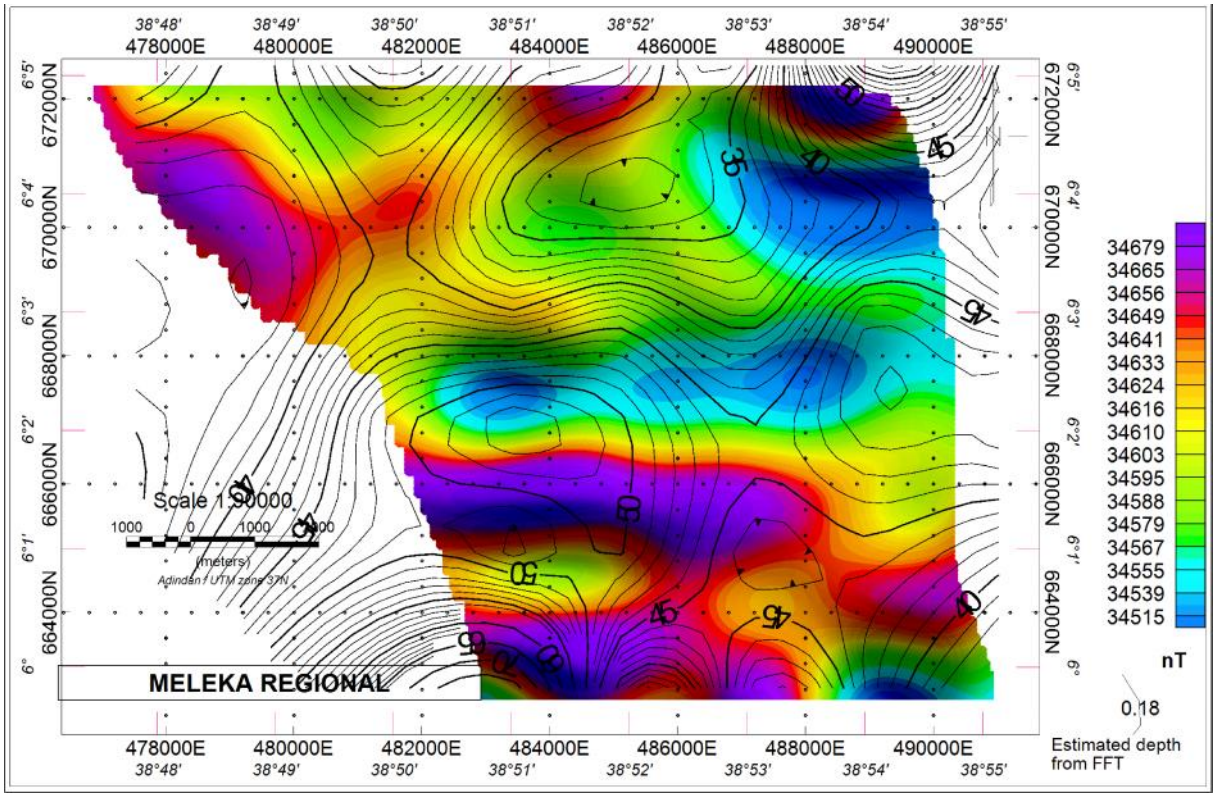

Figure 28 Regional map with a deeper estimated depth contour overlaid

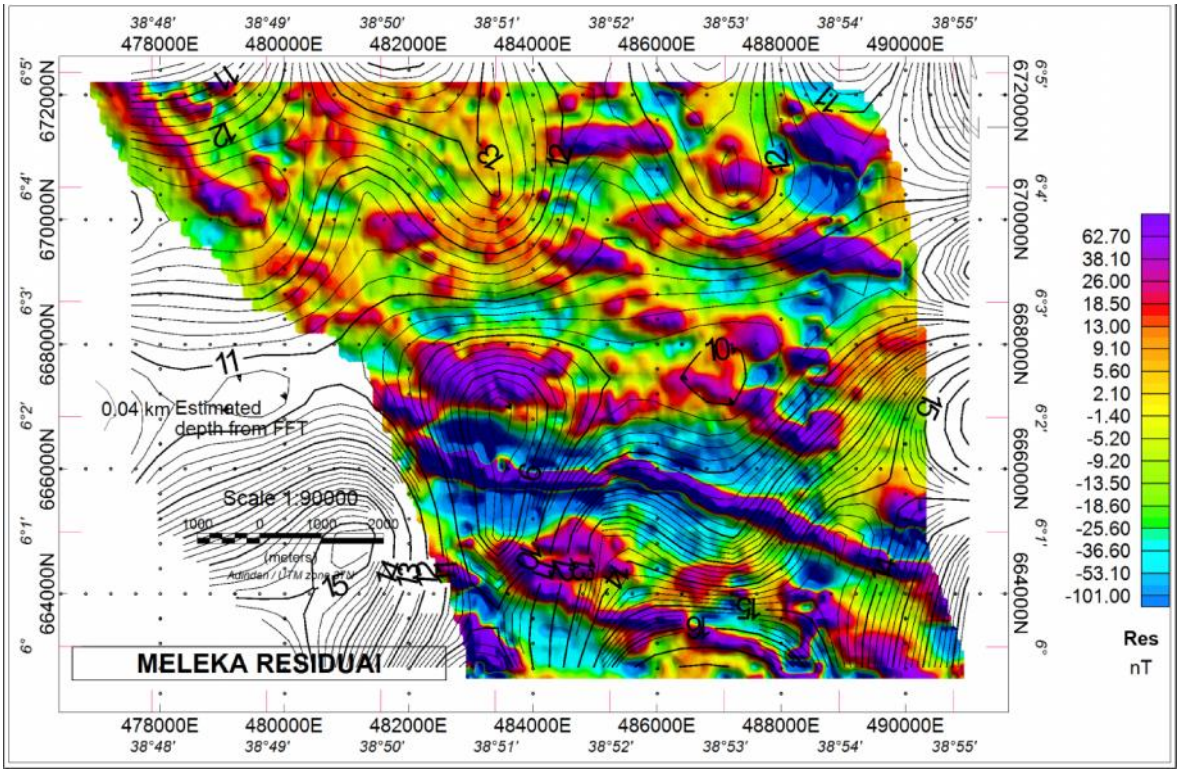

Figure 29 Residual map with a shallower estimated depth contour overlaid

The contour follow the anomaly trends. The contour at the strong anomaly is at deeper depth and to the north eastern part is shallower depth

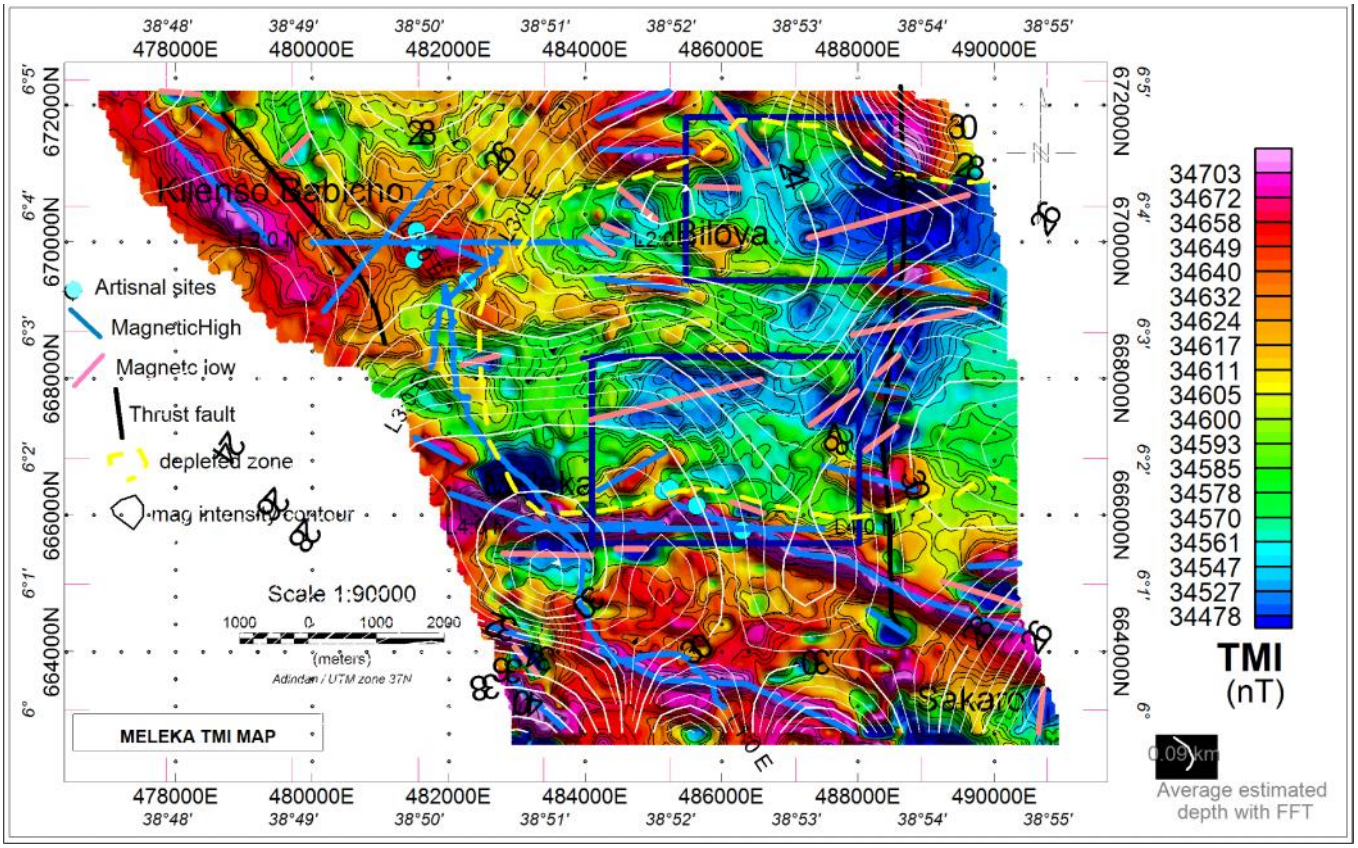

Figure 30 TMI map with average estimated depth contour overlaid

The contour trend make saddle kind of shape. It shows three kind of pattern. one value at the north eastern side, another values at northwestern side and another one at the southern part. At the middle one value sandwiched with the other three. The colour underlaid also shows the same zonation consistent with the contour.

The middle one shows folded kind of pattern. The pattern in the middle is demarcated by the other values. The contour at the southern part is closed up and the pattern has a kind of linear trend following the inferd fault trend. This contour clearly shows a zonation. The map shows the depresion of the basement from east to west, since the value of depth contour increase going from east to west.

5.2.2.7.1 The depth statistics

The depth statistics for each of the three depths (shallower, average and deeper) is presented with respective minimum, mean, maximum and other related information (figure 31 – figure 33).

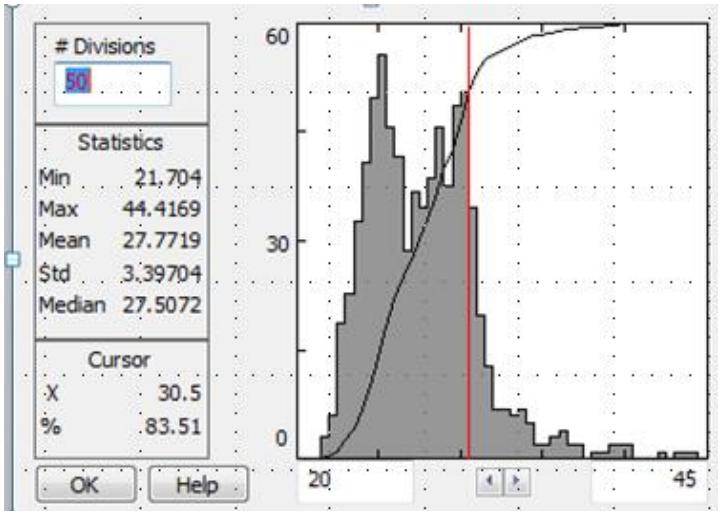

Figure 31 Average depth statistics

This statistics (figure 31) shows the mean depth from the average depth estimate map is 27.7719m and minimum depth 21.704m and that of maximum depth is 44.4169m. The distribution shows most of the depth information comes from body source of depth between 25 to 30.5m. Since the vertical axis shows the population distribution, it is possible to conclude that most of the magnetic signitures are coming from the the depth between 25 to 30.5m.

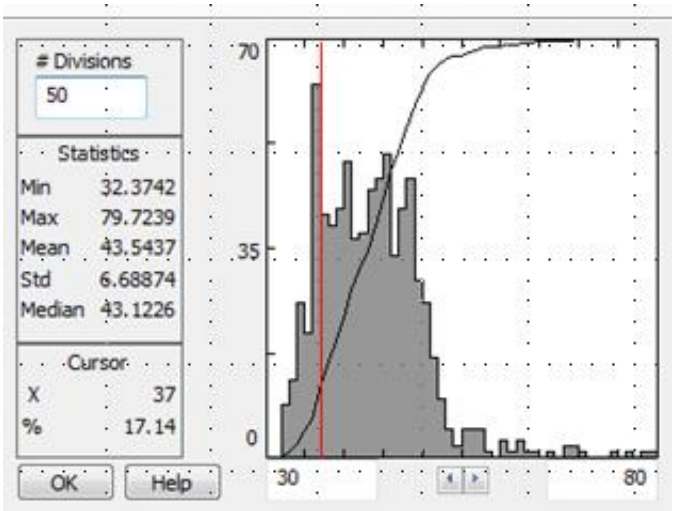

Figure 32 Deeper depth statistics

This statistics (figure 32) shows the mean depth from the deeper depth estimate map is 43.5437m and minimum depth 32.3742m and that of maximum depth is 79.7239m. The distribution of the curve show most of the depth information comes from body source of depth around 37m. We can conclude that most of the magnetic signitures on the regional map are coming from the mean depth of 37m.

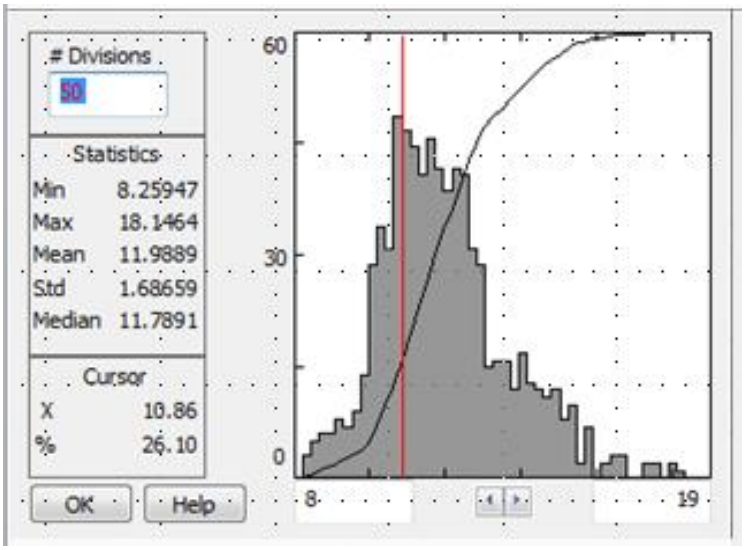

Figure 33 Shallower depth statistics

This statistics (figure 33) shows the mean depth from the shallower depth estimate map is 11.98 and minimum depth 8.25m and that of maximum depth is 18.15m. Most of the depth information comes from body source of depth around 10.86m. Possible to conclude that most of the magnetic signatures on the resigual map are coming from the mean depth of 10.86m. The curve has a normal distribution

5.2.2.8 Comparison of ground and airborne data

The ground magnetic data is compared along three selected profile lines of respective aeromagnetic data (figure 34- figure 36) and one ground radiometry line with that of the helicopter borne gamma ray spectrometric line for each of the four windows TC, K, U and Th (figure 37 - figure 40). All the data found to be corroborated with each other.

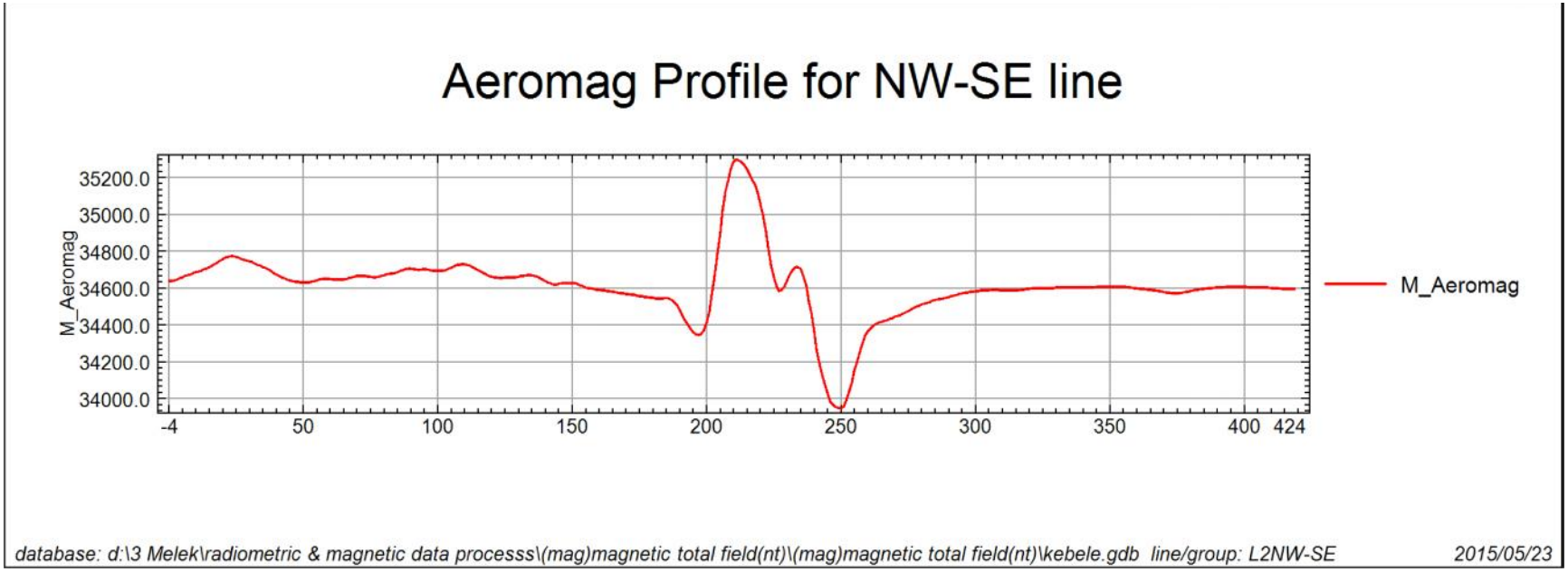

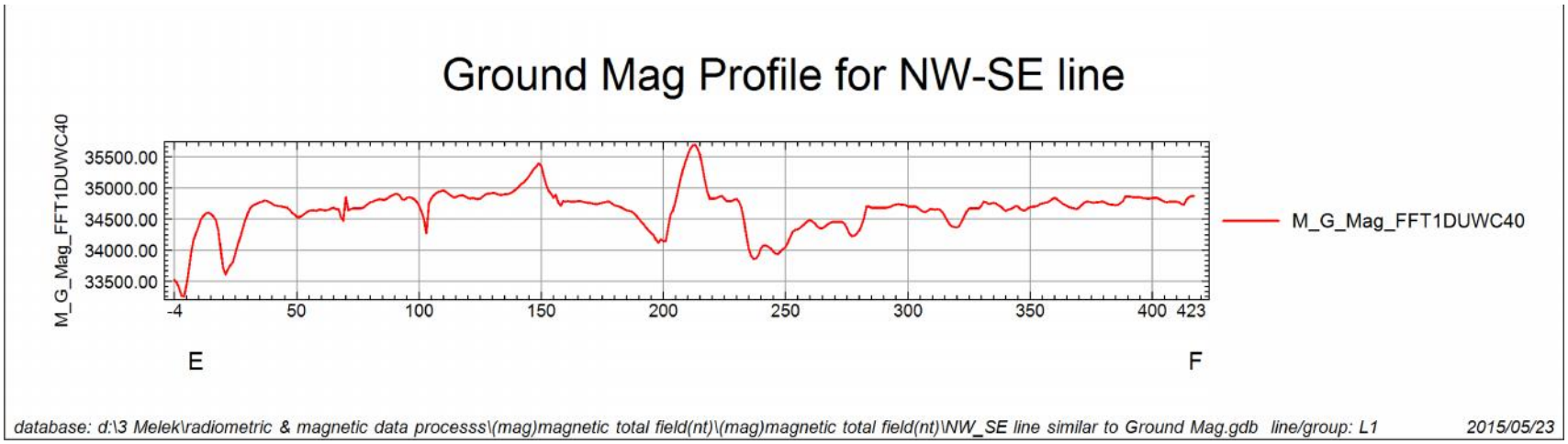

Figure 34 Comparison of the aeromagnetic and ground magnetic profile along the NW_SE direction of the ground magnetic line

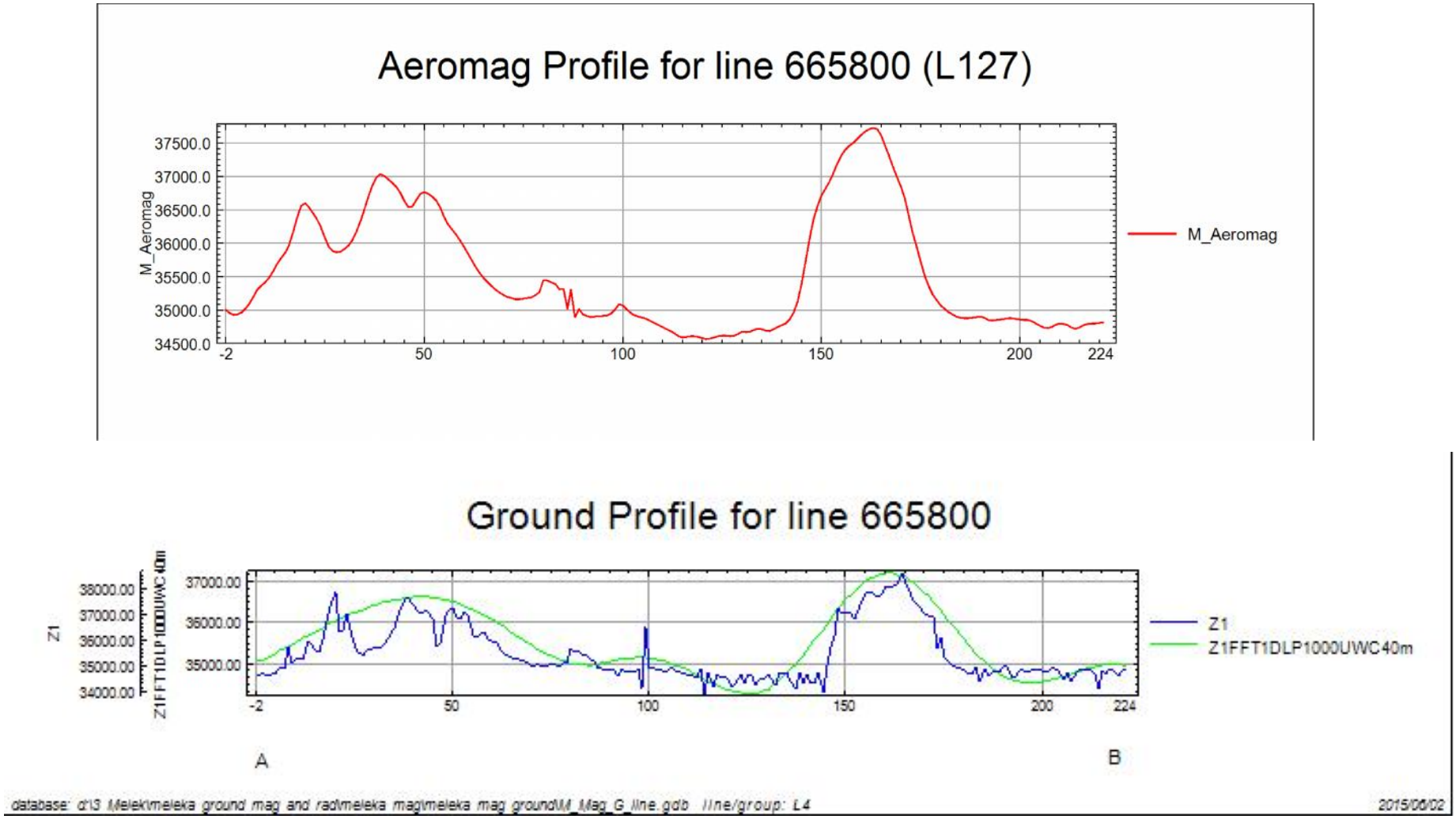

Figure 35 Comparison of the aeromagnetic and ground magnetic profile along the line 665800 of the ground magnetic survey line

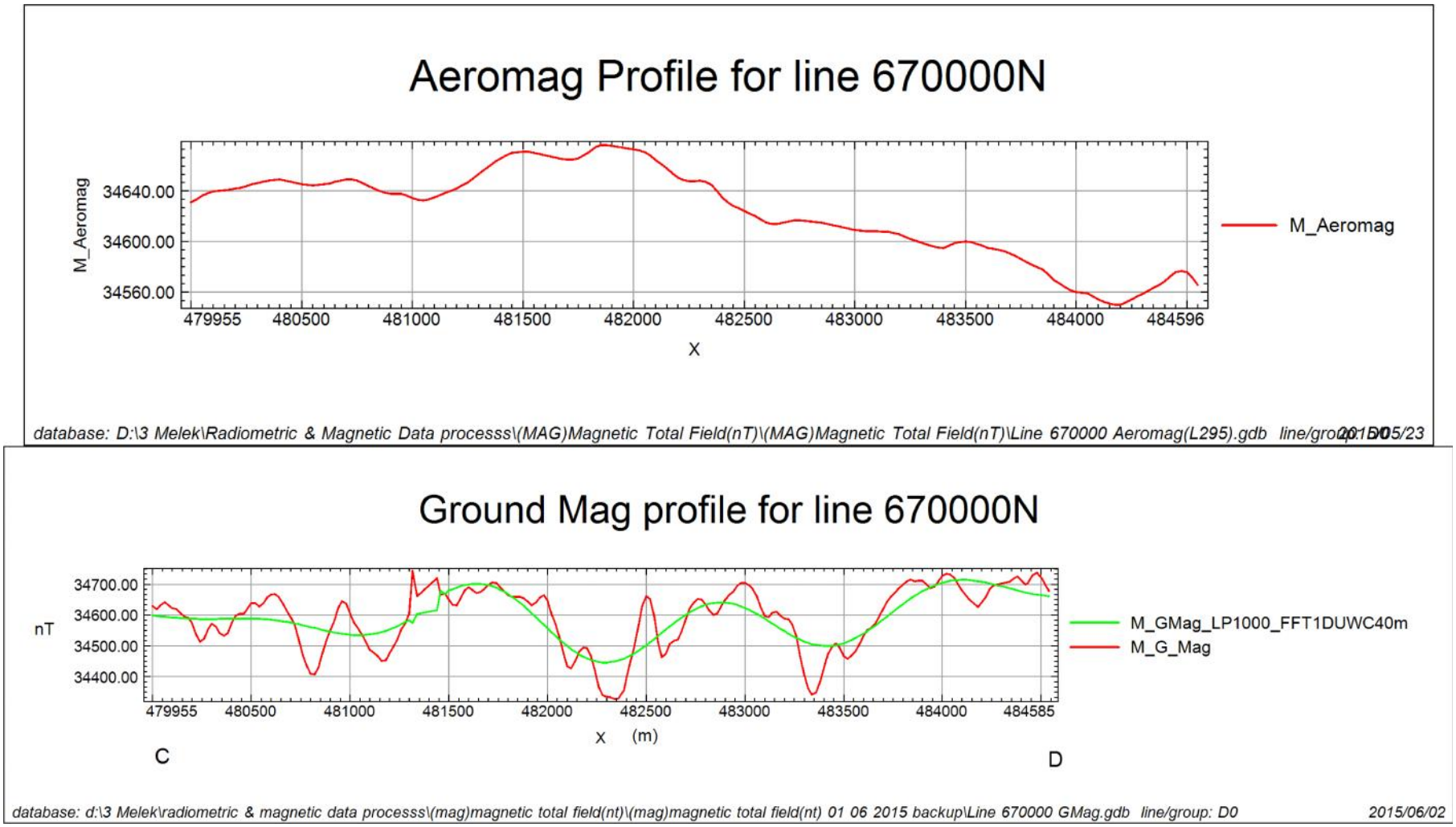

Figure 36 Comparison of the aeromagnetic and ground magnetic profile along the line 670000N of the ground magnetic survey line

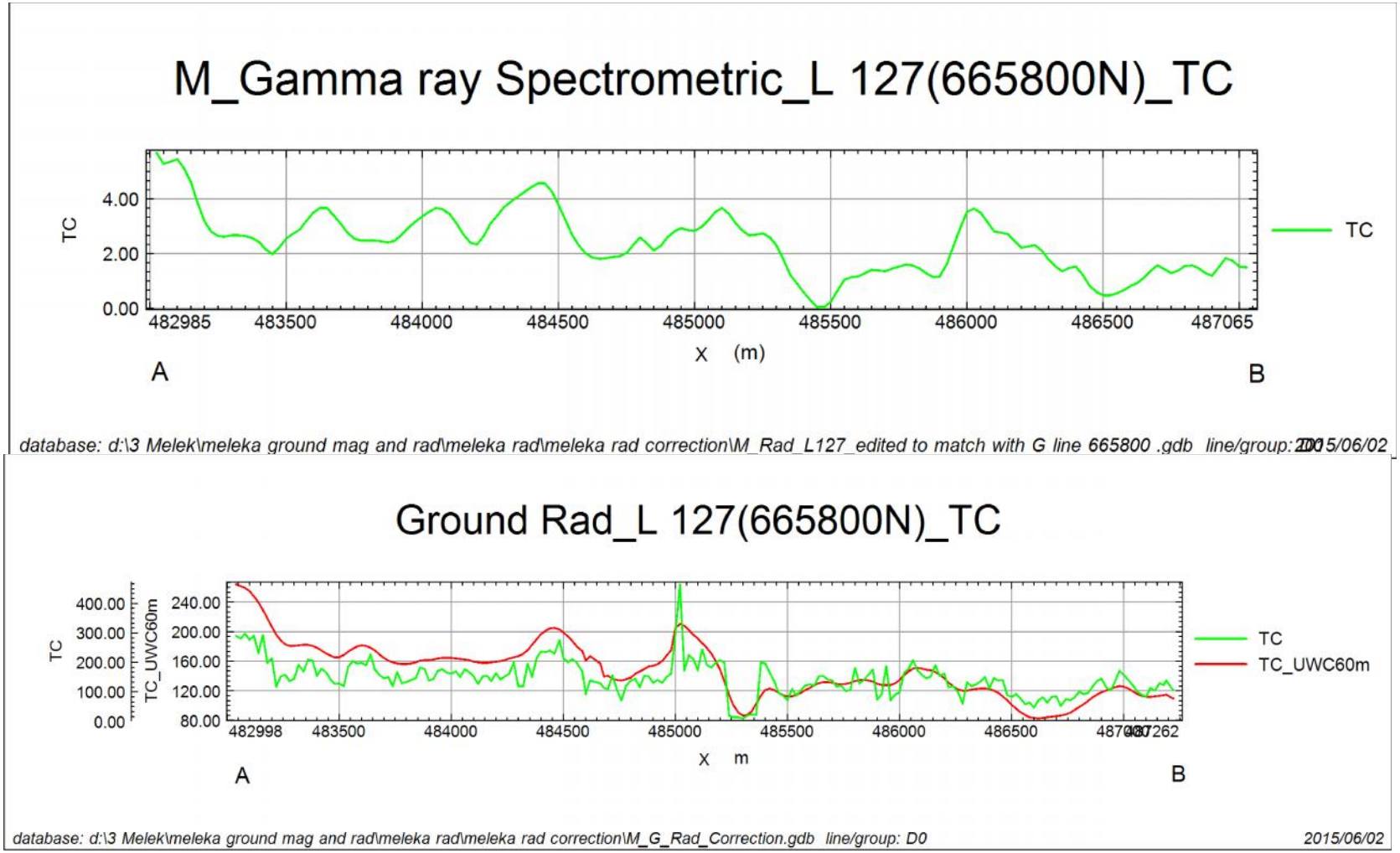

Figure 37 Comparison of the gamma ray spectrometric and ground radiometric TC profile along the line 665800N of the ground radiometry survey line

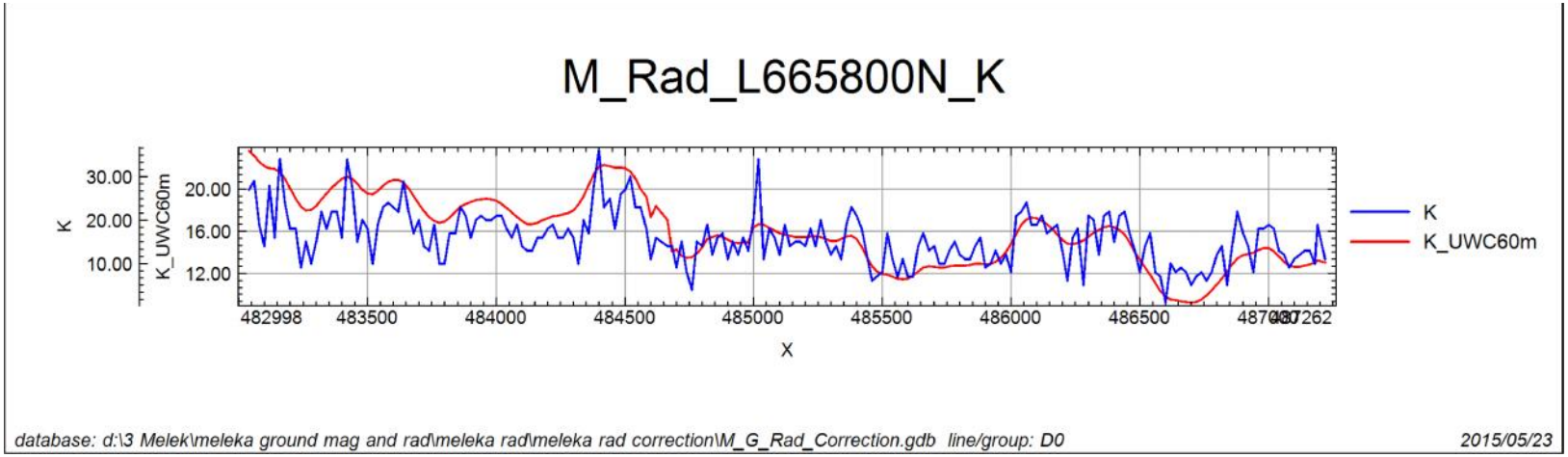

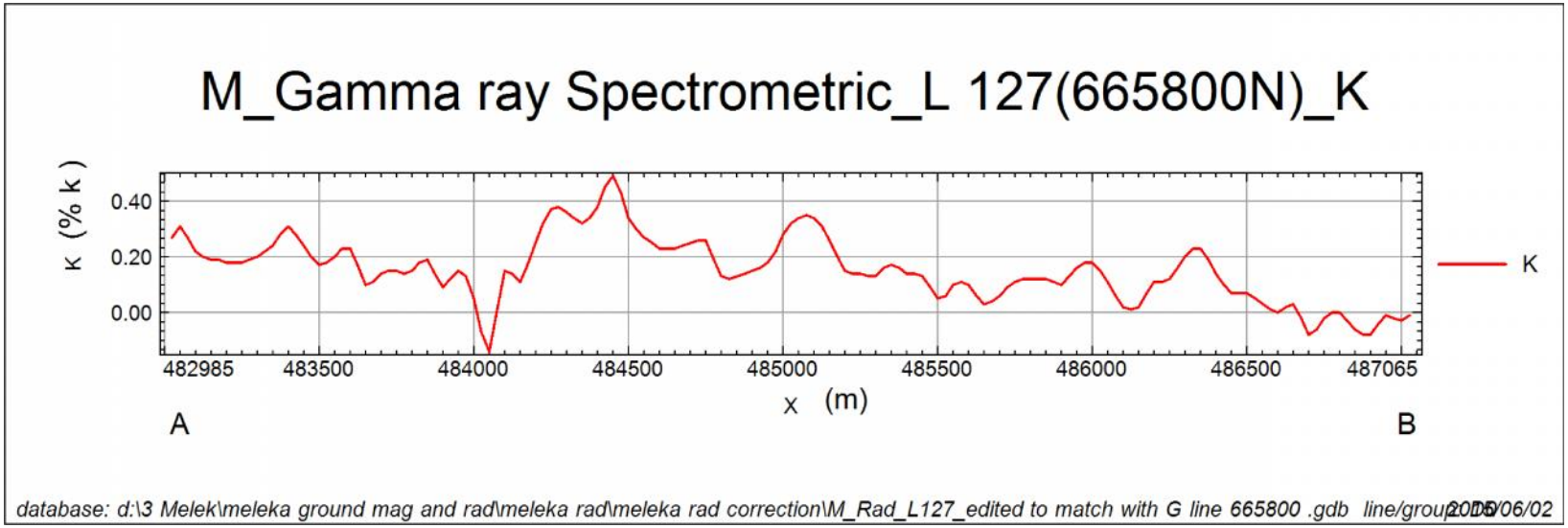

Figure 38 Comparison of the gamma ray spectrometric and ground radiometric K profile along the line 665800N of the ground radiometry survey line.

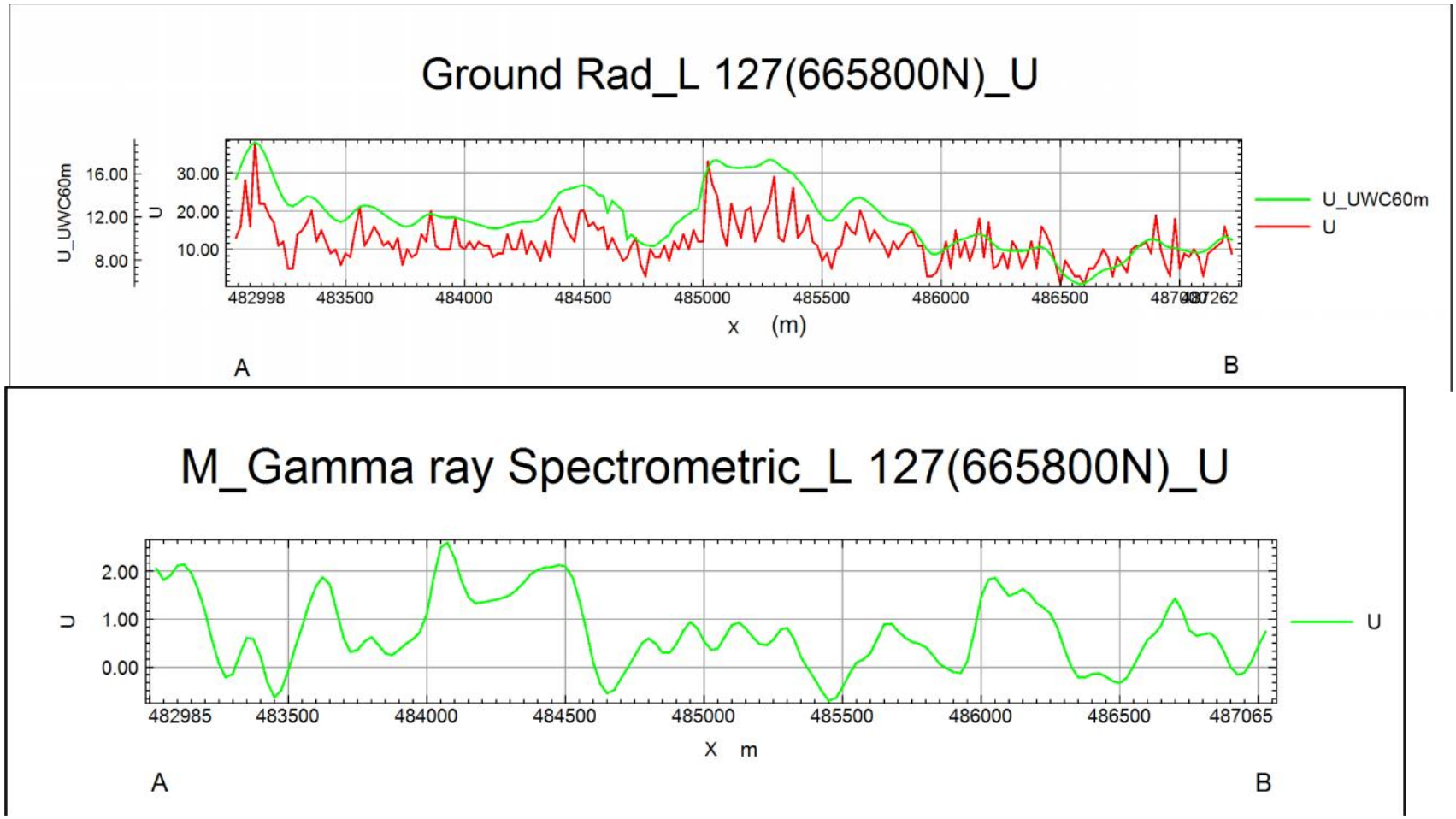

Figure 39 Comparison of the gamma ray spectrometric and ground radiometric U profile along the line 665800N of the ground radiometry survey line

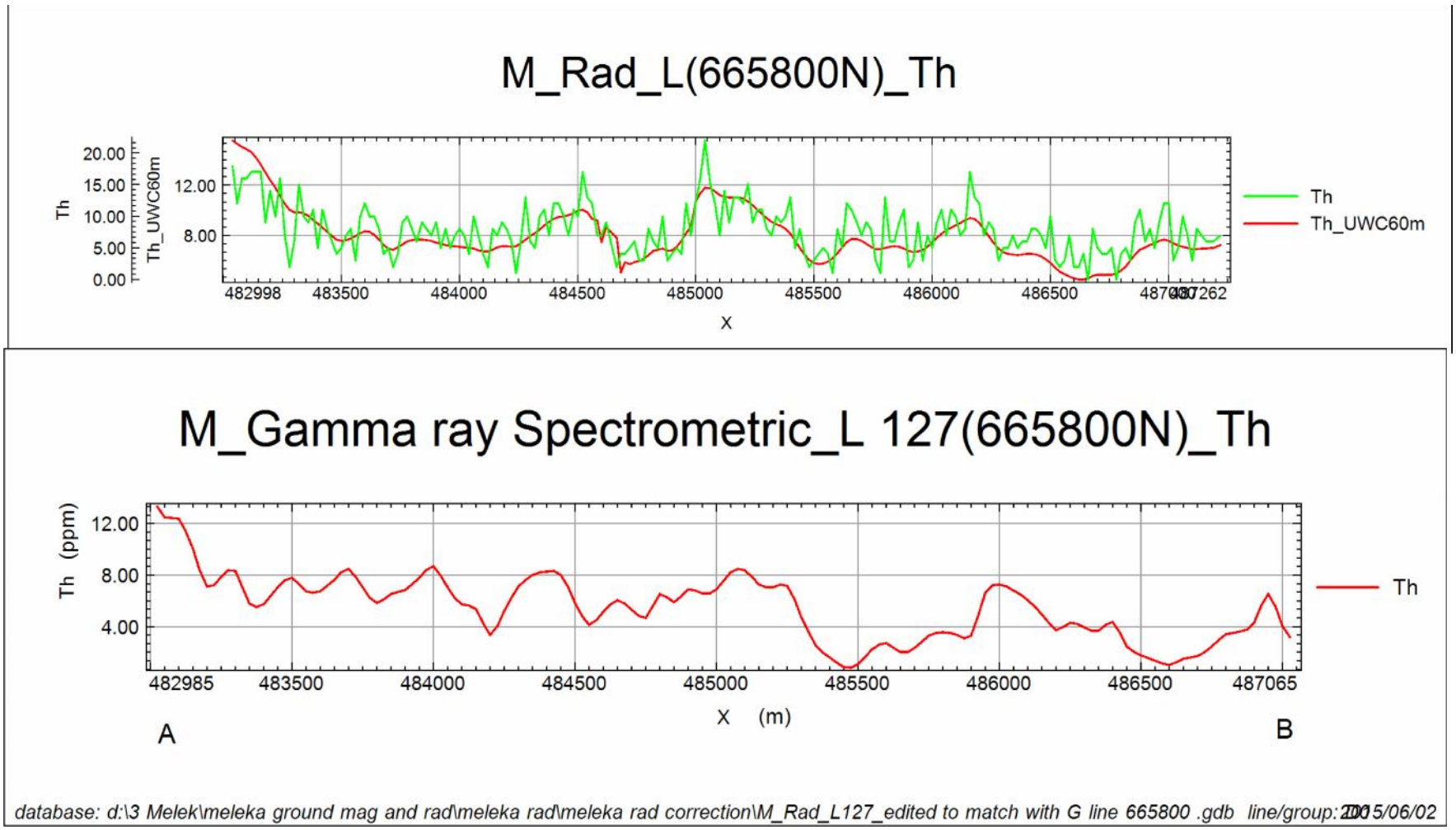

Figure 40 Comparison of the gamma ray spectrometric and ground radiometric Th profile along the line 665800N of the ground radiometry survey line

CHAPTER SIX

Conclusions and recommendations

Conclusions

Aeromagnetic and gamma ray spectrometric data processing together with ground magnetic and radiometry survey have been done and the following results area obtained

- The Total Count map show central part of the area with a low total count from northern end up to the southern covering a wide part of the study area related with central volcano sedimentary belt. It also portrayed area around Kilenso Babicho, Meleka and north Sakaro with a high total count.
- Ternary map demarcates the central volcano sedimentary belt with the bounding eastern and western gneiss, and the thrust fault at the eastern side.
- Th/K ratio shows potassic alteration zones which have exploration significance. Low Th/k value seen scattered within central volcano sedimentary zone following the artisanal sites and at the south western end of Meleka.
- TMI map has revealed magnetically high relief and complex region at the southern part. The eastern part also depicted by semi circular depleted region of low magnetic relief with some minor close-ups inside. This could be due to a shear zone. It also outlines the thrust fault with a N-S trend at the eastern side and NW-SE trend at the North Western side. These thrusts bounds old rock of biotite gneiss and younger amphibolite.
- TMI map also modifies the disposition of the two inferred fault trend with NW– SE direction against the regional geological map.
- Upward continued map shows the two inferred fault at the southern part and one NW-SE trending linear structure at the north western side is coming from deeper source.
- The tilt derivative and first vertical derivative map depict elongated shallow features.
- Regional and residual anomaly map is prepared to investigate deeper (regional) and shallower (residual) magnetic anomaly trend.
- FFT analysis done by dividing the grid in to forty two square helped to estimate the average depth of the shallower source and deeper source. From the statistics calculation of the average depth for the shallower sources is estimated to be 11.98m and the average deeper depth is estimated to be 43.54m
- Comparisons of ground and airborne data on the selected areas are found to be well corroborated
- Airborne Coverage of the country is updated with a new coverage data collected for petroleum

Recommendations

Sufficient constraining data is absent and makes the magnetic interpretation (quantitative) difficult due to the non uniqueness of potential field. With a good constraining geo-data advanced quantitative interpretation using 2D/3D modelling techniques can be made. Finally a prospectively analysis and modelling could be made using information from the geochemistry and new geoscientific data.

Further recommendation on the selected targets

1. Detailed ground geophysics with a 20 m station interval and 100m line spacing Spectral Induced polarization
2. Detailed ground magnetic survey with a 20 m station interval and 100m line spacing
3. Detailed ground gravity survey with a 20 m station interval and 100m line spacing to perform combined potential field modelling
4. Structural geology
5. Detailed geochemistry

These methods could be handled by the graduate student of the school as integrated geoscientific mapping and research.

References

Alemu, T. (2001). Precambrian Geology of Ethiopia: A Summary. 4. Unpublished report.

Alireza Almasi, Alireza Jafarirad, Hasan Kheyrollahi, (2014). Evaluation of structural and geological factors in orogenic gold type mineralisation in the Kervian area, north-west Iran, using airborne geophysical data. Exploration Geophysics , 5-6.

Asrat, A. P. (2001). The Precambrian Geology of Ethiopia: a review. Africa Geoscience Review , 271, 288.

Ayele, T. (1993). Application of frequency domain electromagnetic survays for geologic mapping and mineral prospecting at nun-uttardit area Thiland. MSc Thesis, Chang Mahi.

Bexell, G. (1948). A Preliminary roport on the geological and prospecting survey in the Adola district during the period April 1946 to February 1949. Ethiopian Mineral Resource Development Corporation. Unpublished report.

Breiner, S. (1999). Applications manual for portable magnetometers. 8,119-130. San Jose, California, U.S.A: Geometrics.

Canyon Resources, A. (1997). Meleka Abeba Technical Justification Report -first Project-Year End. 4-5. Addis Ababa, Ethiopia: unpublished report.

Canyon Resources, A. (1998). Meleka Abeba Technical Justification Report -Second Project-Year End. 7- 8. Addis Ababa, Ethiopia: unpublished report.

Canyon Resources, A. (1999). Meleka Abeba Technical Justification Report -Third Project-Year End. 6 - 16. Addis Ababa, Ethiopia: unpublished report.

EIGS, E. I. (1993). Final report on mineral exploration in Adola area. 42- 90. unpublished report.

Ford .K, P. KEATING AND M.D. THOMAS (2007). Overview of geophysical signatures associated with Canadian ore deposits. 14.

Ian. N. Macloed, S. V. (n.d.). Analytic_signal and reduction-to-pole in the interpretation of total magnetic field data at low magnetic latitude. 830 - 835.

Jessel, M. (2002). Manual of Structural Geophysics.

Kazmin, V. (1978b). Geology of the Ethiopian basement and possible relation between the Mozambique.

Kazmin, V. (1978). The Ethiopia basement: Stratigraphy and possible manner of evolution. Geology of Rundschau , 531- 544.

Kearey, P. (2002). An Introduction to geophysical Exploration (Third ed.). Hong Kong: Blackwell Science Ltd.

Last, B. J. (1994). Final mission report. 7 - 32. Addis Ababa, Ethiopia: Unpublished technical report.

Lowrie, W. (2007). Fundamentals of Geophysics (second ed.). Cambridge: Cambridge University Press.

Maha Abdelazeem, E.-S. K.-S. (2012). Analysis of magnetic gradients at North East of Wadi Ar Rika quadrangle, Saudi Arabia, to delineate subsurface linear features and faults. NRIAG Journal of Astronomy and Geophysics , 2-5.

Mahanyele, P. J. (2010). Interpretation of airborne magnetic data over selected areas of Witbank coalfield, South Africa: an aid to mine planning. 22- 33. University Of Pretoria.

Mario Rebolledo-Vieyra, J. U.-F.-L. (2010). Aeromagnetic anomalies and structural model of the Chicxulub. Revista Mexicana de Ciencias Geológicas, , 27, p.185-195.

Mekonnen, T. K. (2004). Interprotation and Geodatabase of Dykes Using Aeromagnetic Data of Zimbabwe and Mozambique. 26-29.

Mita Rajaram, S. A. (2013). Aeromagnetic signatures of Precambrian shield and suture zones. Geoscience Frontiers , 13.

Miyashiro. (1979). Metamorphism and metamprhic belts, .

Muleta, B. (1990). Report on reconnaissance geophysical surveys in Ababa river basin. 4-10. Addis Ababa.

Nabighian M. N. , Grauch. V. J. S., Hansen. R. O. , LaFehr T. R. (2005). The historical development of the magnetic method in exploration. GEOPHYSICS , 70 (6), 1-29.

Nabighian, Missac N. (1972). The analytic signal of two-dimensional magnetic bodies with polygonal cross-section: its properties and use for automated anomaly interpretation. 37 (3), 507 - 517.

Negussie, T. (1990). Geologiccal report of meleka area. 1-26. GSE, unpublished report.

Oasis Montaj. Geosoft Inc.Oasis Montaj user manual.

P.Eng, Douglas L. McConnell. (1994). A report on helicopter electromagnetic and radiometric survay of adola. Ethiopian Institute of Geological Survey, Addis ababa.

Parasnis, D. (1975). Mining geophysics (2nd ed.). New York: Elsevier scientific publishing company.

PS Mining Private Limited Company. (2015). Second Year Annual Report on Gold and Base metals Exploration in Bulbul area. Unpublished, Addis Ababa.

Reeves, C. V. (2005). Aeromagnetic surveys.

S. A. Ganiyu, B. S. (2013). Upward Continuation and Reduction to Pole Process on Aeromagnetic. Earth Science Research , 2 (1).

Scintrex. (1979). Cad-6, Four Channel Stabilized Gamma Ray Spectrometer Manual.

Scintrex. GSP- 4, Portable Gamma - Ray Sensor manual.

Smith, B. A. (2007). Helicopter Electromagnetic and Magnetic Geophysical Survey Data, Oakland, Ashland, and Firth Study Areas, Eastern Nebraska. U.S.G.S open file report 2008.

Solomon, T. (2009). Mineral Resources Potential of Ethiopia. Addis Ababa : Addis Ababa University, p 1-5, 34.

Suze Nei P. Guimaraes, V. M. (2012). Airborne geophysical surveys in the north-central region of Goias (Brazil)Brazil): implications for radiometric characterization of tropical soils. Journal of Environmental Radioactivity , 9.

Sweth. (2009). A proposal for Airborne Geophysical Survey of South western Ethiopia. Addis Ababa.

Tadesse, A. (2010). Introducton to Metamorphic Petrology .

Telford, W. G. (1976). Applied Geophysics (2nd ed.). Cambridge: Cambridge University Press.

Urquhart, W. (2013). Airborne Geophysics. Retrieved October 2014, from Airborne Geophysics: http://www.geoexplo.com/index.html

Weldehaimanot, B. (1995). Structural Geology and geochemistry of the Neoproterozoic Adobha and Adola Belts (Eritria and Ethiopia). Giessen.

Woldetinsae, G. (1997). Aeromagnetic study near Gadawara area,and its implication on the Namada-son lineament, India. National Geophysical Research Instituite.

Woldetinsae, G., Nigussie, M., & Yosef, M. (1995). Integrated Geophysical Survey ForMineral exploration in North MI-Essa and Mi_Essa Areas, Adola District, Southern Ethiopia. GSE. Addis Ababa: Unpublished report.

Worku, H. (1996). Geodynamic development of the Adola Belt (Southern Ethiopia) in the Neoproterozoic and its control on gold mineralizatio. Berlin.

Declaration

This thesis is my original and has not been presented for the degree/masters in any other university, and that all the sources of materials used for the thesis have been duly acknowledged.

Behailu Mammo

Signature_____ Date _____

Dr. Abera Alemu (Advisor)

Signature _____ Date_____

July 2015

Addis Ababa

ETHIOPIA